2009

CFD modelling and analysis of an opposed piston internal combustion engine

George Thomas
University of Wollongong

2009

CFD modelling and analysis of an opposed piston internal combustion engine

George Thomas
University of Wollongong

CFD MODELLING AND ANALYSIS OF AN OPPOSED PISTON INTERNAL COMBUSTION ENGINE

A thesis submitted in partial fulfilment of the
requirements for the award of the degree

MASTERS BY RESEARCH

from

UNIVERSITY OF WOLLONGONG

by

GEORGE THOMAS
MASTER OF ENGINEERING (MECHANICAL)

School of Mechanical, Materials and Mechatronics Engineering
University of Wollongong
August 2009

CERTIFICATE OF AUTHORSHIP AND ORIGINALITY

I certify that the work in this thesis has neither previously been submitted for a degree nor has it been submitted as part of requirements for a degree except as fully acknowledged within the text.

I also certify that the thesis has been written by me. Any help that I have received in my research work and the preparation of the thesis itself has been acknowledged. In addition, I certify that all information sources and literature used are properly referenced in the thesis.

George Thomas
Student Number: **3230843**
Master of Engineering-Mechanical
31 August 2009

Signature of Candidate

ABSTRACT

A Computational Fluid Dynamics (CFD) simulation of an opposed piston Internal Combustion (IC) engine, also known as the NuStroke engine, has been developed. The thesis focuses on the design and analysis of this particular engine using ANSYS CFX, a commercial CFD tool. The primary objectives of this thesis are to analyse the gas flow, effect of heat transfer, and combustion process on the engine performance. The engine geometry is modelled and meshed in ANSYS Workbench V11.0 to minimize any exporting errors that may creep in and cause serious mesh issues during mesh deformation simulation. Several researchers for a wide range of cases, justifying its application in the present study, have extensively validated different versions of the CFD code.

At the initial stage of the project, the engine is modelled with single inlet and exhaust ports, the piston motion is prescribed with a sinusoidal profile, and a polynomial profile based on cam profile motion. The model does not include the combustion process. It is validated against an air-standard cycle process model developed in spreadsheet form. Similar spreadsheet models have been developed and extensively validated against experimental results of other engines by the author as a part of another thesis. To analyse the effects of combustion, the Domain Source Method (DSM) is employed in the CFD model, by which energy of combustion is explicitly fed to the engine model.

A further improved CFD model with multiple inlet and exhaust ports is then applied. This enables the engine CFD model to closely simulate a real world engine, with the combustion model based on the DSM. The results obtained are then compared with the previous modelling results and spreadsheet results. The initial work on using Burning Velocity Model (BVM) and Eddy Dissipation Model/Finite Rate Chemistry (EDM/FRC) models to simulate combustion in the model is done and some results from these models are presented. The in-cylinder flow fields and pressure waves observed show significant vortex generation and heat transfer through the gas and combustion chamber walls.

The present modelling of the engine using CFD techniques, and the analysis are the first attempts of this kind for this particular engine. The advantage of polynomial cam profile in controlling the performance of this engine is observed to be outstanding. The analysis of the obtained pressure and temperature, and the in-cylinder mid-plane pressure and velocity streamline plots show that both the spreadsheet model and CFD model agree qualitatively. These observations lead to a conclusion that the project, if extended further with experimental analysis, will give results that are comparable to the spreadsheet and CFD model results.

The current work successfully presents a numerical simulation of an opposed piston engine. This study has enough potential to boost further research attempts in similar engine configurations, as the opposed piston engines have not been widely used nowadays in industries due to difficulties in attaining a successful design and balancing issues despite of the fact that they are low cost and less complicated engines. At this stage of the thesis, experimental results are not available for a more extensive validation, but at a later stage, if possible, this could be done to validate the current CFD model. Further extensive research on similar engine configurations with the help of good computing facilities and CFD simulation tools would make it possible to develop a successful, designer-friendly, and eco-friendly engine, which could eventually set up a new revolution in the entire engine industry.

ACKNOWLEDGEMENTS

I wish to thank Dr. Buyung Kosasih, for his support, experience, and direction during the course of this project. The support he has given me throughout the project with CFD modelling is really appreciable. His enthusiastic supervision is gratefully acknowledged.

Also I would like to express my appreciation for the contribution of Dr. Oliver Kennedy, who is the co-supervisor of this thesis. I am grateful to him for giving me this challenging project. His support with spreadsheet modelling of the opposed piston ICE is gratefully acknowledged. I also wish to thank him for allowing me to have access to the F SAE computer lab.

I also thank each and every staff in the faculty who directly and indirectly helped me in successfully finishing this project. The support provided by LEAP Australia during some parts of the CFD modelling of IC engine is also acknowledged. I extend my gratitude to Dr. Paul Cooper, Head of the School, for encouraging me to carry out this Masters Thesis project.

The support of Powell Engine Company for providing the concept design of the engine is gratefully acknowledged.

Last but not least, I would like to thank my parents for supporting me both financially and morally with my studies. Without their support I would not be here for my studies. Above all, I wish to thank God for giving me the courage to go on with the project when I faced with lots of limitations, and for helping me to take the project to this level of achievement.

TABLE OF CONTENTS

LIST OF FIGURES

LIST OF TABLES

NOMENCLATURE

Symbols

a	Piston displacement, mm
A	Area, mm^2
A_E	Effective flow area, mm^2
A_p	Port area, mm^2
A_R	Characteristic flow area, mm^2
$A_{surface}$	Piston area, mm^2
b	A constant
B	Bore diameter, mm
c	Clearance, mm
c	Reaction progress
C	Discharge coefficient
C_p	Specific heat at constant pressure, J g^{-1} K^{-1}
C_{stiff}	stiffness model exponent
C_v	Specific heat at constant volume, J g^{-1} K^{-1}
CR	Compression ratio
c_μ	Empirical closure coefficient
d	Distance from nearest boundary, mm
D	Piston diameter, mm
D_v	Valve diameter, mm
e_i	Turbulence eddy dissipation
E	Gas internal energy, J
F_2	Blending function
G	Gas mass flow rate, kg s^{-1}
h_c	Heat Transfer Coefficient, W m^{-2} K
h_p	Port height, mm
k	Thermal conductivity, W m^{-1} K^{-1}
k_e	Effective thermal conductivity, W m^{-1} K^{-1}
k_i	Turbulence kinetic energy, kg m^2 sec^{-2}

l	Cylinder length, mm
l_i	Eddy wave length, mm
L_v	Valve lift, mm
L_ε	Turbulence internal length, mm
L_L	Connecting rod length, mm
m	Molecular weight, mass of air, kg
$\dot{m}$	Mass flow rate, kg s^{-1}
M	Mach number
m_h	Mass fraction of fuel burnt during burn duration
MEP	Mean Effective Pressure, kPa
N_c	Number of cycles
Nu	Nusselt number
p	Cylinder fluid pressure, kPa
P_a	Ambient pressure, kPa
P_A	Downstream pressure, kPa
P_b	Exhaust back pressure, kPa
p_c	Sonic pressure ratio
P_f	Fluid pressure in valve/port, kPa
p_m	Motored cylinder pressure, kPa
P_o	Stagnation pressure, kPa
p_r	Reference state fluid pressure, kPa
Pr	Prandtl number
$\dot{q}$	Heat flux rate, W/m^2
$\dot{Q}$	Heat transfer rate, W
r	Port corner radius, mm
R	Universal gas constant, J K^{-1} mol^{-1}
$\tilde{R}$	Value of R per mole
Re	Reynolds number
R_L	Crankshaft radius, mm
s	Shear strain
S	Stroke, mm
S_L	Flame propogation speed

t	Time, sec
T	Temperature, K
T_b	Temperature of burned particles, K
T_c	In-cylinder gas temperature, K
T_{ac}	Adiabatic core temperature, K
T_g	Gas temperature, K
T_r	Reference state fluid temperature, K
T_s	Local wall temperature, K
T_u	Temperature of un-burned particles, K
T_w	Wall temperature, K
u'	Turbulence intensity, W/m^2
$\overline{U}(\theta)$	Phase averaged velocity
ν_s	Paddle rotation velocity, m s^{-1}
V	Instantaneous cylinder volume, cc
V_c	Clearance volume, mm^3
V_d	Engine capacity, cc
V_m	Molar volume
V_p	Mean piston speed, m sec^{-1}
V_r	Reference state fluid volume, mm^3
V_s	Swept volume, mm^3
V_t	Total volume, mm^3
w	Local average gas velocity, m sec^{-1}
W	Work done, J
^0CA	Degree crank angle
γ	Ratio of specific heats
Γ_{disp}	Mesh stiffness, Nm
δ	Boundary layer thickness, mm
δ_l	Ratio of laminar flame thickness, mm
η_0	Otto cycle efficiency
τ_c	Chemical time scale, sec
θ	Shaft angle, degree

θ_d	Total burn duration, degree
θ_s	Starting angle of fuel ignition
κ	Von Karman constant
μ	Dynamic viscosity, kg m^{-1} s^{-1}
μ_t	Turbulence viscosity, m^2 s^{-1}
v_t	Eddy-viscosity, Pa sec
ρ	Density, kg m^{-3}
ρ_2	Density of gas at vena contracta during flow, kg m^{-3}
ρ_o	Stagnation density, kg m^3
σ	Stefan-Boltzmann constant, kg s^{-3} K^{-4}
ω	Angular velocity, m s^{-1}
ω_p	Paddle rotation speed, rpm
$\forall$	Control volume size

Subscripts

u	Unburned
w	Wall
b	Burned gas
c	Coolant, Cylinder
e	Exhaust

Abbreviations

BDC	Bottom Dead Centre, BC
BVM	Burning Velocity Model
CEL	CFX Expression Language
CFD	Computational Fluid Dynamics
Cd	Discharge coefficient
CI	Compression Ignition
CO	Carbon Monoxide

DNS	Direct Numerical Simulation
DSM	Domain Source Model
EDM	Eddy Dissipation Model
EP	Exhaust Port
EV	Exhaust Valve
EVC	Exhaust Valve Close
EVO	Exhaust Valve Open
FRC	Finite Rate Chemistry
HC	Hydro Carbon
HTC	Heat Transfer Coefficient
ICE	Internal Combustion Engine
IP	Inlet Port
IV	Inlet Valve
IVC	Inlet Valve Close
IVO	Inlet Valve Open
LES	Large Eddy Simulation
NO	Nitrous Oxide
OPE	Opposed Piston Engine
RANS	Reynolds Averaged Navier Stokes
SI	Spark Ignition
SIM	Spark Ignition Model
TDC	Top Dead Centre, TC
WB	Work Bench

Chapter 1

INTRODUCTION

The Internal Combustion (IC) engines have undergone significant advancements since their introduction in the early 16th century, and the latest trend is to make them greener. The influence of fuel-powered mechanical engines in the modern world is substantial enough, so that we cannot avoid them for emission reduction reasons. Their application extends from lawn mowers to powering heavy military ships and jets. The latest trend in the IC engine industry is to develop power plants with higher efficiency and to make them running on alternative fuels to meet modern emission norms.

There are different IC engine configurations used to generate mechanical output from chemical energy, namely reciprocating engines (single and double piston) and rotary engines. In general, a double piston engine delivers more power than a single piston engine for the same configuration. This thesis uses an analytical model developed in spreadsheet form and a Computational Fluid Dynamics (CFD) model to analyse the operating characteristics of an Opposed Piston Engine (OPE).

1. 1 Objective and Scope of the thesis

The analytical methods of designing have been completely replaced by CFD methods. The most prominent reasons behind this changeover are faster design and analysis, less chance for errors, and designs are easily revisable. This thesis uses ANSYS V11 for simulation, which has been validated by several users (Horrocks, 2001, Foster, 1998, Stone, 1999).

The main objectives of this thesis are:

- To project the capability of CFD techniques to model and analyse IC engine processes,

- To compare the spreadsheet analytical model and the CFD model (Thomas, 2008),
- To discuss the advantages of using polynomial profile cam-plate over sinusoidal profile cam-plate for the Opposed Piston IC engine,
- To discuss the advantages of using multiport engine configuration over the uniport engine design,
- To introduce the concept of modelling combustion using Domain Source Model (DSM), and
- To discuss CFD combustion modelling using the Burning Velocity Model (BVM) and Eddy Dissipation Model/Finite Rate Chemistry (EDM/FRC).

The scope of the thesis is limited to CFD simulation of the Opposed Piston gasoline engine which is a unique design. The study can be extended to experimental analysis to validate the CFD and analytical models. The methods of combustion analysis discussed in this thesis can be used in the future for analysis of IC engines and combustors, and the results from this method can be used as benchmark values for comparison.

1. 2 Introduction to Internal Combustion Engines (ICE)

In conventional IC engines, the reciprocating motion of piston inside the cylinder imparts rotary motion to the output shaft of the engine. An exception to this kind of engine is the rotary IC engine developed by Wankel in 1957 (Heywood, 1988). However, rotary engines are not widely used because of their complicated design, and higher cost of manufacture and maintenance compared to reciprocating engines.

The motion of the piston is transmitted to the output shaft using a connecting rod and crankshaft assembly. Figure 1.1 shows a simple assembly of this concept of engine. The crankshaft rotary motion will impart reciprocating motion to the piston. The piston has two extreme positions during its motion inside the cylinder, called the Top Dead Centre (TC/TDC) and the Bottom Dead Centre (BC/BDC) (Thomas, 2008).

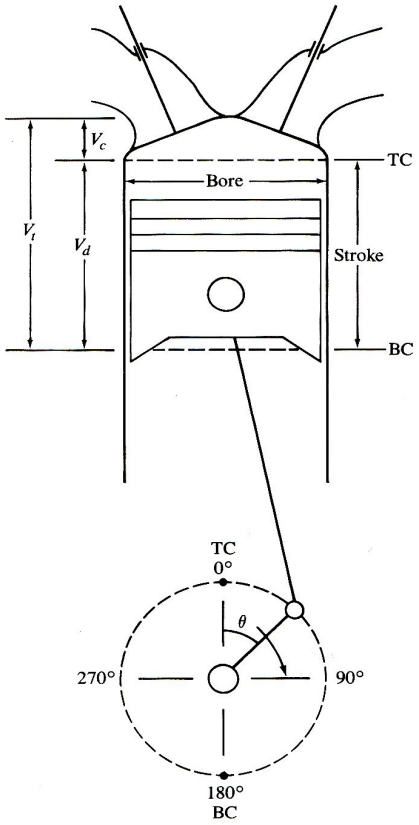

Figure 1.1: Geometry of a reciprocating ICE (Heywood, 1988)

The cylinder block keeps the cylinder in position with the top of the cylinder block covered by cylinder head, and at the bottom is the crankcase that is normally of wet type where lubricating oil is filled in the case. The combustion chamber volume is designated as the instantaneous volume occupied between the top of the piston and upper portion of the cylinder during combustion (Mathur and Sharma, 2003). In the case of gasoline engines, an electric spark ignites the highly compressed air-fuel mixture above the piston at the TC/TDC position. The resulting explosion imparts a downward force to the piston, which results in transmission of motion to the rotary output shaft.

1.2.1 Conventional ICE

Figure 1.2 shows the four strokes in a conventional four stroke reciprocating engine. The working fluid inside the combustion space exerts force on the piston to move it inside the cylinder. In a four stroke engine, each cylinder needs four strokes of the

piston, i.e two revolutions of the crank shaft for one complete engine cycle (Heywood, 1988).

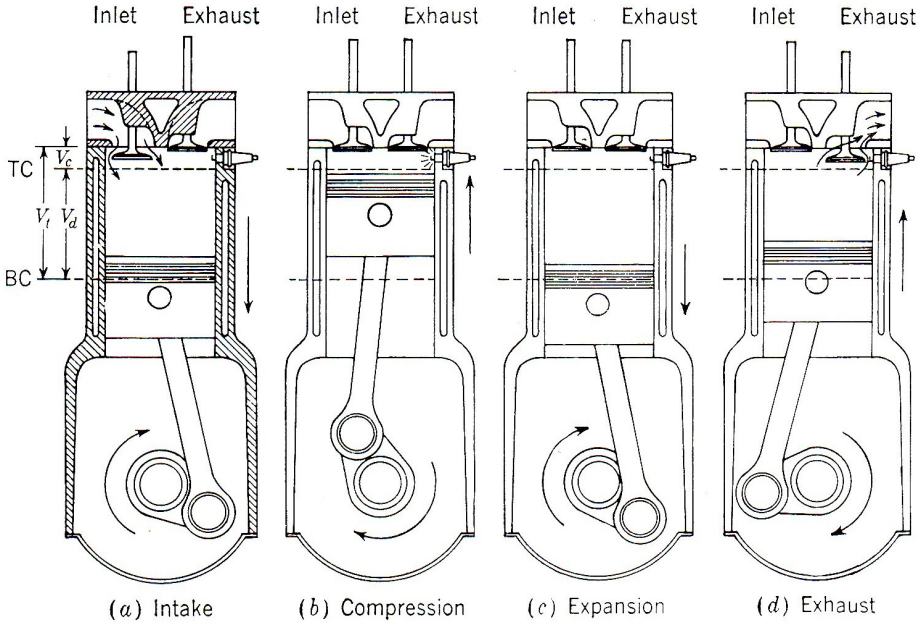

Figure 1.2: Four stroke engine cycle (Heywood, 1988)

Beginning with the intake stroke (a), the piston is at TC/TDC, advancing towards BC/BDC. During this process the air-fuel mixture is drawn through the inlet valve into the cylinder. In the compression stroke (b), all the valves are closed, the piston moves from BC/BDC to TC/TDC, compressing the air-fuel mixture, and making it ready for combustion. At the specified spark advance angle, the spark plug is activated and energy is released into the compressed air-fuel mixture to initiate combustion.

During the expansion/power stroke (c), power is generated in the engine. During this stroke the expanding gas due to combustion push the piston from TC/TDC to BC/BDC. The burnt gas is removed from the cylinder during the exhaust stroke (d). The gas removal is aided by factors like the sudden opening of exhaust valve at the end of expansion stroke, the pushing of gases through the valves by the piston, and the turbulence imparted by fresh charge entering the system through inlet valves.

Otto Air Standard Cycle

The Otto cycle is the theoretical cycle followed in a Spark Ignition (SI) engine. A thorough knowledge of the working of this cycle is essential for the successful modelling of cam-plate engine.

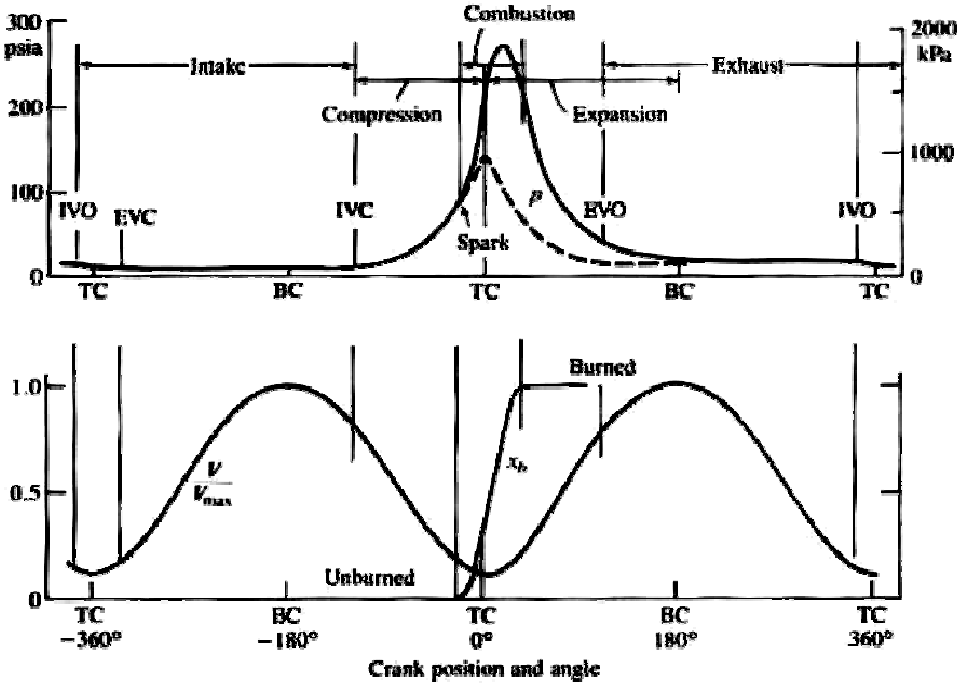

Figure 1.3: Figure shows different events in a four-stroke SI engine cycle. Variation of cylinder pressure, cylinder volume V/V_{max}, and mass fraction burned x_b are been plotted. (Solid line – firing cycle; Dashed line – motored cycle) (Heywood, 1988)

The Otto cycle is also called the constant volume cycle. This section discusses the air-standard cycle analysis, and hence the suction and exhaust processes generally shown in two-stroke engine analysis are not shown in the Figure 1.4.

The air standard cycle analysis for the CFD model was performed earlier by the author (Thomas, 2008), and the results obtained were compared against the analytical model results. The purpose of air-standard cycle analysis was to check the mesh quality and simulation stability, before performing the complete combustion model simulation.

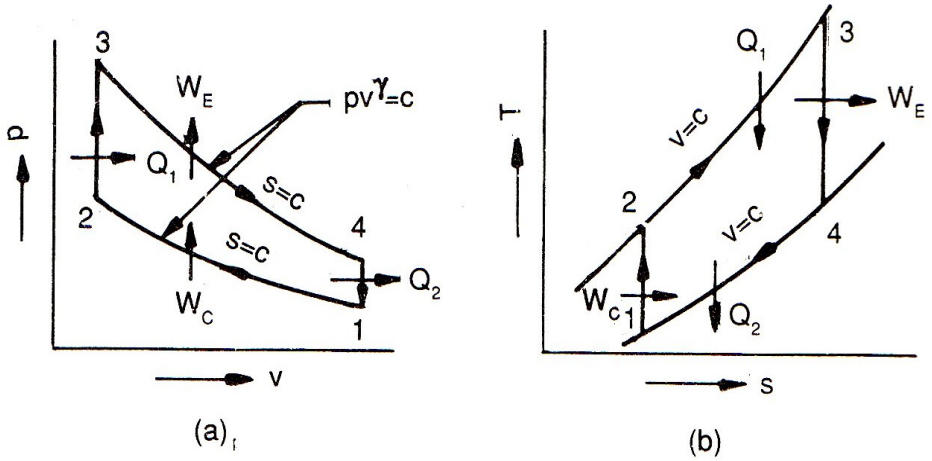

Figure 1.4: The Otto air standard cycle: (a) P-V and (b) T-S diagram (Nag, 1995).

1. 3 Historical development of Opposed Piston Engines

An opposed piston engine assembly is a configuration with a single cylinder housing two oppositely moving pistons, with each of these pistons driving a separate crankshaft. This design helps the engine to be highly balanced. In addition, these engines do not need cylinder heads as both the pistons are in a single cylinder. As these engines assemble two pistons inside a cylinder, the relative piston velocity is double for a particular crank and piston speed.

The gas flow in and out of the engine is quite easy as this engine uses ports instead of valves. The pistons control the ports, and thus the complexity of valve motion and the corresponding arrangements are absent (Mathur and Sharma, 2003). One of the major drawbacks of these engines is their lengthy construction configuration, as the two connecting rods linking the pistons and crankshafts extend in both direction. This may eventually affect the design of the vehicle (Singh, 2004).

The inventor of the first-ever practical opposed piston engine is Hugo Junkers, in 1859. The design was not a complete success due to difficulties in power collection and proper synchronization of the multiple crankshafts. Junker's Jumo 205 diesel aircraft engine is one of the famous examples of this kind of engine configuration (Hofbauer, 1999). The evolution of opposed piston engines began in the early 20th century. In 1907, Raymond Koreyvo who was an engineer in Kolomna Works, patented and designed the first opposed piston engine.

A major application of this kind of engine is in the nuclear powered submarines for auxiliary power supply. In all the different kinds of design like Koreyo, Jumo, or Deltic in the earlier times, the two pistons themselves as in the case of the NuStroke engine operated engine ports. The piston linked to the exhaust port is termed as the exhaust piston and that linked to the inlet port is the intake piston. As the ports are located on the cylinder wall for these engines, the charge enters the cylinder in a radial direction, by which the charge motion is optimized inside the cylinder for proper combustion (Hofbauer, 1999).

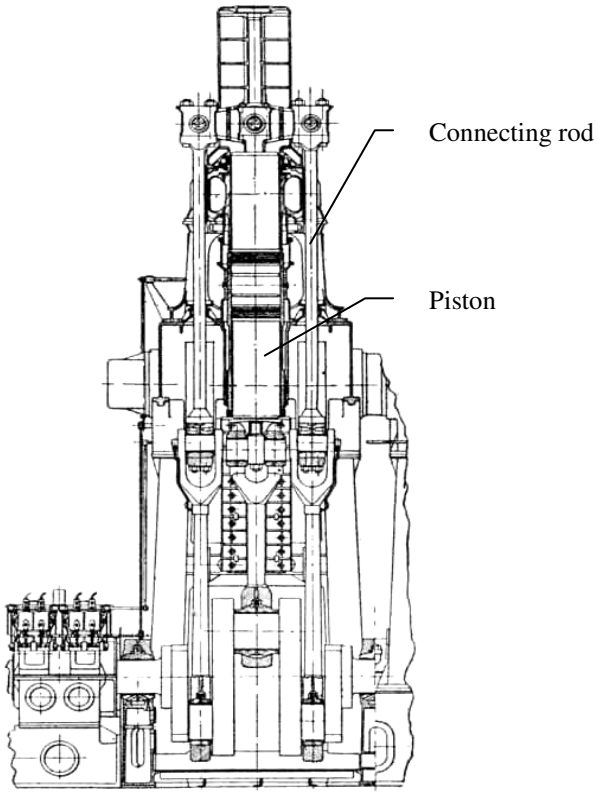

Figure 1.5: Side Sectional view of the Doxford Opposed-Piston Main Propulsion Marine Engine, showing cylinder and connecting rods (DFD, 1947)

The Doxford engine (Figure 1.5), adapted from the Jumo and Fairbanks design is a different design. It has an external connecting rod that connects the upper and lower pistons. This results in a design advantage requiring only a single crankshaft. Karl Otto Keller first developed a design adaptation of this engine in 1912. The free piston engines later developed in different parts of the world are the followers of Opposed Piston engine configurations.

D. Napier & Sons, Ltd developed another version of the Opposed Piston engine in 1950 (Figure 1.6). The engine is liquid-cooled, and it uses a mechanically driven turbo-blower. The engine has a lightweight and modular construction compared to other opposed piston engines developed until then. The Deltic engines have higher power output, and due to fewer moving parts they have low maintenance cost. The engine assembly is shaped like an equilateral triangle, with the three crankshafts in the corners of the triangle.

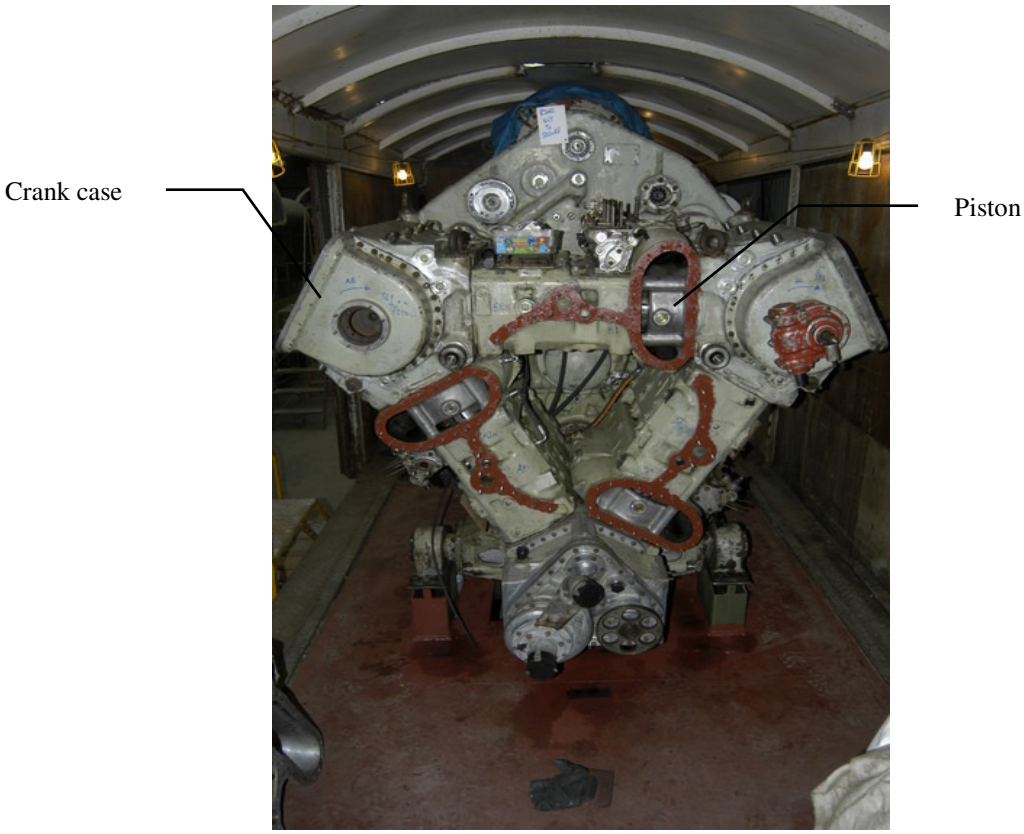

Figure 1.6: Napier engine (Deltic, 1960)

1.3.1 Design challenges in Opposed Piston Engines

Even though Opposed Piston engines deliver higher efficiency and better performance compared to the conventional engines, the difficulties in developing a fool-proof engine are many. Some of the prominent disadvantages and limitations of Opposed Piston engines are discussed here.

These Opposed Piston engines are restricted to two-stroke operation. The engine uses port-scavenging to increase the reliablity and simplicity of the design. Because of this reason, the premixed-charge engine may suffer from short-circuiting, as some of the inlet mixture may be lost through the exhaust port (Mikalsen and Roskilly, 2007). This can affect the fuel efficiency, and can cause exhaust gas emissions as normally observed for SI two-stroke engines.

As mentioned earlier, the Opposed Piston engines are lengthy, either in the vertical direction or in the horizontal direction. This is unavoidable as the connecting rods and crankshafts need to be at either end of the pistons. This will affect proper streamlining of the vehicle and hence these engines are not used in commercial automobiles any more. However, it is claimed that this disadvantage is overcame by the NuStroke design by replacing the crankshafts and associated parts with simple camplate assemblies at either end of the engine, which is less space consuming.

Only an experienced person can work on these engines as the piston motions and spark ignition in case of multiple sparks need to be synchronized. Another challenge is, whether the two-stroke Opposed Piston engine can meet modern emission and sound regulations. According to the Powell Engine Company (Powell, 2006), these problems have been rectified in the NuStroke engine by using easily replaceable and cheaper parts for the engine, and the exhaust emission is controlled by using stratified charging for these engines.

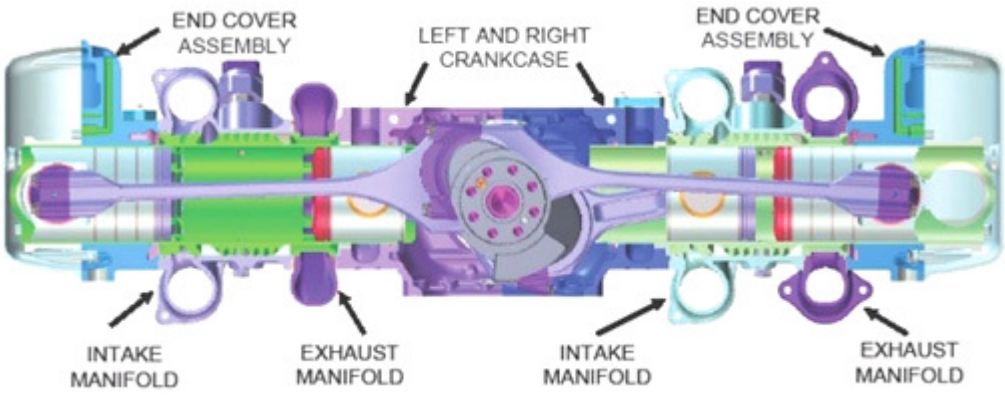

Figure 1.7: A revolutionary opposed piston engine configuration, developed by DARPA for the US defence industry ((TARDEC), 2009)

An efficient engine cooling system is vital in the case of Opposed Piston engines as a multi-cylinder engine configuration is too thickly packed, and this will limit the engine cooling efficiency. Another design challenge is to provide proper lubrication for the piston, crankshaft and piston rings. As the cylinders are either in transverse or vertical arrangement, crank-case lubrication as observed in wet crank-case engines is not possible for these kind of engines. Many innovative designs like providing lubrication through the piston holes are under consideration as observed in a new project by DARPA (Figure 1.7).

1. 4 Camplate engines

The main difference of cam-plate engine from the conventional engine is that this engine use cam-plate instead of a crankshaft for transferring reciprocating motion of piston to rotation of the output shaft. Therefore, the cam-plate engine has fewer moving parts. The dynamic stability and reduced friction loss characteristics of these engines are attractive features for engineers working towards crankless cam-plate engines.

Figure 1.8: 8 Cylinder Slipper Pad Crankless Engine (DFD, 1947)

A British-born Australian named Michell Anthony, in 1917, developed the first patented cam-plate engine design. Figure 1.8 shows an eight-cylinder crankless

engine, which has the geometry of an oblique slice of a solid cylinder mounted on a horizontal shaft. The engine cylinders are arranged circumferentially around the shaft inside the assembly. The Michell slippers help to maintain contact between the pistons and the slant (Walker, 1996).

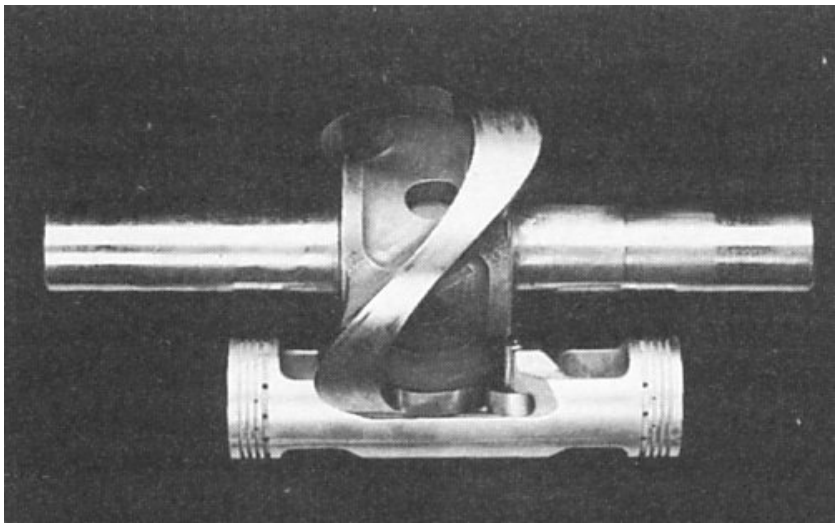

Figure 1.9: A Dyna-cam configuration to which pistons are connected. The thickness of cam-plate varies, appears thinner when it is at a more oblique angle
(Newton and Steeds, 1927)

The Dyna-cam engine (Figure 1.9) is another kind of cam-plate engine, which uses a sinusoidal cam-plate for linking the connecting rods and output shaft. The cam-plate used in the Michell engine is simply a metal disc that is located at an angle in a rotating shaft. The plate wobbles with piston motion and the resulting motion is available on the output shaft. However, in the Axial Vector Engine (Figure 1.10) the cam-plate is of polynomial profile.

The axial vector engine (Figure 1.10) is another version of the Dyna-cam engine developed by the Nevis Engine Company. The engine is quite long, but has several sets of pistons co-axially arranged around the periphery of the cam-plate. The inherited cooling challenges with other similar arrangements are also seen in this engine. However, the engine is capable of delivering low piston velocities, constant acceleration and deceleration for the pistons (Nevis, 2009).

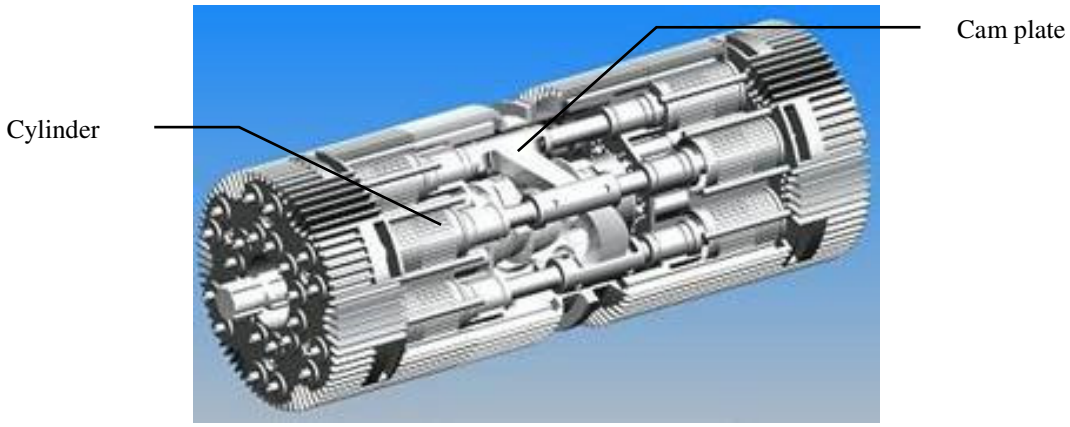

Figure 1.10: Axial Vector Engine (Nevis, 2009)

In Batoni's model of opposed-piston engine (Figure 1.11) the gas exchange process happens in two phases, scavenging and charging. The engine has two cylinders of different displacements. Both the cylinders have a series of intake ports, whereas the small cylinder has the normal exhaust ports sealed off. During operation, the large cylinder is first charged with air only, and following this the small cylinder is charged with a very rich mixture (air:fuel ratio ≈ 4:1). In the next stage the rich mixture is fed to the upper part of the main cylinder. During the compression stroke the rich mixture at the upper part is diluted by fresh air to make it a lean mixture (Heywood and Sher, 1999).

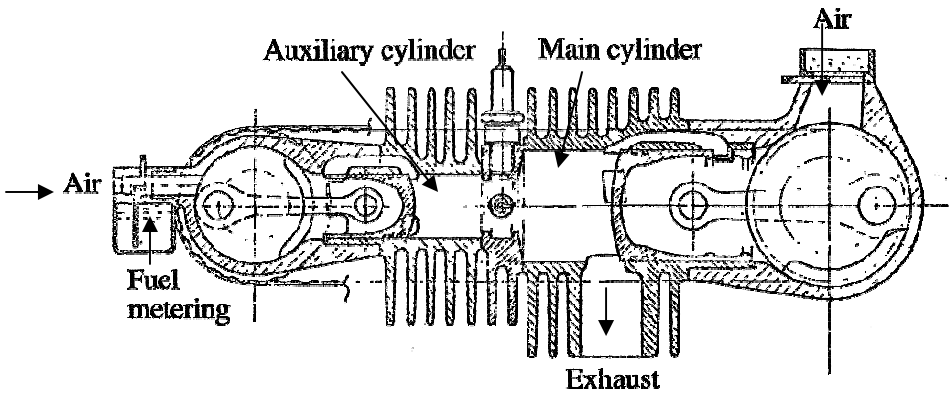

Figure 1.11: Batoni's engine, opposed piston stratified charge configuration (Heywood and Sher, 1999)

1. 5 NuStroke Engine

The NuStroke engine (Figure 1.12), also known as Powell engine, is developed by the Powell Engine Company in Australia. Brian Powell, the founder of the company, proposed the idea of the NuStroke Engine. The engine is an opposed piston polynomial cam-plate guided engine, with the designer having complete control over piston motion. The cam profile can be configured within safe operational limits based on the type of motion needed for the piston and the required duration of port opening (Powell, 2006).

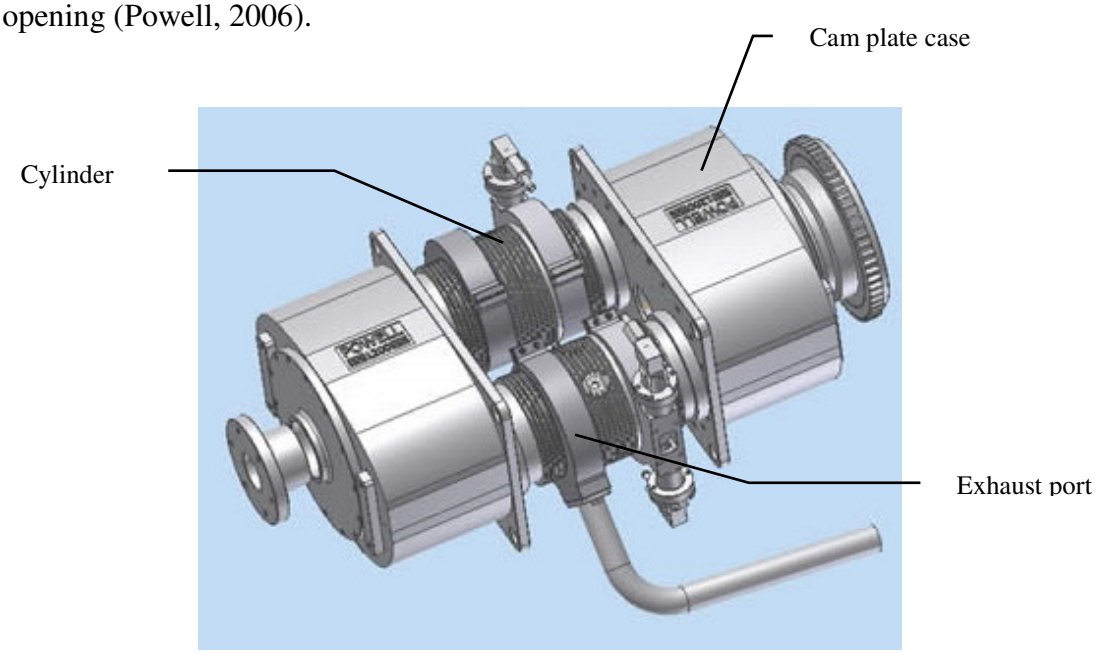

Figure 1.12: NuStroke engine (Powell, 2006)

The NuStroke engine is different from other Opposed Piston engines because of the highly configurable cam-plate used in this engine that enables variable compression ratio, controlled piston motion, and port functioning. The polynomial cam profile generated using a spreadsheet is shown in Figure (1.13).

A set of rollers connected to the end of the connecting rod help it to maintain contact with the upper and lower faces of the cam-plate in order to transmit motion from the piston to the output shaft. Since the upper roller takes most of the load in a cycle, the upper roller is bigger than the lower roller. The carefully designed cam-plate profile can control the acceleration, jerk, and high velocity overshoot of the rollers.

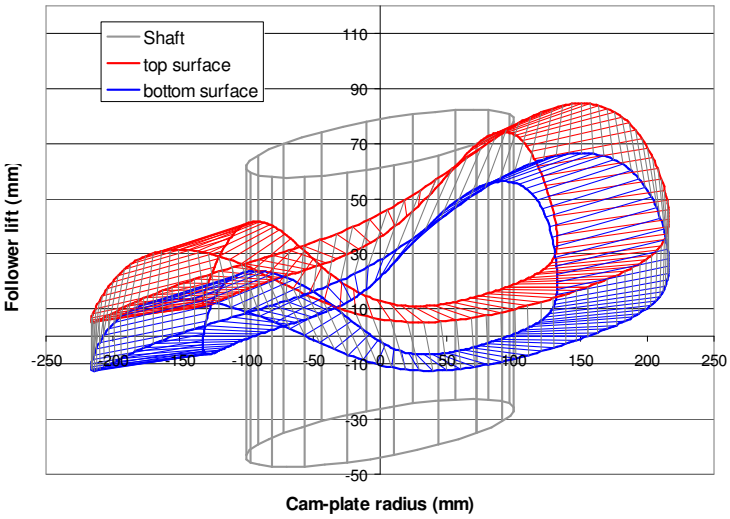

Figure 1.13: Polynomial cam profile generated in spreadsheet (Thomas, 2008)

The user can configure the number of lobes required in the cam-plate for the engine. A large number of lobes in a cam-plate make it possible to assemble several pistons on a single cam-plate, and to achieve more strokes during a rotation of the cam-plate. The rise and dwell as observed in the cam-plate corresponds to different strokes in the engine process cycle. Figure 1.14 shows an actual cam-plate produced for the NuStroke engine.

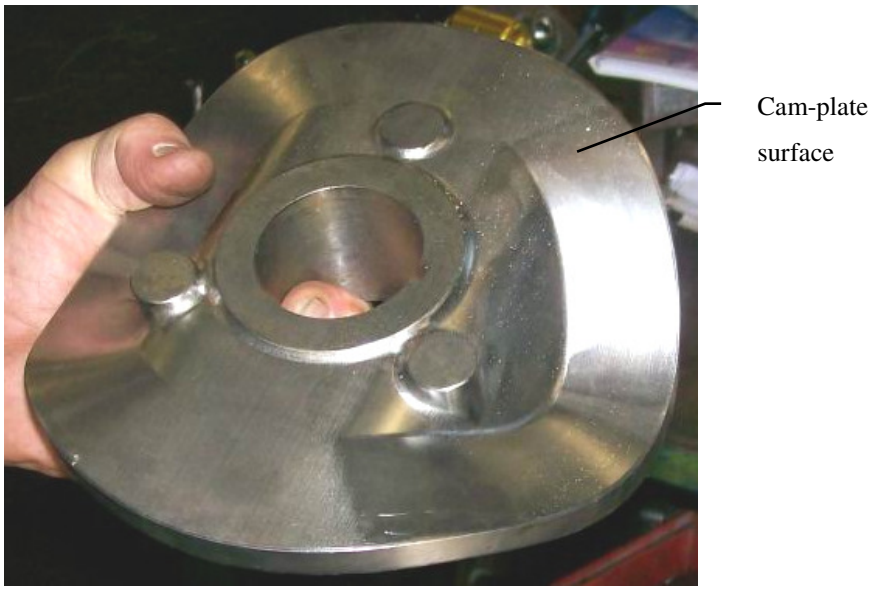

Figure 1.14: Photograph of the polynomial cam-plate (Powell, 2006)

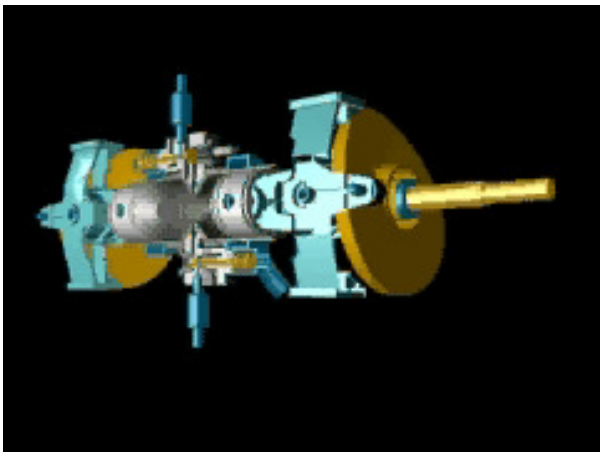

Figure 1.15: Cut-way diagram of the Nustroke engine (Powell, 2006)

Figure 1.15 shows the cut-way diagram of the Nustroke engine. The two opposedly moving pistons and cam plates assemble on the output shaft are shown in the picture.

Table 1.1: Nustroke engine operation parameters

Process	Commences	Finishes
Suction	136^{o}CA	180 ^{o}CA
Compression	0 ^{o}CA	85.5 ^{o}CA
Combustion	86 ^{o}CA	135.5 ^{o}CA

1. 6 Overview of the current thesis

The CFD process modelling and analysis of the Opposed Piston cam-plate engine is discussed in this thesis; and the CFD model is validated against the spreadsheet-generated analytical model.

Chapter 2 discusses the basic theory of IC engines. The chemistry of the combustion process and the effect of turbulence in combustion is discussed, specifically referring to combustion in gasoline engines where turbulence influence the combustion chemistry. Heat transfer analysis based on Woschni model is discussed for evaluating Heat Transfer Coefficient (HTC) in the engine.

Chapter 3 deals with spreadsheet-based analytical modelling of the engine, which was done at an earlier stage by the author (Thomas, 2008). Important empirical relations used in the analytical modelling are discussed. The modelling includes heat transfer and gas flow analysis during an IC engine process, and other features like modelling of the polynomial cam-plate.

Chapter 4 gives an overview of the CFD analysis of engines. This chapter presents the governing equations of CFD and turbulence modelling. Some theory on combined Eddy Dissipation Model/Finite Rate Chemistry (EDM/FRC) and Spark Ignition Model (SIM) for combustion modelling is discussed.

Chapter 5 discusses in detail the Opposed Piston engine modelling using ANSYS. The geometry modelling, mesh generation, grid deformation, mesh quality, and the boundary conditions applied for this engine model are also discussed here. The implementation of Domain Source Model (DSM) for simulating combustion, analysis of uniport and multiport configurations and sinusoidal and polynomial cam-plate guided piston motions are discussed here.

Chapter 6 is mainly intended to discuss the ongoing work on the CFD engine model to simulate combustion using SIM and EDM/FRC methods. The Burning Velocity Model (BVM) model is used for the first time to simulate combustion in Opposed Piston engines.

Chapter 7 gives results on the comparison of the Opposed Piston engine model based on different configurations of ports, and piston motions. Also, the results from the analytical model and CFD model are compared to draw conclusions.

Chapter 8 presents conclusions from the modelling and analysis performed on the engine models and the recommended future works on the CFD model. The major problems faced during CFD and analytical modelling are also discussed. Suggestions to perform experimental analysis of the engine to validate both the CFD and analytical models are mentioned here.

Chapter 2

BASIC THEORY OF ICE ANALYSIS

Combustion in internal combustion engines is one of the most difficult processes to model, because it includes many chemical reactions and physical factors that are hard to describe accurately and completely using empirical relations. Usually the parameters used to characterize engine performance are torque output, total power output and other factors like mass flow rate and volumetric efficiency. Another important factor essential for analysis is the heat transfer within and outside the process engine.

2. 1 Combustion in Internal Combustion Engine

The process of combustion in IC engines is a series of chemical reactions, initiated by kickers that depend on the type of engine, and the reactions result in release of high amount of energy both as heat and mass. The kicker is spark ignition in the case of a gasoline engine and higher compression in the case of a diesel engine. In the chemical reaction associated with combustion, a combination of oxygen with hydrogen and carbon which is present in the fuel, happens at elevated temperature and pressure (Judge, 1955).

The factors that are essential for combustion process in an IC engine are as follows:

1. There must exist a combustible mixture for burning,
2. There must be something to initiate the combustion process, and
3. The flame must propagate inside the combustion chamber (Mathur and Sharma, 2003).

In the case of gasoline engines, once combustion is initiated with the help of spark ignition, the spreading of the flame is completely controlled by turbulence, and the density and homogenity of air-fuel mixture in the surrounding volume. Ricardo

defines combustion as taking place in two different stages: (1) growth and development of a semipropagating nucleus of flame which is called as ignition lag or preparation phase, and (2) spreading of flame throughout the combustion chamber, Figure 2.1(a). Figure 2.1(b) shows the different stages of combustion in an SI engine. Point A shows the instant at which spark is introduced into the cylinder, point B shows the instant at which pressure starts to build up inside the cylinder, and point C shows the instant of peak pressure in the cylinder.

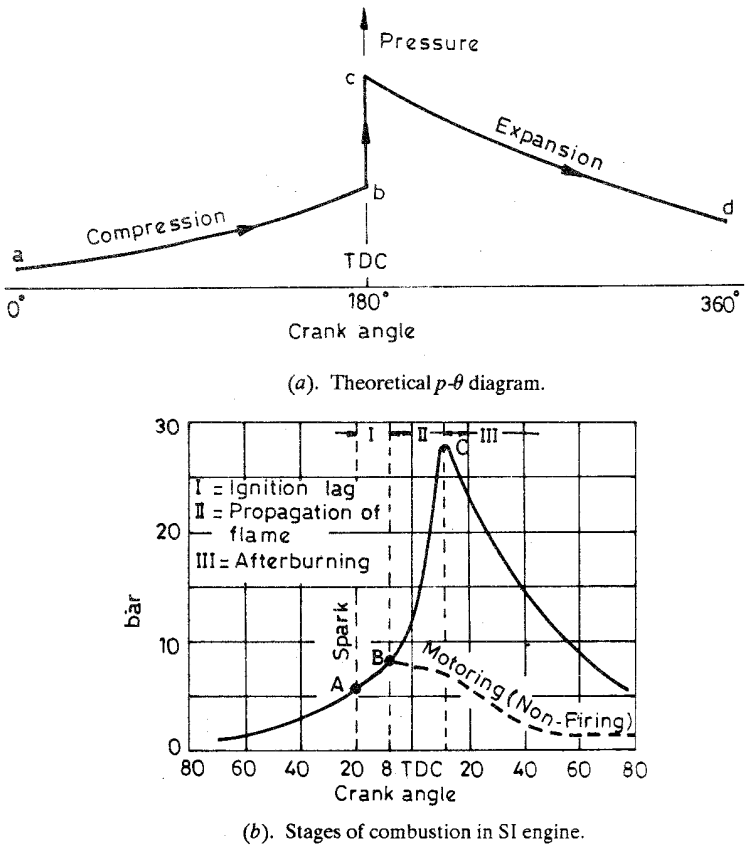

Figure 2.1: (a) Pressure Vs Crank angle diagram, (b) Stages of combustion (Mathur and Sharma, 2003)

2.1.1 Chemistry of SI engine Combustion

The combustion process is a series of chemical reactions in which oxidation of the hydrocarbon fuel happens at special conditions achieved inside the combustion chamber. To effectively represent the chemistry of combustion of an organic compound at elevated temperatures, several thousands of elementary reactions are

needed. A best possible way to assemble all these equations is to perform this function using computer softwares. Several papers on the use of computers to develop mechanisms of pyrolysis, combustion and oxidation are discussed in detail by researchers (Battin-Leclerc et al., 1999).

If a hydrocarbon fuel is represented by the chemical formula C_xH_y, the equation for combustion can be given as:

$$C_xH_y + \left(x + \frac{y}{4}\right)O_2 = xCO_2 + \frac{y}{2}H_2O \qquad (2.1)$$

The above equation means that one mole of C_xH_y reacts with $\left(x + \frac{y}{4}\right)$ moles of O_2 to produce x moles of CO_2 together with $\frac{y}{2}$ moles of water vapour (Judge, 1955).

2.1.2 Theory of spark ignition

Spark ignition is used as a triggering action in gasoline engines to initialize the combustion of fuel. It is needed to provide the necessary conditions to initiate combustion at the right time and location inside the cylinder. During the sparking process, an electric discharge occurs between the plug electrodes for some milliseconds of time with the release of a large amount of heat energy. It is assumed that the temperature of the dissociated and ionized gas reaches around 60,000 K. If the spark ignition is successful, a uniform combustion and flame propagation is expected inside the engine cylinder. The best way to achieve this is to use a continuous power source for sparking as suggested by Deshaies and Joulin (Weaving, 1990).

2. 2 Effect of Turbulence in Internal Combustion Engine

The flow inside a combustion chamber is highly turbulent in nature. The in-cylinder turbulence amplifies the flame speed during spark advance, agitates the heat transfer, and helps in the proper mixing of burnt and unburnt gas particles in the flame front. These help to increase the velocity of the turbulent flame. The turbulent flow entirely

depends on its environment, is highly unstable, and undergoes variations from cycle-to-cycle. In maintaining the overall turbulent nature of a flow, both large-scale and small-scale turbulent motions are of great significance (Heywood, 1988).

The parameters normally used for describing turbulent flows are the mean velocity, fluctuating velocity about the mean, and several length and time scales. Even though the cycle itself repeats every time in the same fashion, the flow characteristics need not to do the same. In order to analyze quasi-periodic flows, it is suggested to perform either ensemble-averaging or phase-averaging (Veynante and Vervisch, 2001).

At any specific crank-angle θ, the instantaneous velocity in the i^{th} cycle of an engine operation is,

$$U(\theta,i) = \overline{U}(\theta,i) + u(\theta,i) \tag{2.2}$$

The $\overline{U}(\theta)$, which is ensemble-averaged or phase-averaged velocity, is defined as the average value at any specific crank-angle. Figure 2.2 shows this technique applied to a two-stroke cycle engine. The ensemble-averaged (EA) velocity is,

$$\overline{U}_{EA}(\theta) = \frac{1}{N_c}\sum_{i=1}^{N_c} U(\theta,i) \tag{2.3}$$

where

N_c = number of cycles for which data are averaged

The difference between mean velocity in a particular cycle and the ensemble-averaged mean velocity over many cycles is the cycle-by-cycle variation in mean velocity;

$$\hat{U}(\theta,i) = \overline{U}(\theta,i) - \overline{U}_{EA}(\theta) \tag{2.4}$$

Therefore, the instantaneous velocity shown by the earlier equation is divided into three components,

$$U(\theta,i) = \overline{U}_{EA}(\theta) + \hat{U}(\theta,i) + u(\theta,i) \tag{2.5}$$

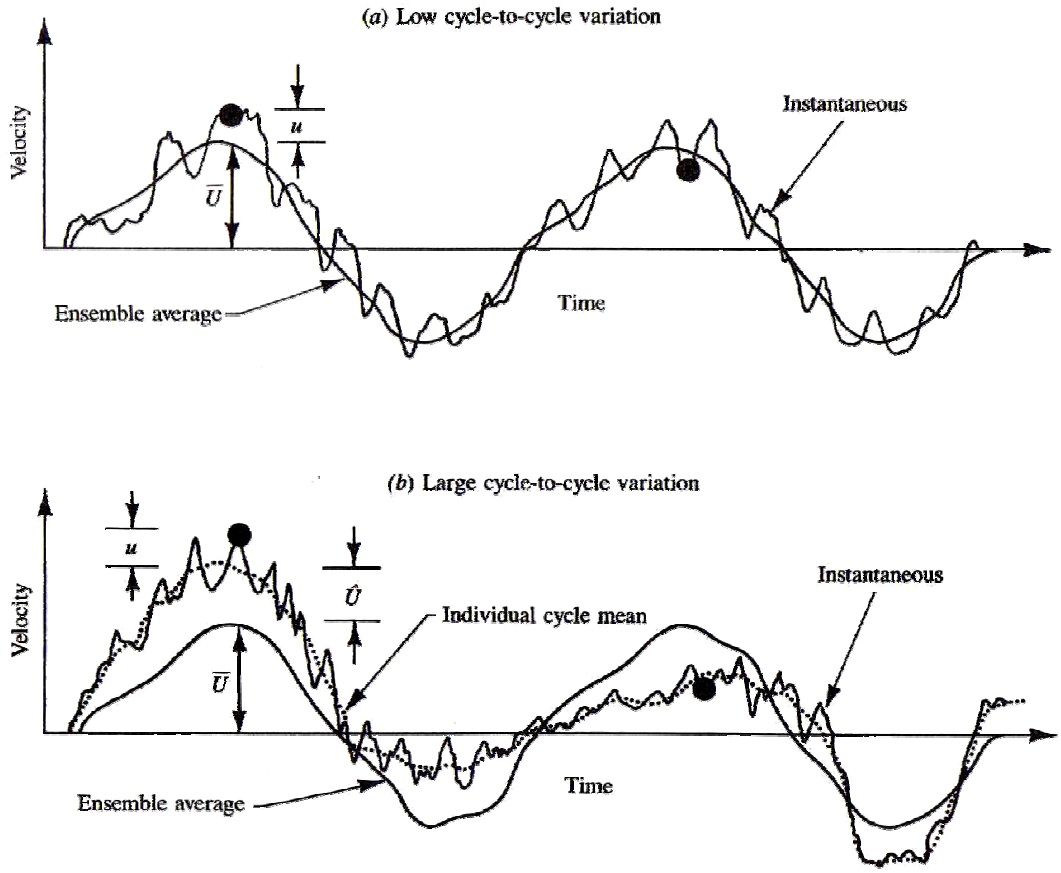

Figure 2.2: Figure shows the variation of velocity with crank angle at a fixed point in the cylinder during two consecutive cycles of an engine. Dotted line shows instantaneous velocity. Solid smooth line shows ensemble / phase-averaged velocity (Heywood, 1988).

Figure 2.2 (a) shows small cycle-to-cycle variations, and Figure 2.2 (b) shows large cycle-to-cycle variation. The turbulent fluctuation 'u' is defined with respect to the mean of individual cycle (Heywood, 1988). The nature of this turbulent velocity fluctuation depends on whether the cycle-to-cycle variations are small or large scale.

Figure 2.3 shows the effect of turbulence on flame propagation with the help of photographs taken using high-speed Schlieren movie in an SI engine at 1400 rpm and 0.5 atm inlet pressure. The flame development and advancing are important during the early stages where rise in pressure due to combustion is negligible. The steady growth of spark flame to a ball shaped flame is illustrated in Figure 2.3.

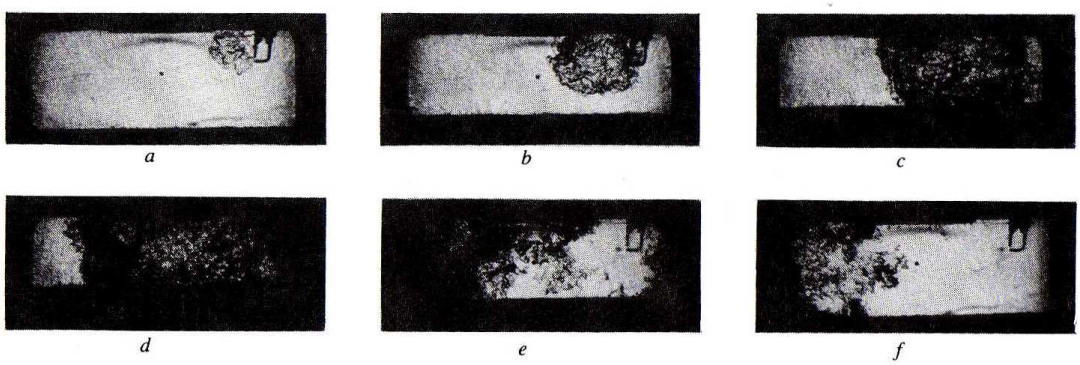

Figure 2.3: The sequence of photographs taken during one engine cycle in a square cross section cylinder (Heywood, 1988)

The convoluted flame surface visible in Figure 2.3 (a) itself shows the effect of turbulence. The volume ignited by the advancing flame front that expands in a spherical fashion, while some of them later hit the cylinder surface as shown in Figures 2.3 (b & c). The maximum cylinder pressure is expected to occur at the time when the flame touches the far end wall (Figure 2.4) in the square cross section cylinder as shown in Figure 2.3 (e). Towards the end of the cycle, the unburned mixture inside the cylinder will completely burn out and the density gradients in the flame reaction zone completely disappear, and this is shown in Figure 2.4.

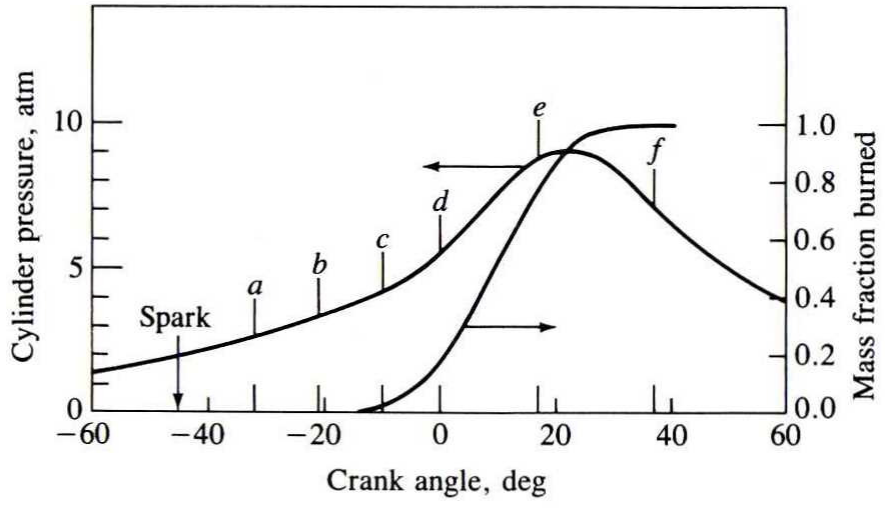

Figure 2.4: The pressure and mass fraction burned are shown in the graph (Heywood, 1988)

Turbulence occurs due to instabilities in the flow that results from the interaction of viscous and inertia forces that are significantly nonlinear in nature. The turbulent field contains regions of vorticity where vortex stretching happens in order to maintain or increase the magnitude of vorticity. The vortex stretching process is important for the turbulence to sustain for prolonged time, which otherwise will die out rapidly. This explains the dissipative nature of turbulent flows (Weaving, 1990).

A turbulence model can predict the heat release rate approximately. The reaction progress value 'c' describes the turbulent flame for laminar flame analysis. In case of premixed combustion, the value of reaction progress will be $c = 0$ for fresh gas and $c = 1$ for a completely burnt gas. The position of the flame varies with the value of c from zero to one. The chemical reaction is strongly influenced by turbulence (Veynante and Vervisch, 2001).

2.2.1 Premixed turbulent combustion

In SI engines fuel is mixed with air at the intake manifold, and this air-fuel mixture is then fed into the cylinder. There the mixture is compressed to form a homogeneous charge for combustion. At this point, when the piston reaches TDC the mixture is ignited by the spark, followed by generation of a laminar flame kernel. This kernel then changes to a turbulent kernel, which later grows out to become turbulent flame. This turbulent flame, because of the low mean velocity inside the cylinder, grows spherically as it hits the combustion chamber walls. Figure 2.5 shows Schlieren photographs of flame propogation inside a disc-shaped combustion chamber for a 1.6L transparent piston engine at 2000 rpm.

In Figure 2.5, the larger of the lower arcs shows the inlet valve, and the smaller one is the exhaust valve. The dark semicircle visible in the photographs shows the spark plug. For this engine operation ignition is started at 40^{o}CA before TDC. The flame kernel is grows more at around 22^{o}CA before TDC. Large turbulent structures are visible at around 14^{o}CA before TDC. By around 4^{o}CA before TDC the burnt gas region is visible as shown by the dark region behind the flame front. As the piston reaches TDC the flame is observed to have propagated across a majority of the visible part of combustion chamber (Peters, 2000).

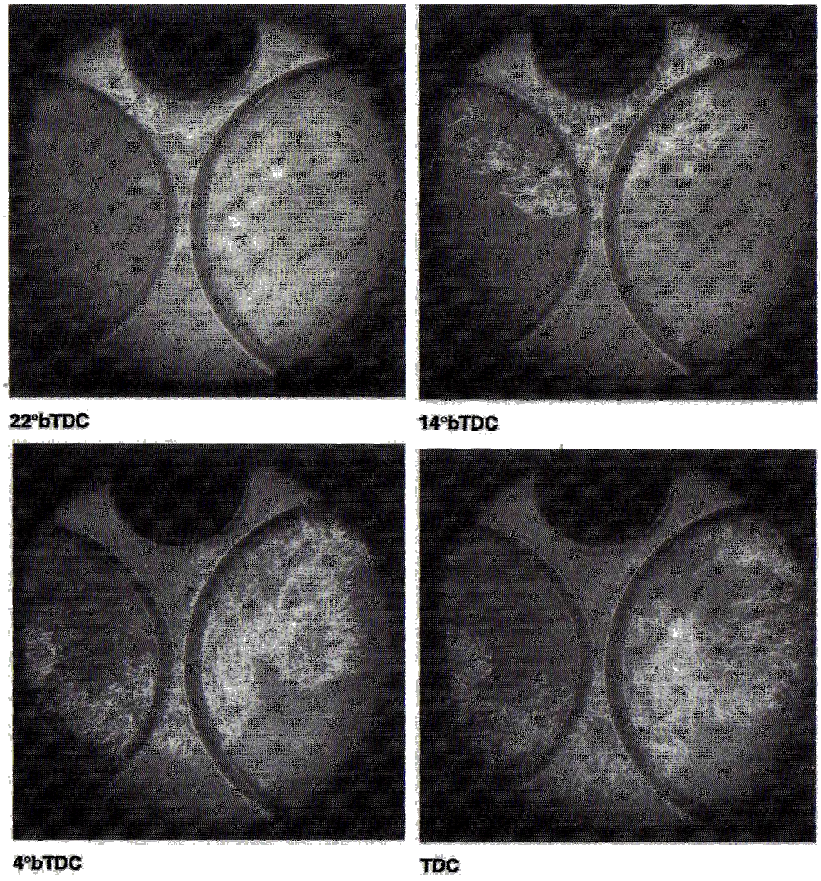

Figure 2.5: The sequence of photographs showing turbulent flame propagation as observed through a transparent piston. The large semicircles show the edges of valves (Peters, 2000).

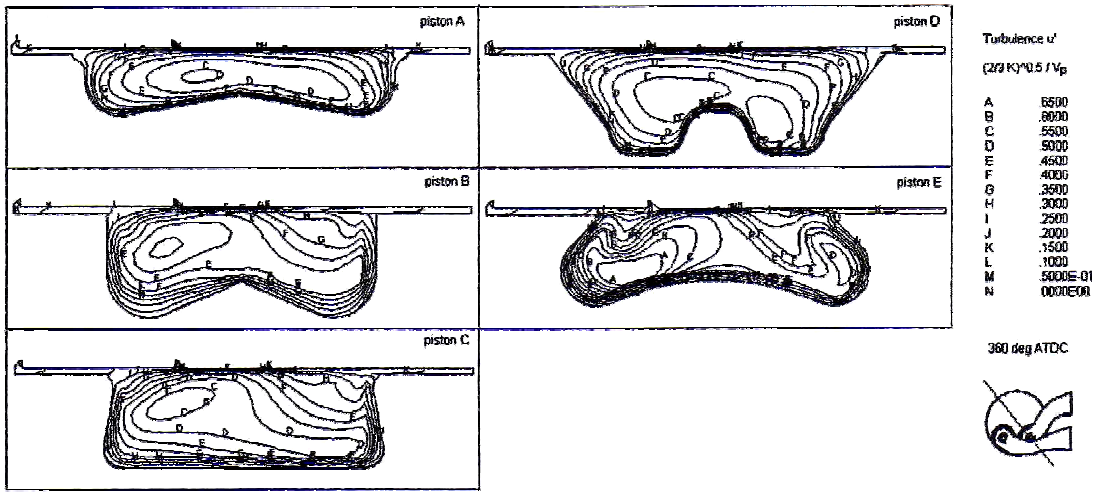

Figure 2.6: The non-dimensional turbulent velocity fields generated for five different kinds of pistons at TDC position (Payri et al., 2003)

Figure 2.6 shows the turbulent intensity contours inside the cylinder at TDC position for different types of piston at same crank angle. The dependence of turbulence on piston shape is clearly visible from the figures. Pistons A, B and C show similar velocity fields, and the fields are almost homogeneous throughout the engine cylinder. However, for the re-entrant chamber of piston E, the intensity fields are not homogeneous as observed for other piston types (Payri et al., 2003).

2.2.2 Turbulence and chemistry relations

Turbulence in the reaction zone, in both the premixed and non-premixed flames, has a significant effect on the functionality of combustion models. The turbulence field is influenced by the mass fraction of species, and also by the critical species (Barlow and Frank, 1998). The temperature fluctuations can effectively increase the rate of reactions, which means that the chemical source term can increase or decrease the turbulent fluctuations. Both the RANS approach and LES approach of turbulent flow simulations need the proper modelling of turbulence-chemistry interactions (Pope, 2000). In effect, the in-cylinder turbulence can singificantly affect the transport of momentum, heat, and species. In LES models these are represented with the help of resolved fields.

In the case of a single-step irreversible combustion process the reaction progress 'c' can be expressed in terms of temperature as (Veynante and Vervisch, 2001),

$$c = \frac{T - T_u}{T_b - T_u} \tag{2.6}$$

In the case of turbulent premixed flames, the ratio of laminar flame thickness δ_l and the flame propogation speed S_L gives the chemical time scale τ_c. The burn rate is defined in terms of the turbulent mixing of gases inside the cylinder. A large Damkohler number $\left(Da = \tau_t / \tau_c\right)$, the ratio of the turbulent characteristic time τ_t and chemical characteristic time τ_c, means that the rate of reaction is controlled by the turbulent mixing which is defined in terms of scalar dissipation rates (Bray, 1996).

2. 3 Heat Transfer in Internal Combustion Engine

The heat transfer process in IC engines needs to be adequately described for the conceptual and detailed design of engine. It can affect the engine performance, efficiency, emissions and the engine life. Heat transfer imposes high level of thermal loading on different engine components, and so the engine should have a good cooling system. The heat transfer between the unburnt fuel mass inside the engine and the cylinder wall can cause knocking in engines. The heat transfer can cause the gas to generate pollutants from engine due to after-burning of CO and HC within the engine and in the exhaust system (Heywood, 1988).

Uncontrolled heating of the engine can cause expansion of the piston and piston rings, which will increase frictional losses. The viscosity of cooling and lubricating oils used in the engine, and the cooling system pump requirements are influenced by the heat transfer. However, the use of computer technologies for designing and simulating engines help to foresee the design requirements prior to their actual production.

2.3.1 Modes of heat transfer

Heat transfer in an IC engine happens due to three modes of heat flow: conduction, convetion and radiation. Figure 2.7 shows the energy flow in an IC engine with reference to all these three modes of heat transfer.

Conduction

In conduction, the heat flows due to molecular vibrations. This mode accounts for majority of heat transfer from the engine. The heat will flow through fluids at rest, oil and carbon particles, and through cylinder walls, pistons etc. The one-dimensional conduction heat flux is given by Fourier's law:

For a steady one-dimensional heat flow (Heywood, 1988):

$$\dot{q} = \frac{\dot{Q}}{A} = -k \frac{dT}{dx} \tag{2.7}$$

Convection

Convection heat transfer occurs in moving media, and at a fluid-solid interface.. Significant amount of heat is transferred between fluid and solid surfaces, cylinder head, cylinder walls, and pistons during an engine cycle. Convection in the inlet system can be used to increase the temperature of intake charge.

The heat transfer due to convection is given by the equation:

$$\dot{q} = h_c \left(T - T_w \right) \tag{2.8}$$

Radiation

In radiation heat transfer, the heat flows through emission and absorption of electromagnetic waves. Here, the heat flow happens from high temperature combustion gases and flame region to the cylinder walls and further to the environment (Heywood, 1988). The emissivity of flame will vary both in intensity and in wavelength distribution, and this depends on the time, air-fuel ratio, fuel consumption and the amount of detonation present. The radiation accounts for nearly 5% of the total heat transfer from the engine (Taylor and Taylor, 1950).

The radiant heat flux from a body can be given by the relation:

$$\dot{q} = \sigma \left(T_1^{\,4} - T_2^{\,4} \right) \tag{2.9}$$

2.3.2 Heat transfer pattern in an IC engine

Figure 2.8 shows the heat release diagram showing different phases of heat transfer during an engine cycle. The vapourized fuel collected during the ignition delay period is burned abruptly at the end of the delay period. The resulting pressure rise is not too high, because the chemical kinetics control combustion here. The air-fuel

ratio and oxygen availability controls the combustion phenomenon. The second peak observed is due to the effect of air entering the system. The remaining heat transfer is controlled by the diffusivity and turbulent mixing that controls the rate of combustion (Mathur and Sharma, 2003).

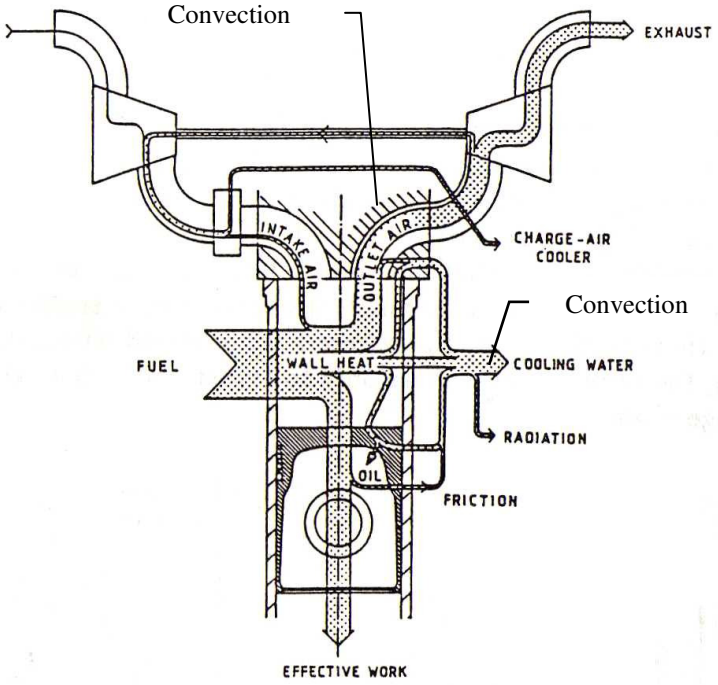

Figure 2.7: The energy flow indicated in a turbocharged engine with air-charge cooling is shown (Spalding and Afgan, 1989)

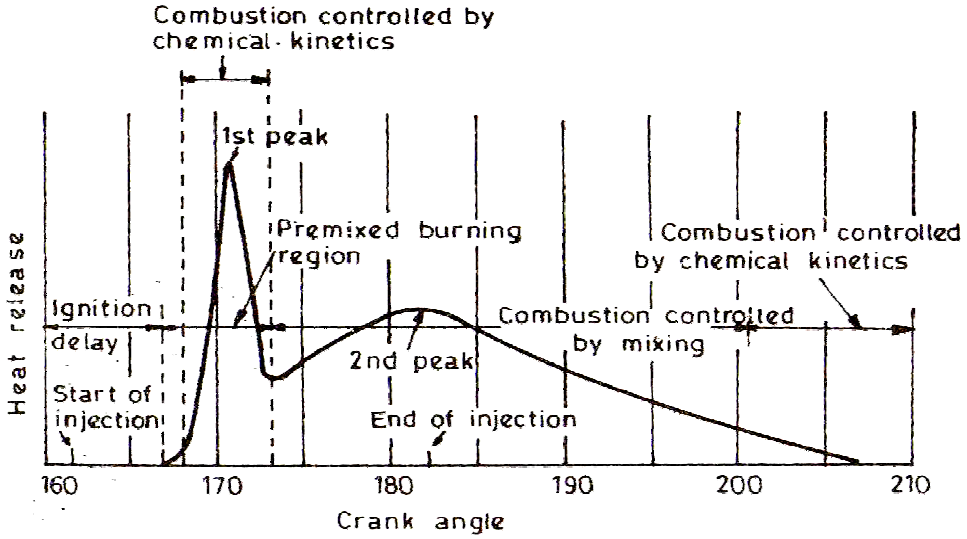

Figure 2.8: The different phases of heat release during a cycle of operation (Mathur and Sharma, 2003)

The process of heat release can affect the pressure rise rate that may give rise to noise and vibrations inside the engine. Heat release rate can affect the cycle efficiency, as during the initial part of combustion the heat release rate is considerably higher, but later it drops to a very low value. Figure 2.9 shows the heat release in an SI engine, together with the pressure data and mass fraction of mixture burned, plotted against crank angle.

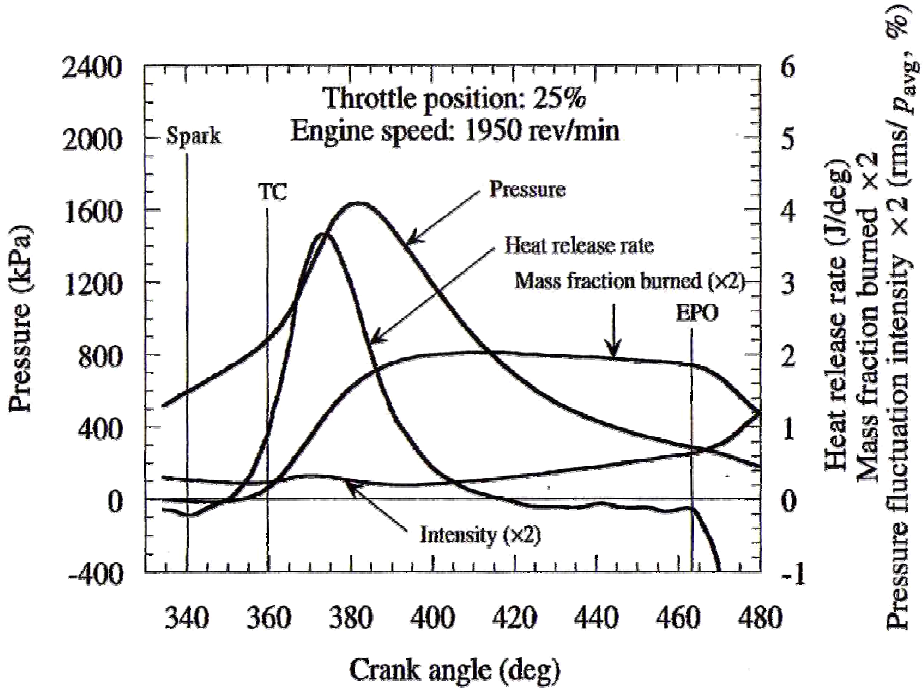

Figure 2.9: Heat release rate, mass fraction burned and pressure variation during a cycle of operations for a crankcase-scavenged two-stroke SI engine is plotted as a function of crank angle (Heywood and Sher, 1999)

Wendy et.al (Kurniawan et al., 2007) performed an analysis of a CNG-DI engine using multidimensional CFD to predict the heat release rate. The heat release rate is recorded directly from the reacted species. This method of analysis can be used to estimate the combustion duration and hence to optimize the work output. Figure 2.10 shows the heat release rate for this engine. The maximum heat transfer is observed to be around 118.11 J/degree, which then drops to a value of 4.203 J/degree at the beginning of exhaust stroke. This is also influenced by the engine speed, as a higher piston speed will cause faster heat transfer to the cylinder walls (Kurniawan et al., 2007).

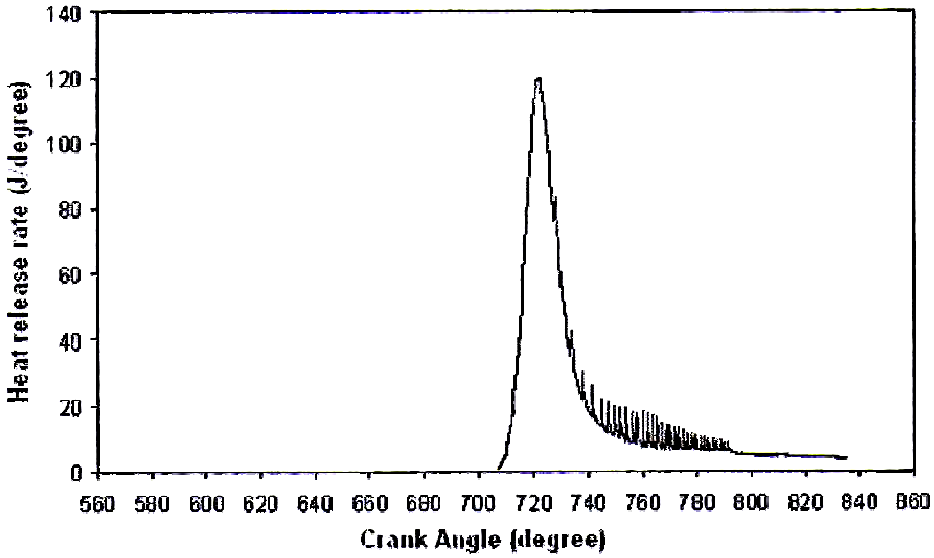

Figure 2.10: The heat release rate as a function of crank angle is plotted for CNG-DI engine (Kurniawan et al., 2007)

Chapter 3

ANALYTICAL PROCESS MODELLING

The spreadsheet-generated analytical model is a very important part of this thesis. The fluid dynamics and thermodynamics equations used for analysis in this model are discussed in this chapter. In addition, the chapter also discusses some of the major results including the pressure, temperature, and mass flow rate diagrams.

3. 1 Description of the spreadsheet

The analytical model is versatile in all respects in that it can be used for predicting the performance of almost all Opposed Piston engine configurations. The results produced as graphs provide an easy visualization of the engine performance. The analytical model developed in spreadsheet form contains a set of worksheets for different aspects of the process modelling. Among them, one of the main sheets is the one devoted to the modelling of polynomial cam-plate profile using mathematical expressions.

Figure 3.1 is a screenshot of the main worksheet. The major parameters used in modelling are shown. The engine configuration sheet includes information on the number of pistons, number of cylinders, compression ratio, air-fuel ratio, fuel energy etc. In the main sheet, prediction of thermodynamic properties and mass flow characteristics through the ports are carried out. This includes evaluation of thermal and gas flow characteristics, together with the velocity and mass flow rate predictions.

Another important section in the main sheet is the heat transfer analysis using various HTC models. During the analytical model analysis, it was observed that the Woschni model for evaluating HTC is more suitable in the current context. Therefore, this HTC model is used as the default choice in the analytical engine model. Other

models for finding the HTC included in the spreadsheet are the Annand model, Nusselt model, Eichelberg model, a constant HTC etc (Finol and Robinson, 2005).

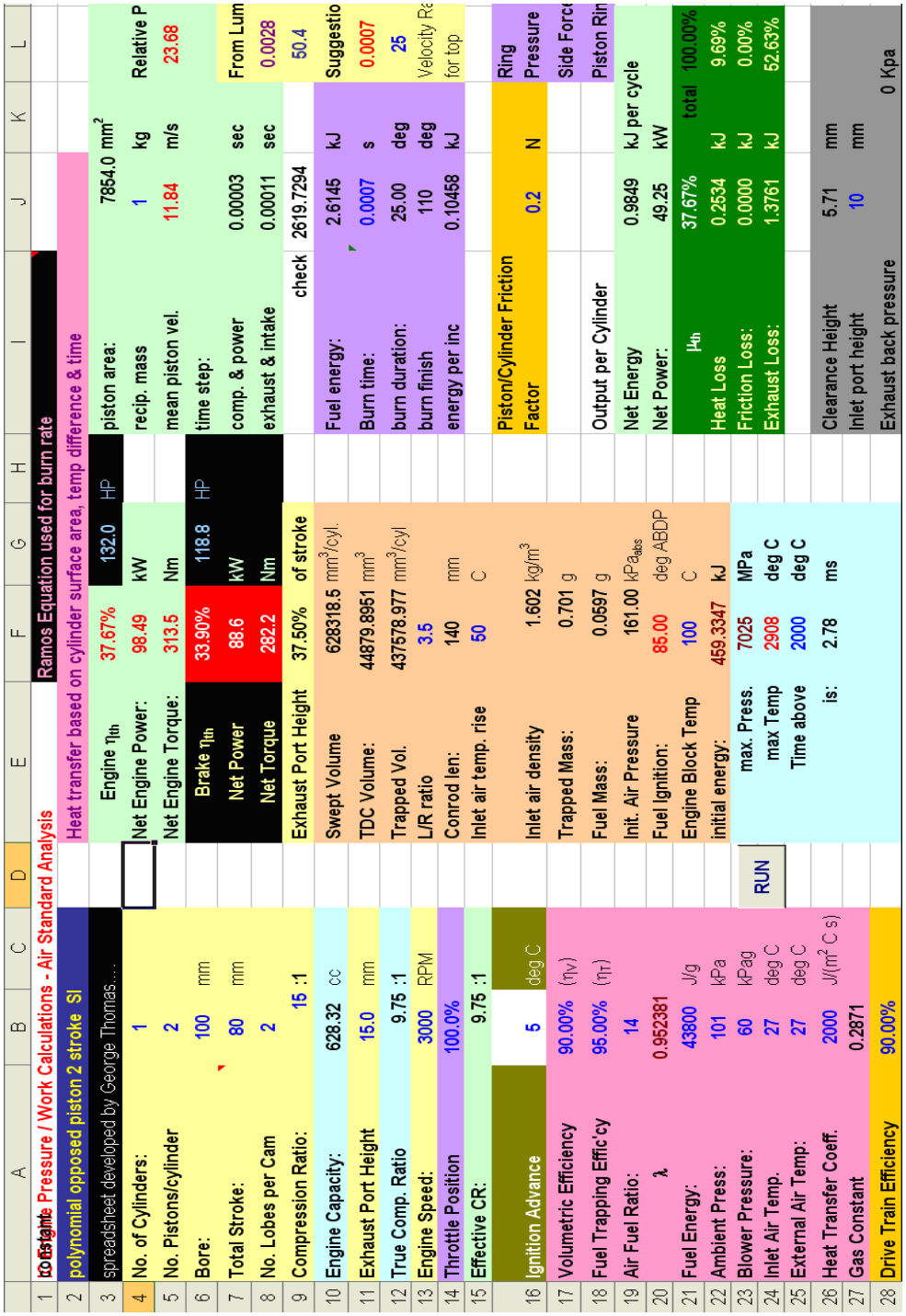

Figure 3.1: Spreadsheet process model (screenshot of main sheet in the file) developed for cam-plate engine (Thomas, 2008)

Similarly, the Demtchenko (Benson, 1960) method is used as default choice for predicting discharge coefficient (C_d). Other options available for evaluating C_d in analytical model are the Busemann model, Witchenko model, Nusselt model etc (Finol and Robinson, 2005). Since the C_d value is a function of valve / port opening area, a constant value of C_d is not a suggested option.

The design of polynomial profile cam-plate using analytical method is a complicated work. The cam-plate design considers all the relevant cam-follower motion characteristics as shown in Figure 3.2. Explanation of mathematics behind the generation of cam-plate profile and related motion characteristics are beyond the requirements of current thesis, as the analytical model is used here only for comparing results from the numerical model.

Moreover, rather than the mathematics behind generation of the cam-plate profile, importance should be given to the advantages offered by polynomial profile cam-plate over a conventional crankshaft assembly or a sinusoidal profile cam-plate. Chapter 5 in the thesis discusses the comparison of these features in detail. A larger dwell time during the exhaust stroke to aid complete removal of the burnt gas, and a slower motion of the piston during expansion stroke to harness the maximum output from the engine, are easily achievable with the polynomial profile cam-plate.

Figure 3.3 shows outline of the polynomial cam profile. The image on the left shows the cam-plate assembled in the camshaft, which is the engine output shaft. The image on the right shows the top view of the cam plate and roller assembly. The axis of the profile corresponds to the dimensions of the cam-plate assembly. The connecting rods from the reciprocating pistons are connected to the cam-plate using rollers attached to the connecting rod. Two similar cam-plates are assembled on either side of the engine to transfer motion from both the pistons to the output shaft.

3. 2 Vital in-cylinder conditions

For the successful prediction of engine characteristics like turbulence, heart transfer etc., several parameters need to be defined, initialised and used. In the analytical model, data like the initial pressure, temperature, mass flow etc are assumed initially.

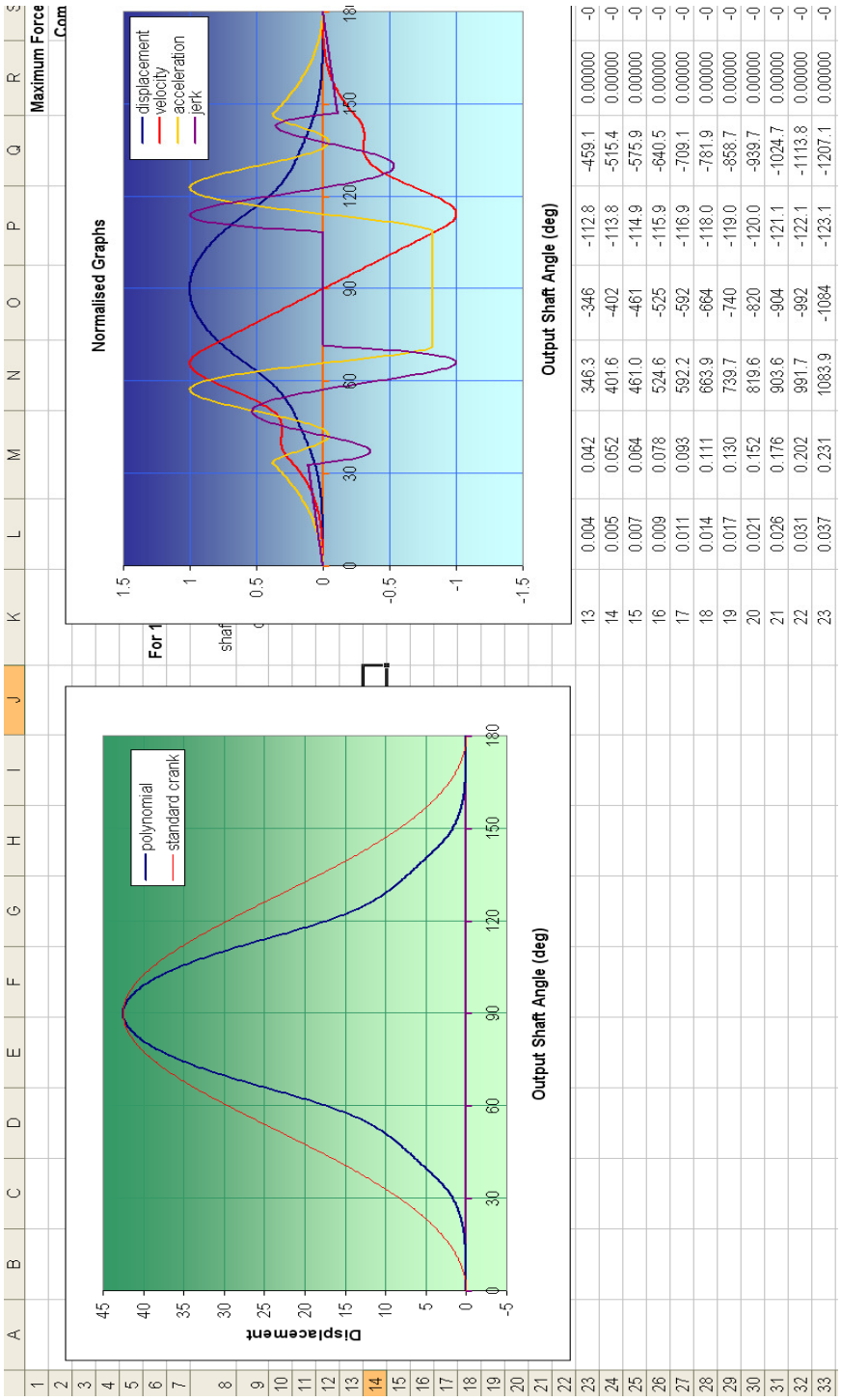

Figure 3.2: Spreadsheet model showing comparison of polynomial cam profile generated piston motion and sinusoidal profile based piston motion, and the follower motion characteristics for the design with respect to crank angle (Thomas, 2008).

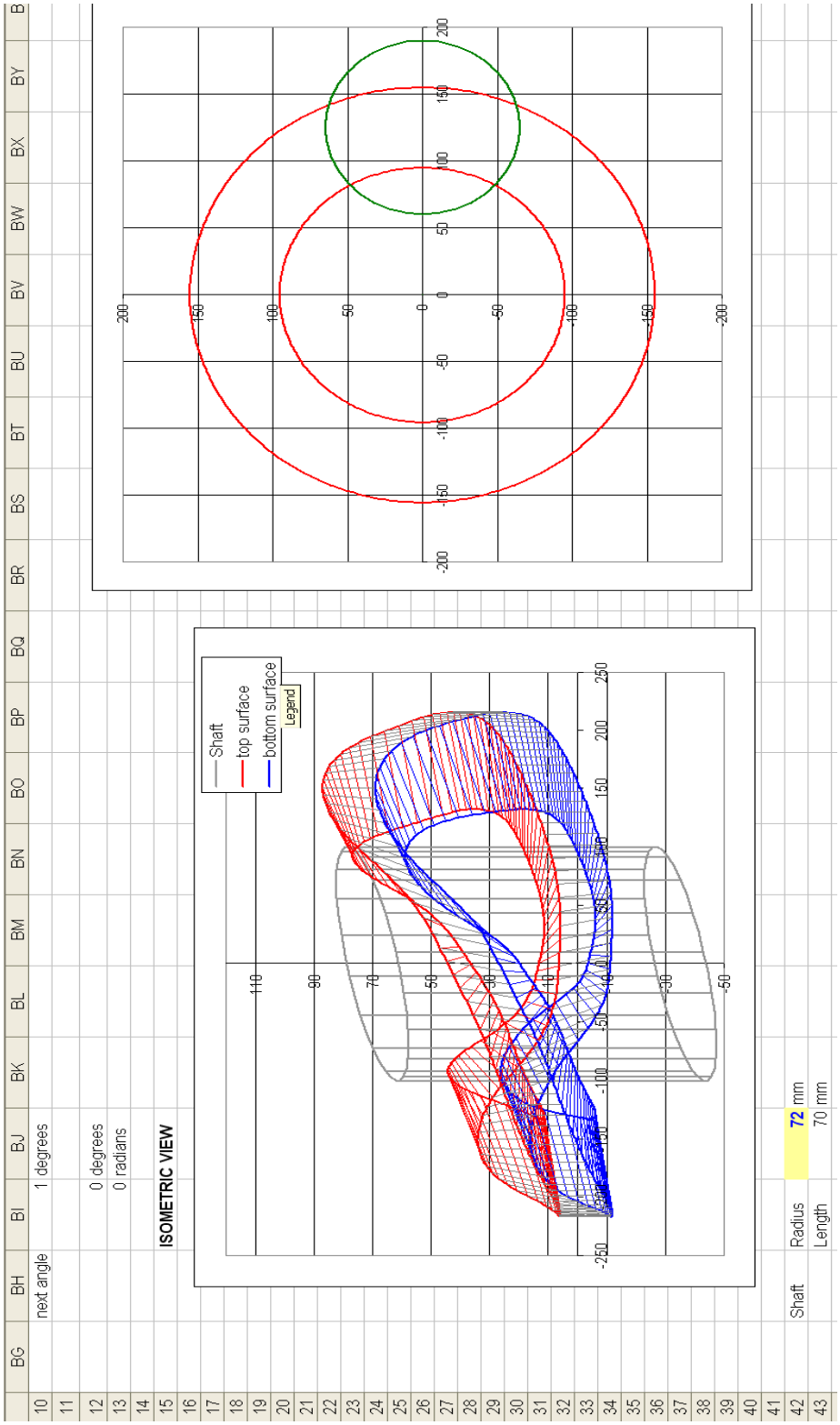

Figure 3.3: The polynomial cam profile as assembled on the rotating shaft, developed in spreadsheet (Thomas, 2008).

Later, the analytical engine model is run for four cycles using macros to predict the engine parameters accurately. Though the same can be done also with CFD model, it is not done here due to the high computation costs it will incur.

Fuel burn rate:

The fuel burn rate is obtained using Ramos equation (Ramos, 1989).

$$m_h = \frac{\left[1-\cos\left((\theta-\theta_s)\times \pi/\theta_d\right)\right]}{2} \times \text{Fuel heating value} \qquad (3.1)$$

In-cylinder gas pressure

The instantaneous in-cylinder pressure is evaluated using the Redlich-Kwong relation. This equation is one of the most acceptable for evaluating the state of a real gas, and the major attraction of the equation is its simplicity. The equation can be represented as (Nag, 1995):

$$p = \left[\frac{R\,T}{V_m - b}\right] - \left[\frac{a}{T^{1/2}\,V_m\,(V_m+b)}\right] \qquad (3.2)$$

where

$$a = \frac{0.42748\,R^2\,T_c^{2.5}}{p_c}$$

$$b = \frac{0.08662\,R\,T_c}{p_c}$$

where, p_c = 37700 kPa, and T_c = 133 K, are the critical pressure and temperature.

Instantaneous volume:

The P-V plot is drawn with instantaneous volume on the x-axis and pressure on y-axis. The instantaneous volume is found by using the following relation:

$$V = \text{total volume} - (\text{piston displacement} \times \text{piston area}) \tag{3.3}$$

where

$$\text{total volume} = \text{trapped volume} + \text{swept volume}$$

$$\text{piston displacement} = R_L\,(1 - \cos(\theta)\,) - L_L\,(1 - \cos(\phi)\,)$$

$$\text{piston area} = \frac{\pi D^2}{4}$$

Heat transfer:

Heat transfer through the engine block is obtained by using the following relation (Heywood, 1988):

$$\dot{q} = HTC \times A_{surface} \times \Delta T \tag{3.4}$$

where

$$\Delta T = (\text{gas temperature} - \text{engine block temperature})K$$

Throat pressure:

Pressure of the charge flowing through a port is given by the following expressions:

For choked flow, where $\frac{P_a}{p} \leq p_c$

$$P_f = (P_b + P_a) \times p_c \tag{3.5}$$

where

$$p_c = \frac{2}{\gamma + 1}^{\gamma/\gamma - 1}$$

For non-choked flow:

$$P_f = p$$

Throat temperature:

The following relations for different flow conditions obtain throat temperature. For choking flow, the value of pressure can be given as:

$$T_{throat} = T_{cylinder} \times T_{sonic\ ratio} \tag{3.6}$$

where

$$T_{sonic\ ratio} = \frac{2}{\gamma + 1}$$

For non-choking flow, temperature can be given as:

$$T_{throat} = T_{cylinder}\, e^{\frac{R}{C_p} \ln \frac{P_{throat}}{P_{cylinder}}} \tag{3.7}$$

Throat velocity:

Velocity of flow of gas at throat can be given as:

For choking flow:

$$V_{throat} = \sqrt{\gamma\, R\, T_{throat}} \tag{3.8}$$

For non-choking flow:

$$V_{throat} = \sqrt{2\ \Delta h} \tag{3.9}$$

where

$$\Delta h = C_p \left(T_{cylinder} - T_{throat} \right)$$

Volume flow rate:

The following relation can obtain volume flow rate:

$$\dot{v} = V_{throat} \times A_{throat} \tag{3.10}$$

where

$$A_{throat} = \pi D_{valve} L_{valve}$$

Pressure Work:

Pressure work output from the IC engine is represented by the equation:

$$W = (P_a - p) \times A_{surface} \tag{3.11}$$

3. 3 Heat transfer model

In the case of reciprocating engines, heat transfer is highly nonuniform and unsteady as the heat flux between fluids and solid surfaces changes considerably during an engine cycle as a function of both space and time. The heat flux fluctuates considerably over the combustion and intake processes. Different models are used to predict the heat flux arising from combustion. Based on the heat flux predicted and the purpose of calculation, different correlations are used to find the time-averaged heat flux, the spatially averaged heat flux, and instantaneous local heat flux.

The total heat released by gases can be evaluated by time-averaged heat flux, and this is used to obtain engine heat balance (Taylor, 1985). The instantaneuos heat flux coefficients are used to predict the power output, efficiency, and emissions from the engine, which needs temporal variation in heat flux. The heat flux is generally used to predict chances of pollutant generation and emission, and also for predicting in-cylinder wall temperatures. A successful prediction of temperature distribution in the engine body will help to improve engine design considering the bore distortion that will result in less frictional losses and blow-by and reduced specific fuel consumption and increased durability.

Woschni model

The heat transfer in IC engines is due to forced convection. The basis of the Woschni equation is forced convection and turbulent flow (Incorpera and DeWitt, 1990), while the other early-developed models for evaluating HTC like Annand, Nusselt etc. wrongly assumed free convection heat transfer. The Woschni equation is widely used by researchers due to its stability and ability to predict the results with appreciable accuracy (Finol and Robinson, 2005) (Mohammadi et al., 2007) (Borman and Nishiwaki, 1987).

For evaluating the Reynolds number in the above expression, the characteristic length considered is the bore of the cylinder, and the velocity is the in-cylinder gas velocity. With P_r and T_r showing the available properties of the working fluid corresponding to the instantaneous cylinder volume V_r, the HTC proposed by Woschni is (Woschni, 1967):

$$h_c = 127.9\, B^{0.2}\, p^{0.8}\, T_g^{-0.53} \left(C_1\, V_p + C_2 \left(\frac{V_s\, T_r}{P_r\, V_r} \right) (p - p_m) \right)^{0.8} \qquad (3.12)$$

The values of C_1 and C_2 in the above expression are shown in Table (3.1)

Table 3.1: Values of C_1 and C_2 (Thomas, 2008)

Process	**C_1**	**C_2**
Intake & Exhaust	6.18	0
Compression	2.28	0
Combustion & Expansion	2.28	3.24×10^{-3}

The pressure gradient between motoring and combustion helps to find the value of C_2 in the above equation. In effect, the constant C_2 imparts the effect of combustion on the velocity of gas. For simplicity, it is assumed that radiation effect on the gas energy is also taken into consideration by the additional term used for combustion (Finol and Robinson, 2005).

In the case of high-speed engines with swirl, the values for C_1 and C_2 are evaluated using the relations:

For intake and exhaust:

$$C_1 = 6.18 + 0.417 \frac{\upsilon_s}{\overline{S}_p}$$

and, for the remaining cycle:

$$C_1 = 2.28 + 0.308 \frac{\upsilon_s}{\overline{S}_p}$$

where

$$\upsilon_s = \frac{B\,\omega_p}{2}$$

The Woschni correlation obtained above is thus rewritten as:

$$h = 3.26\, B^{-0.2}\, p^{0.8}\, T^{-0.55}\, w^{0.8} \tag{3.13}$$

The above relation suggested by Woschni was later modified by Hohenberg to better predict the time-averaged fluxes. It was done by directly measuring the heat flux from Direct Injection (DI) engine using probes. In contradiction to Woschni using cylinder bore as the characteristic length, Hohenberg used a length based on the instantaneous cylinder volume, changes in effective gas velocity, and exponential of the temperature term (Hohenberg, 1979).

Figure 3.4 shows that the Woschni model predicts area-averaged heat flux with reasonable accuracy. Comparing the Annand and Woschni models for similar operating characteristics, the Annand correlation predicts higher heat flux at the same crank angle for different engine loads. The reason for lower HTC prediction by the Woschni model is that the combustion-induced velocity term is smaller for this model. However, the consistency shown by Woschni model in heat transfer prediction made it the preferred choice for IC engine researchers, and the model is highly validated (Finol and Robinson, 2005).

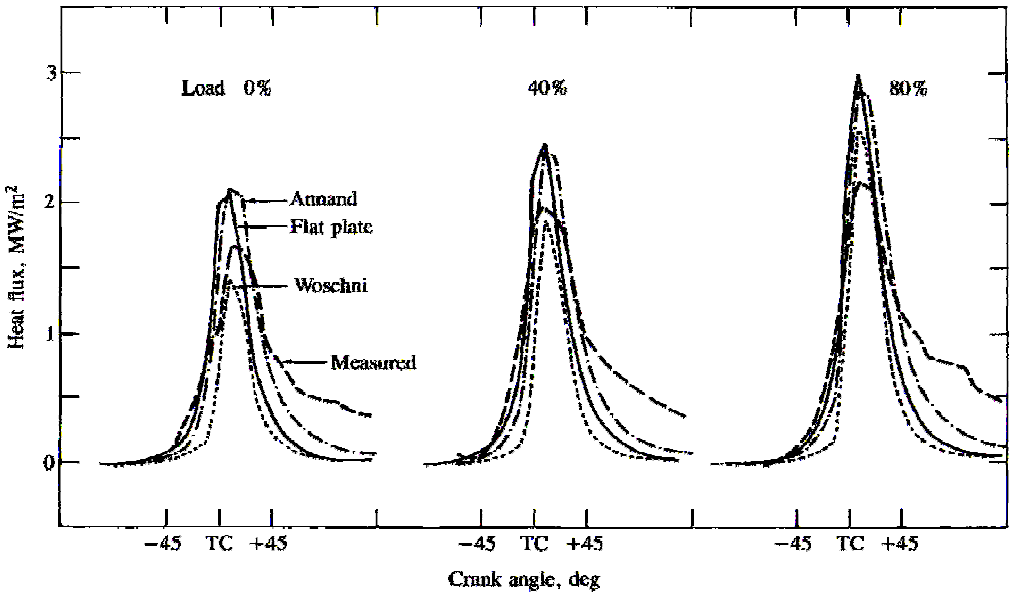

Figure 3.4: Comparison of heat flux measure which varies with crank angle at 1050rpm for a fired high-swirl DI engine is shown (Heywood, 1988).

3. 4 Gas flow analysis through ports

The gas flow in and out of the engine cylinder is of great significance for the proper functioning of the engine. In two-stroke engines, the gas flow to and from the cylinder is controlled by ports. A discharge coefficient term is used to represent the functionality of the ports. The size, shape, and orientation of the ports can significantly influence the gas addition and removal in an engine.

Mass flow rate through port

The mass flow rate through a port depends on the port geometry and the port gas-flow parameters. Figure 3.5 gives different port parameters as observed in a rectangular port with rounded edges. The relation (3.14) can give the open area in a partially opened port:

$$A_p = X\, h_p - \frac{r^2 (4 - \pi)}{2} \tag{3.14}$$

The equation (3.15) gives the mass flow rate through a partially opened port as a function of pressure ratio across the port.

$$\dot{m} = \frac{Cd\, A_R\, p_0}{(R\, T_0)^{0.5}} \left(\frac{p_T}{p_0}\right)^{1/\gamma} \left\{ \frac{2\gamma}{\gamma - 1} \left[1 - \left(\frac{p_T}{p_0}\right)^{\gamma - 1/\gamma} \right] \right\}^{0.5} \tag{3.15}$$

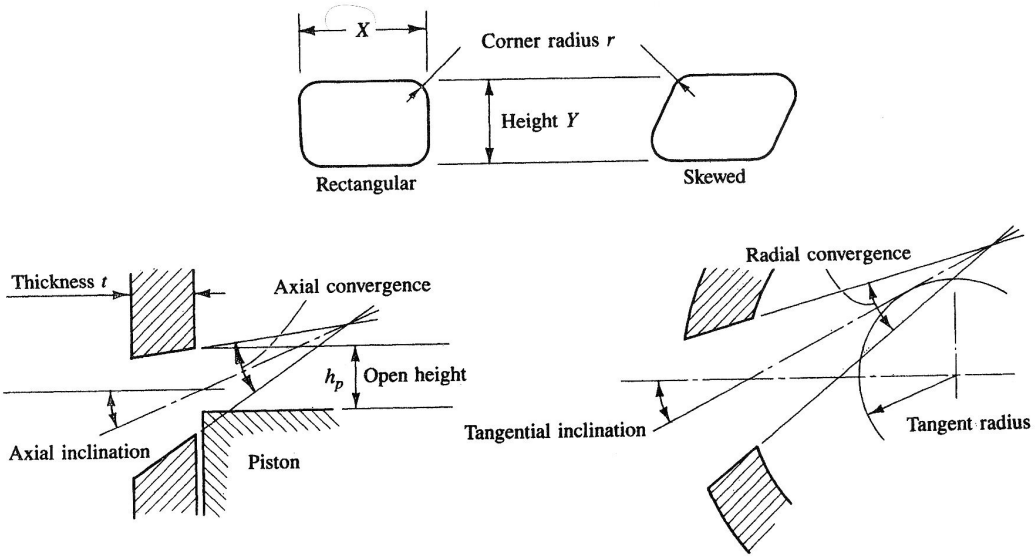

Figure 3.5: The port parameters (Heywood and Sher, 1999)

For a choked flow, which occurs when, $\frac{p_T}{p_0} \leq \frac{2\gamma}{\gamma + 1}^{\gamma/\gamma - 1}$; the value of mass flow rate can be obtained as (Heywood and Sher, 1999):

$$\dot{m} = \frac{C_d\, A_R\, p_0}{(R\, T_0)^{0.5}} \; (\gamma)^{1/2} \left\{ \frac{2\gamma}{\gamma - 1} \right\}^{\gamma + 1/\gamma - 1} \tag{3.16}$$

For intake flow through the port, p_0 is the scavenge flow pressure p_{sc}, and p_T is the cylinder pressure. For exhaust flow through a port, p_0 is the cylinder pressure and p_T is the exhaust pressure. The product of $C_d \times AR$ is given as the effective flow area, A_E. The C_d varies with pressure ratio.

Coefficient of discharge models

The C_d evaluation methods like Demtchenko, Nusselt, Busemann etc. are basically designed for flow through sharp edged ports (Benson, 1960). These models were thoroughly analysed by the author (Thomas, 2008), and it was observed that the Demtchenko model predicts the flow accurately.

Demtchenko model

The Demtchenko equation is developed based on tangent gas approximation, and is the first attempt to develop an approximate method to evaluate C_d by taking the ratio of jet width at the vena contracta to the width of the slit from lower values of pressure to sonic values (Benson, 1960).

$$C_d = \frac{\pi}{\pi + 2\left(1 - \frac{1}{\gamma}\left(1 - \frac{P_A}{P_0}\right)\right)} \tag{3.17}$$

3. 5 Analytical model results

This section discusses some of the results obtained from analytical model developed for the engine.

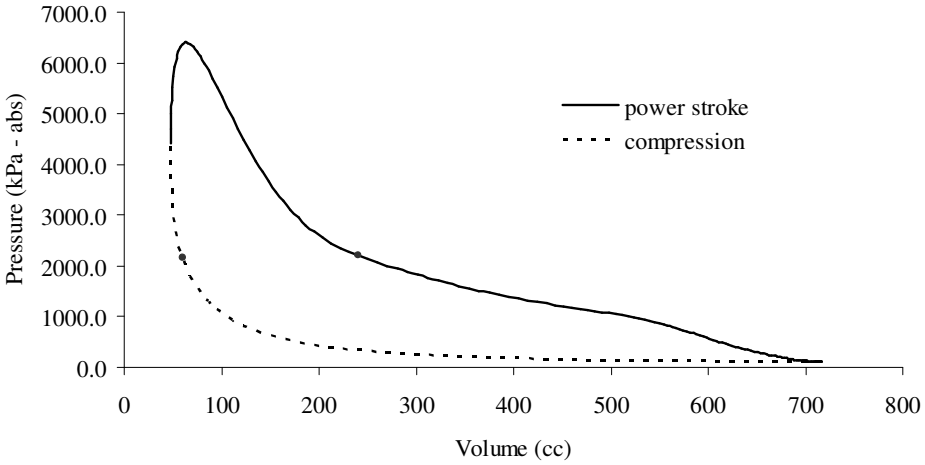

Figure 3.6: The P-V diagram (Thomas, 2008)

Figure 3.6 shows the P-V plot obtained from the analytical model. The analysis predicted a peak pressure of around 6.5 MPa. The pressure plot is drawn against the crank angle in Figure 3.7. The maximum pressure is observed to be at around 180°CA.

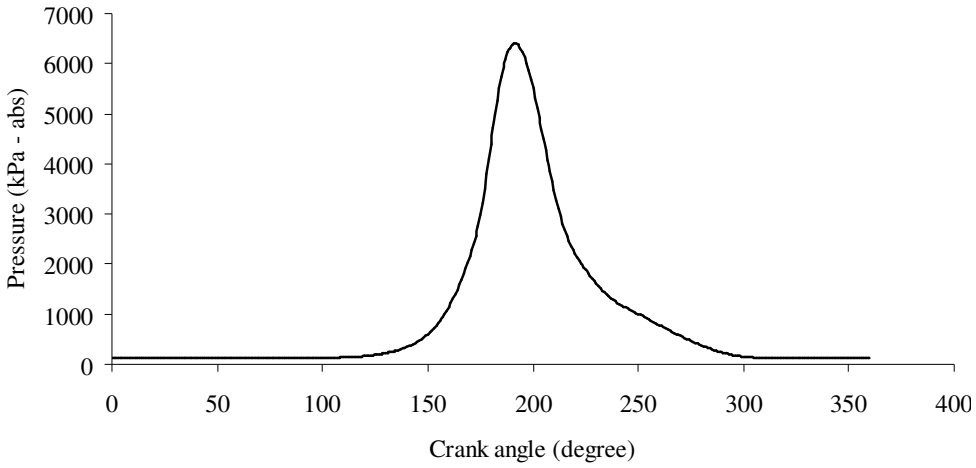

Figure 3.7: The Pressure-Crank angle diagram (Thomas, 2008)

Figure 3.8 shows the variation of in-cylinder temperature as a function of different crank positions during an engine cycle. The temperature starts to rise at around 85°CA, reaches maximum temperature of 2900 K at around 113°CA. The small drop in gas temperature at TDC is due to the increased heat transfer predicted soon after combustion when both the pistons are at TDC. Similar to that observed in the pressure plot, the second half of the temperature plot drops slowly compared to the initial section of rise in temperature due to compression and ignition.

Figure 3.9 shows mass flow through ports and the in-cylinder pressure plotted in a single chart, with respect to the crank angle. Reverse flow is predicted by the analytical model at the inlet port, in the beginning of exhaust stroke. The reason for this is the high pressure prevailing in the cylinder after combustion and expansion strokes. The flow through exhaust port in the beginning of exhaust stroke is also predicted quite high due to the same reason, but normalises gradually. Considering the mass flow rates in and out of the system the volumetric efficiency is calculated as 98% by the analytical model.

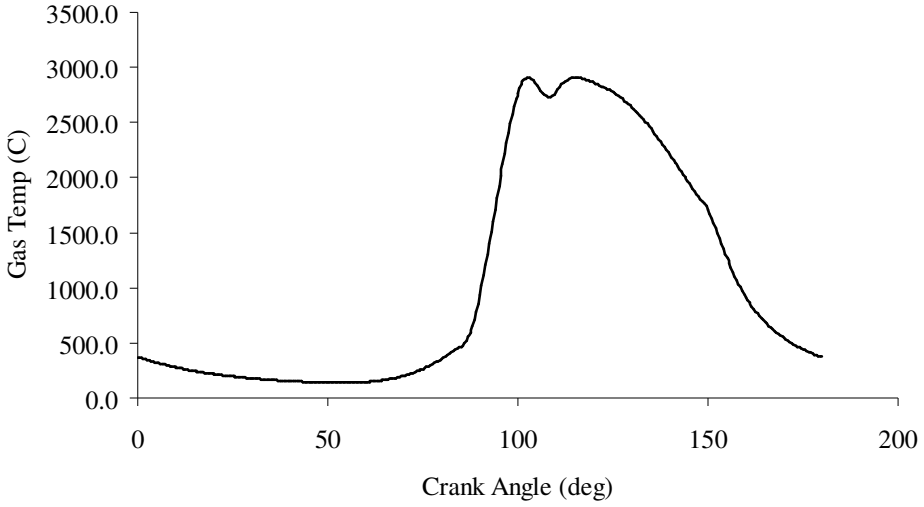

Figure 3.8: The Temperature-Crank angle diagram (Thomas, 2008)

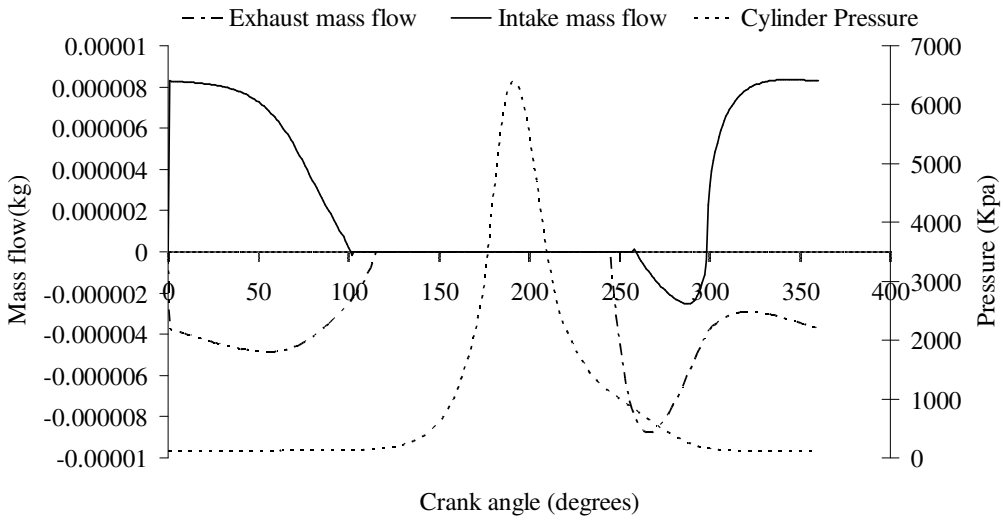

Figure 3.9: The Mass flow and Pressure Vs Crank angle diagram (Thomas, 2008)

Chapter 4

CFD ANALYSIS OF ENGINES

The chapter discusses the some of the principles of CFD. CFD tools are available for purchase commercially and some are developed in research facilities for special purposes. Though they differ in their names and are meant for different applications, all of them share the same basic concepts of mass, energy and momentum conservations, transport equations, and material properties. The combined Eddy Dissipation Model/Finite Rate Chemistry (EDM/FRC) widely used for modelling premixed-combustion and the newly added Spark Ignition Model (SIM) can effectively simulate combustion in CFD models.

4. 1 Conservation equations

The governing equations in CFD, the continuity of mass, momentum, and energy relations are given in vector notation.

Continuity equation

$$\frac{\partial \rho}{\partial t} + \nabla \cdot (\rho\, u) = 0 \tag{4.1}$$

Momentum equation

$$\rho \frac{\partial u}{\partial t} + \rho (u \cdot \nabla)\, u = -\nabla p + \nabla \cdot \left\{ \mu \left[\nabla u + (\nabla u)^T \right] + \lambda (\nabla \cdot u) \right\} + \rho\, g \tag{4.2}$$

Energy equation

$$\rho c_v \frac{\partial T}{\partial t} + \rho c_v (u \cdot \nabla) T = -p(\nabla \cdot u) + \nabla (k \nabla T) + \lambda (\nabla \cdot u)^2 + \nabla u \cdot \left\{ \mu \left[\nabla u + (\nabla u)^T \right] \right\} \tag{4.3}$$

4. 2 Turbulence modelling

Turbulence in IC engines is one of the major factors considered while designing and analyzing the combustion chamber. Turbulence modelling is highly complicated in a combustion chamber because of its three dimensional and unsteady nature. As the inertia forces in fluid overcomes viscous forces, it will cause the turbulence, which is often described in relation to a Reynolds number (Mameri et al., 2008). Even after the introduction of Direct Numerical Simulation (DNS) and Large Eddy Simulation (LES) methods of turbulence predictions, the two-equation method is still widely used because of the good compromise they give in numerical effort and computational accuracy. The most prominent among them is the $k-\varepsilon$ model, which accounts for almost 95% of the present industrial use (George et al., 2001).

The turbulence velocity scale is evaluated from the turbulent kinetic energy (k) obtained from the solution of its transport equation. Similarly the turbulent length scale is evaluated in terms of k and its dissipation rate (ε) from turbulent kinetic energy and its dissipation rate (ANSYS, 2006). The reaction zones in both partially premixed and fully premixed combustion are significantly influenced by the turbulence. The transport of momentum, heat and species in combustion reactions are greatly influenced by turbulence factors (Aglave et al., 2008). During combustion, molecular mixing and chemical reactions occur at the smallest scales, and so these are modelled using statistical modelling in Reynolds Averaged Navier Stokes (RANS).

4.2.1 Reynolds Averaged Navier Stokes (RANS) equations

Among the classical methods of evaluating turbulence the RANS equations are either time averaged or ensemble averaged equations, which reduces the requirements of resolution by several orders of magnitude. The equations thus obtained are called the Reynolds Averaged Navier Strokes (RANS) equations. The information lost because of the averaging procedure can be fed back into the equations by using any turbulence model. The RANS methods are widely used in industrial applications because of their low computational cost they require and due to the simplicity of the model. In RANS modelling the simplest models that can offer sufficient level of

generality and flexibility are the two-equation models. Because of the statistical averaging procedure employed for obtaining the equations, the RANS equations are also referred to as Statistical Turbulence Models (STM) (ANSYS, 2006).

The additional terms that comes into action in RANS models because of the averaging process are called the turbulent stress or Reynolds stress terms. Because of these additional terms the Reynolds stress needs to be modelled with the help of additional equations for available quantities for achieving closure (ANSYS, 2006). One example of such models is the $k-\varepsilon$ model, which gives the required number of equations for getting all the unknowns including the Reynolds-Stress tensor resulting from averaging process.

$k-\varepsilon$ model

The $k-\varepsilon$ model is the most widely used two-equation model. Even though the two-equation turbulence model has tendency to be inaccurate in large separation flows, it is preferred in most cases due to the compromise they offer between complexity, accuracy and robustness of the model (Chow et al., 2006). The in-cylinder flows in a combustion chamber are prone to high amount of swirl motions. Plenty of researches have already been performed in studying the swirl flow characteristics inside the engine cylinder.

One of the inabilities of $k-\varepsilon$ model is its insensitivity to streamline curvature and system rotation, which results in exaggerating the predictions of turbulent mixing and causing a critical decay of the core vortex. Use of the $k-\varepsilon$ model for combustion modelling has been subject of discussion for a long time due to the assumptions made by the model in isotropic eddy viscosity concept and gradient diffusion model. The 'k' and 'ε' used to define the velocity scale 'υ' and length scale 'l' that represents the large-scale turbulence are given by:

$$\upsilon = k^{1/2} \qquad l = \frac{k^{3/2}}{\varepsilon} \tag{4.4}$$

The standard $k-\varepsilon$ model when applied with the Newtonian closure becomes:

$$\overline{-\rho u' \otimes u'} = \mu_t \left(\nabla \cdot U + (\nabla \cdot U)^T\right) - \frac{2}{3}\delta(\rho k + \mu_t \nabla \cdot U) \tag{4.5}$$

The term μ_t in the above equation is the turbulence viscosity. The turbulence diffusivity is defined based on the turbulence viscosity. The following relation gives the Reynolds fluxes as:

$$\overline{-\rho u' \phi'} = \Gamma_t \cdot \nabla \cdot \phi \tag{4.6}$$

In the above equation Γ_t is the turbulence diffusivity (Mameri et al., 2008).

The turbulence diffusivity and turbulence viscosity is related by the equation:

$$\Gamma_t = \frac{\mu_t}{Pr_t} \tag{4.7}$$

The turbulent viscosity can be obtained from the relation:

$$\mu_t = C_\mu \cdot \rho \cdot \frac{k^2}{\varepsilon} \tag{4.8}$$

In the two-equation $k-\varepsilon$ model, the general conservation equations for k and ε are:

$$\frac{\partial \rho k}{\partial t} + \nabla \bullet \rho(U k) = \nabla \bullet \left[\left(\mu + \frac{\mu_t}{\sigma_k}\right) \cdot \nabla k\right] + P_k - \rho\varepsilon \tag{4.9}$$

$$\frac{\partial \rho \varepsilon}{\partial t} + \nabla \bullet \rho(U c) = \nabla \bullet \left[\left(\mu + \frac{\mu_t}{\sigma_\varepsilon}\right) \cdot \nabla \varepsilon\right] + \frac{\varepsilon}{k} \cdot \left(C_{\varepsilon 1} P_k - C_{\varepsilon 2} \rho \varepsilon\right) \tag{4.10}$$

4. 3 Combined Eddy Dissipation Model / Finite Rate Chemistry (EDM/FRC)

The EDM/FRC model is developed based on a phenomenological analysis of turbulent combustion which assumes Reynolds number (>1) and Damkohler number (>1) (Veynante and Vervisch, 2001). In these models, the rate at which fuel is consumed is specified as a function of the local flow properties (Versteeg and Malalasekera, 2007). For the EDM/FRC model, the minimum of the reaction rate calculated for both the models is used. The flow must be turbulent to use the EDM/FRC model efficiently. The EDM/FRC model is used in this thesis, because in some regions of the combustion chamber the reaction rates are limited by the turbulent mixing, and in some other areas by chemical kinetics.

Defining the initial condition for the FRC model is very critical. For this model, the initial temperature depends on the reaction temperature. In the EDM model the reaction zone is considered as an assembly of fresh and burnt gas pockets (Veynante and Vervisch, 2001). The turbulence existing in the domain will leads to a breakdown of fresh gas structures based on the Kolmogorov cascade. In the EDM model, the mean reaction rate is limited by the turbulent mixing time τ_t. In a situation where the oxidiser is in excess in the reaction zone, the mean reaction rate is:

$$\bar{\dot{\omega}} = -C_{EBU}\bar{\rho}\frac{\sqrt{\tilde{Y}_F''^2}}{\tau_t} \tag{4.11}$$

In the above relation, Y_F'' is the mass fluctuation of fuel, and C_{EBU} is the model constant.

The turbulent mixing time, τ_t is:

$$\tau_t = \frac{k}{\varepsilon} \tag{4.12}$$

The reaction rate obtained earlier in terms of turbulent mixing rate, when written in terms of progress variable' c ' becomes:

$$\overline{\dot{\omega}} = -C_{EBU}\overline{\rho}\frac{\sqrt{\widetilde{c}_F''^2}}{\tau_t} \tag{4.13}$$

For use in practical simulations, the EDM can be given as:

$$\overline{\dot{\omega}} = C_{EBU}\,\overline{\rho}\,\frac{\varepsilon}{k}\,\widetilde{c}\,(1-\widetilde{c}) \tag{4.14}$$

The EBU/EDM model can be given in terms of fuel mass fraction as (Veynante and Vervisch, 2001):

$$\overline{\dot{\omega}}_F = C_{EBU}\,\overline{\rho}\,\frac{\varepsilon}{k}\,\frac{\widetilde{Y}_F}{Y_F^0}\left(1-\frac{\widetilde{Y}_F}{Y_F^0}\right) \tag{4.15}$$

In the expression Y_F^0 gives the initial mass fraction of fuel in the reactant stream with the earlier assumption of excess oxidizer.

The FRC model is used in regions where the chemical scale is the rate-limiting factor. An assumption used in CFX for the FRC model is that, the rate of reaction progress of the elementary reaction ' k ' is reversible only if the backward reaction is pre-defined. The reaction rate as done for the EDM model can be given as:

$$R_k = \left(F_k \prod_{I=A,B}^{N_c}[I]^{r'_{kI}} - B_k \prod_{I=A,B}^{N_c}[I]^{r'_{kI}}\right) \tag{4.16}$$

In the relation above, '[I]' shows the molar concentration of the component 'I', and 'F_k' and 'B_k' gives the forward and backward rate constants respectively. The term r', shows the reaction order of the component (ANSYS, 2006).

The following relations obtain the forward and backward rate constants:

$$F_k = A_k T^{\beta_k} \exp\left(-\frac{E_k}{RT}\right), \text{ and} \tag{4.17}$$

$$B_k = A_k T^{\beta_k} \exp\left(-\frac{E_k}{RT}\right) \tag{4.18}$$

here:

A_k - The pre-exponential factor,

β_k - The temperature exponent,

E_k - The activation energy, and

T - The absolute temperature

4. 4 Spark Ignition Model (SIM)

The spark ignition model is the latest addition to CFX, by which the combustion in an IC engine can be modelled with more accuracy. This model is incorporated with the Burning Velocity Model (BVM). The BVM can be used for both the premixed and partially-premixed combustion with an inbuilt term for spark ignition.

According to the literature provided by Ansys Inc. (ANSYS, 2006), the spark ignition model has two purposes: to provide the necessary initial conditions to start the combustion process at the exact time and location, and to specify the initial growth of the spark kernel, so that once it reaches the specified transition radius the model will automatically change to a normal combustion model. The flame is assumed to grow spherically as a ball shape with spark kernel radius r_k, time of ignition given as t_{ignite}, and the initial spark volume is given by $V_{initial}$.

An expression connecting all these terms can be given as:

$$\frac{d}{dt} r_K(t) = \frac{\rho_u}{\rho_b} \cdot s_{T,k} \tag{4.19}$$

where

$$r_K(t_{ignite}) = \sqrt[3]{\frac{3V_{initial}}{4\pi}} \tag{4.20}$$

As mentioned earlier, the spark is expected to grow as a ball shape with the radius of the ball given by a term called transition radius r_{trans}. The center of the spark is given by $\vec{x}_{spark}$. In SIM, the reaction progress 'c' is used to control the combustion inside the domain. This value can be specified while modelling the simulation in CFX-Pre. The integration of the spark kernel into the combustion domain is necessary for proper transition from spark advancing to the actual combustion model. This is done in CFX by averaging the progress of reaction over the phantom region (ANSYS, 2006).

The reaction progress variable can be given by the relation,

$$c = \left(\frac{r_K}{r_{trans}} \right)^3 \quad \text{for} \quad \left| \vec{x} - \vec{x}_{spark} \right| \leq r_{trans} \tag{4.21}$$

$$c = 0 \quad \text{for} \quad \left| \vec{x} - \vec{x}_{spark} \right| > r_{trans}$$

When the spark ignition is intiated in the model, an Initial Value Problem (IVP) is solved until the kernel radius r_K, reaches the transition radius r_{trans}. As the transition radius is reached, the IVP model is switched over to the BVM model.

The Turbulent Burning Velocity (TBV) determines the growth rate of flame kernel radius r_K. When the kernel is too small, a modification is applied for the high curvature as:

$$s_{T,k} = \max\left(s_L, s_T - \frac{2}{r_K} D_t \right) \tag{4.22}$$

where

$$D_t = \frac{C_u}{\sigma_t} \cdot \frac{k^2}{\varepsilon}$$

The initial value problem makes use of the laminar burning velocity s_L, turbulent burning velocity s_T, and the 'k' and 'ε' factors in the turbulence model, together with the burnt mixture density 'ρ_b', and unburnt mixture desntiy 'ρ_u' (ANSYS, 2006).

Chapter 5

CFD ANALYSIS USING DOMAIN SOURCE MODEL (DSM)

It is desirable to test the engine CFD models for stability and mesh quality using some simple methods prior to using the complicated combustion models. The main aim of this chapter is to introduce the concept of Domain Source Model (DSM) for the engine process modelling, before using more complicated combustion models, which needs the chemical reaction parameters. Some of the relevant validation cases of CFX in IC engine process modelling are done by Horrocks (Horrocks, 2001), Foster (Foster, 1998), Stopford (Stone, 1999) etc. This chapter discusses the geometry modelling, meshing and grid deformation done for the engine model using CFX.

5. 1 ANSYS CFX – An Introduction

ANSYS CFX basically is a general purpose analysis tool used in CFD environment (ANSYS, 2006). The V11.0 of the tool is used for the current study, in which Spark Ignition Model (SIM) is a new addition as compared to the previous versions of the same tool. The latest version, V12.0, is incorporated with a dedicated combustion model to simulate combustion in IC engines. The parallel running capability, periodic wall motion with permitting no interfaces between boundaries are few of the attractions of this particular CFD tool. Apart from the CFX, ANSYS has several categories of tools that can aid design and analysis. For instance, the ANSYS Work Bench is used in current analysis to model the engine and port geometries.

5. 2 Geometry modelling and meshing

Attempts to model the engine using dedicated modelling software were found to be troublesome when the model was imported into CFX for simulation. The moving boundary simulation was highly unstable with the geometry was generated by stand-alone design tools. So, the geometry of the engine was modelled using ANSYS

Design Modeller V11.0. The model includes the cylinder volume, the inlet ports and the exhaust ports. In the original engine prototype the inlet and exhaust ports run all around the cylinder geometry. The model in CFX is designed as a series of ports instead of a single opening, assuming maximum volumetric efficiency and perfect removal of burnt gas.

Figure 5.1, shows the engine geometry as observed in the CFX-Pre module. The smaller ports running all around the cylinder geometry are the inlet ports, and the large sized ports running around the cylinder geometry are exhaust ports. The arrows show the direction of fluid flow through these boundaries. A single port opening running around the engine cylinder geometry is not advisable in practical situations as that may cause the piston rings to project outside through the ports when hot. However, the spark plug is not explicitly shown in the geometry the spark ignition is assumed to be occurring in the middle of the cylindrical domain. The spark ignition location is defined using an algebraic equation for modelling using the EDM/FRC combustion model which needs a heat source term for initialising combustion.

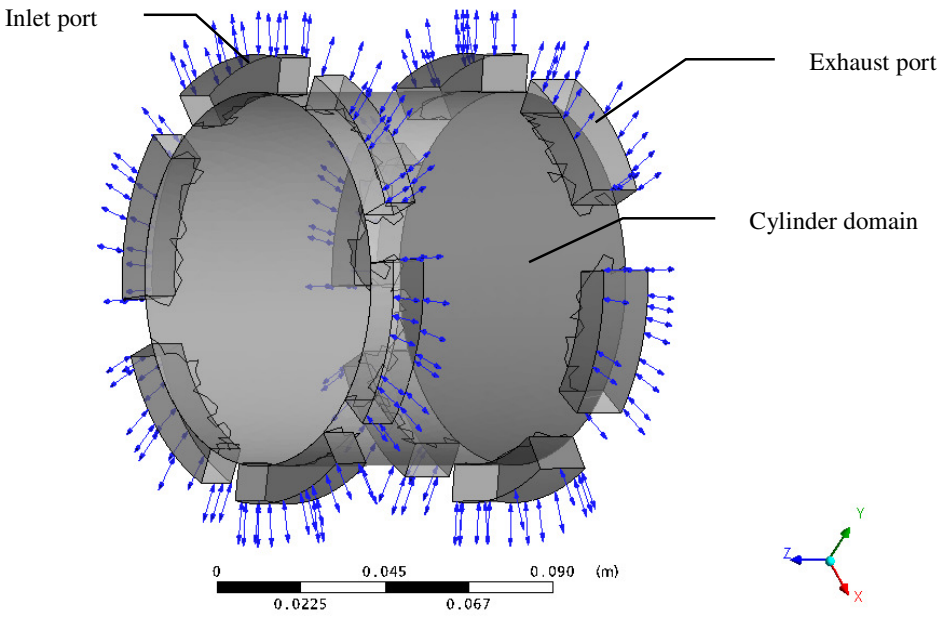

Figure 5.1: The cam-plate engine model developed using Ansys DM

The cylinder is of $100\,\text{mm} \times 85\,\text{mm}$ configuration, and the inlet ports are smaller than the exhaust ports. This is done due to the following reasons: to open the exhaust port prior to the inlet port and a smaller inlet port serves the purpose for this engine due to turbocharged pressure available at the inlet port. Compared to conventional engines with valves controlling fluid flow, this engine follows the two-stroke engine design with the pistons controlling flow through the ports. The piston motion follows the polynomial profile of cam-plate that is generated in the spreadsheet.

The mesh used in present model is a patch-independent tetrahedral mesh, while all the other meshes failed to prove worthy during the high level of deformation applied to the model. With the available ANSYS educational license in the University, it was not possible to use another mesh or to refine the current mesh beyond a limit as the available license restricts the number of elements possible in a domain. The CFX-Mesh gave consistent results throughout the simulations, and so this mesh was used for all further simulations.

5. 3 Mesh deformation

One of the major attractions of IC engine CFD modelling is that the mesh undergoes a high level of deformation to simulate different processes in the engine. In the present CFD model a compression ratio of 10:1 is applied as used in the spreadsheet model. The cylindrical domain is modelled to deform according to the motion specified for the double pistons at the either end of the cylinder. The clearance volume left at the TDC position of the pistons is 5 cm, with the spark ignition occuring at 10 degrees BTDC to give enough time for combustion. Achieving the mesh deformation without any error was one of the difficult tasks faced during the engine CFD modelling. The difficulty in achieving a stable simulation was observed to increase with the increase in compression ratio.

Figure 5.2, shows the different stages of mesh deformation as observed in the CFX-Post module for the multiport opposed-piston cam-plate engine. The series of ports around the geometry also contributes towards the complexity in achieving a stable and accurate CFD result due to the tremendous CFD load it puts on the system and software capability. Even though symmetry could have been used to advantage, this

was not used here so as to avoid any chances of errors due to symmetry assumptions. The mesh deformation modules applied to the simulation supposedly increase the CPU usage approximately 50% per time step as compared to normal steady state and transient non-deformation simulations (ANSYS, 2006). Only a powerful computing setup can handle such a mesh deformation task without any difficulty as the mesh deformation demands higher memory to store the volume flows for the mesh, and also for storing the large sets of mesh coordinates in case of transient simulations.

The motion of the nodes on the boundaries and sub-domain regions are specified using CFX Expression Language (CEL), and the mesh motion model called Displacement Diffusion determines the remaining node movements. Displacement Diffusion was performed in CFX by solving the relation (ANSYS, 2006):

$$\nabla \bullet \left(\Gamma_{disp} \nabla \delta\right) = 0 \tag{5.1}$$

where

δ, gives the relative displacement from the previous mesh location

Γ_{disp}, is the mesh stiffness

The mesh stiffness, during a deformation simulation, will increase near small volumes. In this case the mesh stiffness is given by the relation:

$$\Gamma_{disp} = \left(\frac{1}{\forall}\right)^{C_{stiff}} \tag{5.2}$$

where

C_{stiff}, gives the stiffness model

$\forall$, is the control volume size

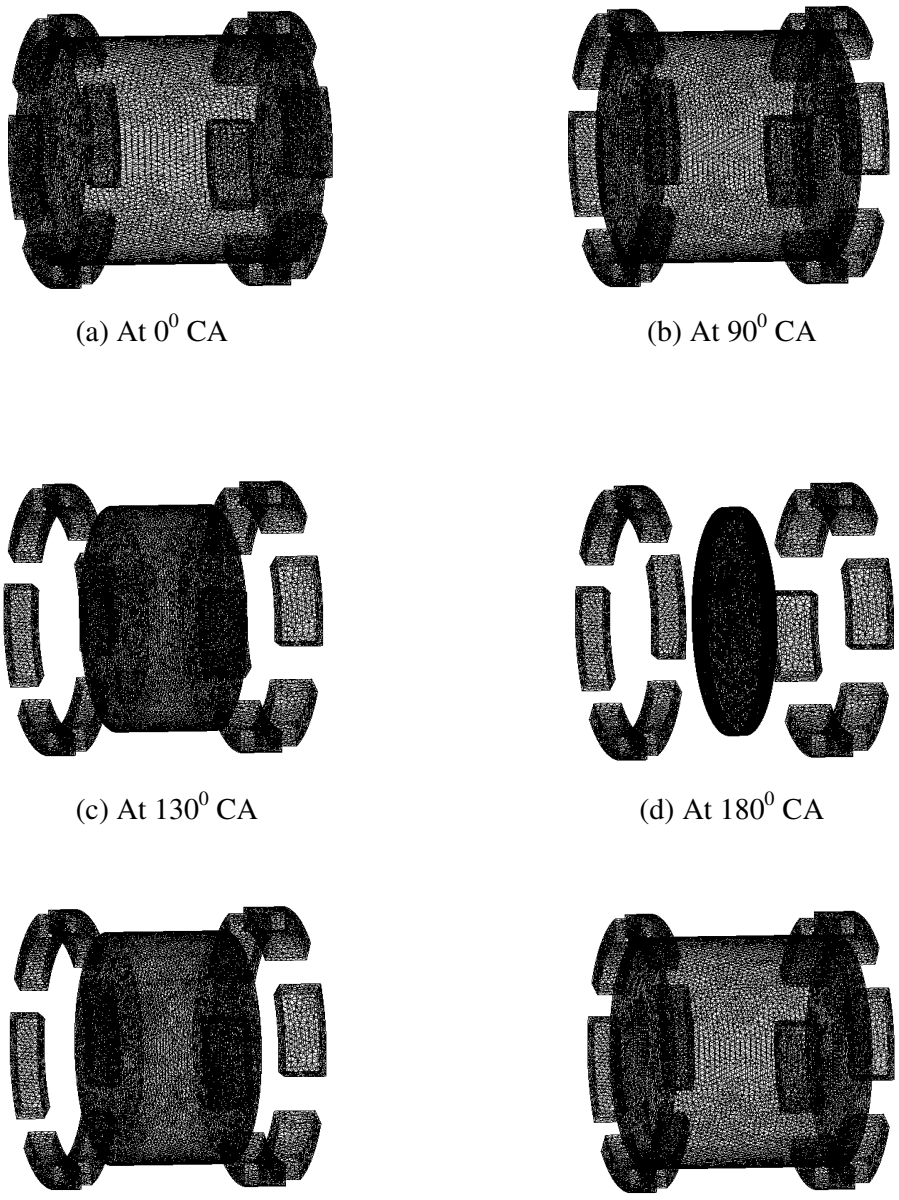

(a) At 0^0 CA (b) At 90^0 CA

(c) At 130^0 CA (d) At 180^0 CA

(e) At 240^0 CA (f) At 280^0 CA

Figure 5.2: The mesh deformation obtained from CFX-Post for the cam plate engine at different crank angles

For the present CFD model, a sinusoidal profile based piston motion and a polynomial profile based piston motion are compared. The sinusoidal motion was applied in the CFX model using CEL expression. The polynomial motion was originally modelled in spreadsheet form using a set of complex polynomial equations and so it was not used directly in CFX. Instead, the motion parameters were read into

CFX as a function that imparts the same motion to the piston boundary in CFX as observed in the spreadsheet model.

5. 4 Boundary conditions and parameters

Setting appropriate boundary conditions is a critical step in the case of transient simulations. The initially assumed boundary values were the starting point of all the calculations in the simulation. It was necessary to specify these values at all the solution points in the domain in the case of a transient simulation (Versteeg and Malalasekera, 2007). In the present model, the boundary conditions were set at the inlet ports, exit ports, cylinder walls, pressure values at the boundaries etc. Different CEL expressions used performed different tasks including the piston motion simulation, reaction initialization etc.

At the inlet boundary, a turbo-charged constant pressure of 60 kPa is applied, and in the outlet, the pressure gradient is set as 0 kPa. The DSM model used air as an ideal gas as the working fluid whiles the EDM/FRC and BVM used a predefined fuel mixture material. Interfaces are used to permit relative motion between pistons, cylinder, and ports. 'Opening'-type boundary conditions are applied to both the inlet and outlet ports in order to handle any backflows through the ports, which is quite normal in case of engines.

The walls were set to permit heat transfer by specifying a fixed wall temperature of 373K. The same temperature applied at all the boundaries in order to initiate the engine model. Other major features included the expressions used to simulate the polynomial piston motion as a function of time, and the positioning of the spark ignition in the cylindrical domain. A discrete heat transfer condition applied to model the heat transfer inside and outside of the cylinder domain.

5. 5 Uniport Domain Source Model

Compared to the multiport model, this engine model was different in that it had only a single port each for inlet and outlet gas flows as compared to the series of ports

used in the multiport engine model, Figure 5.3. The blue double arrowed lines show the opening boundary condition applied to the port boundaries.

The main aims of this section are to:

- To introduce the DSM technique as a substitute for analyzing the CFD model prior to applying more complicated combustion models, and
- To distinguish between the functionalities of engines using sinusoidal profile based piston motion and polynomial profile based piston motion.

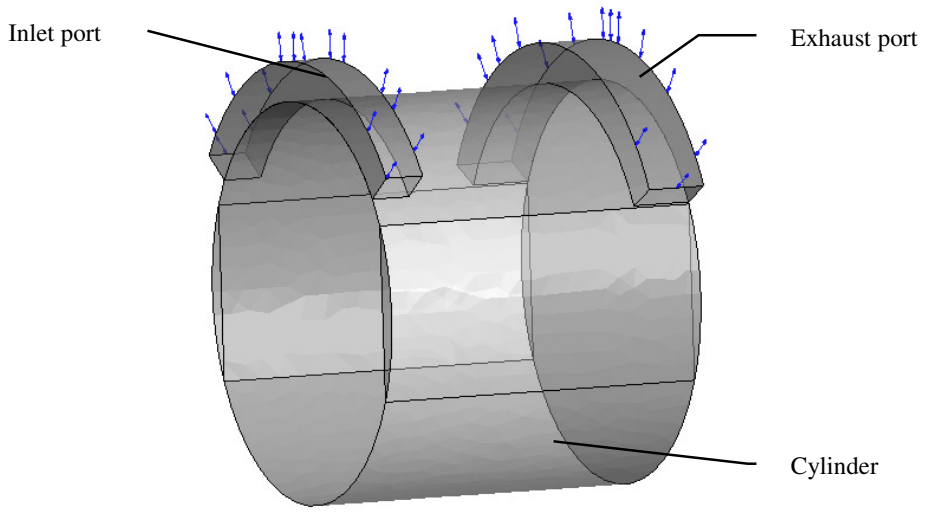

Figure 5.3: Uniport cam-plate engine, modelled in Ansys DM V11.0

5.5.1 Sinusoidal profile piston motion

A sinusoidal profile-based piston motion has been used for a long time in similar kind of cam plate guided engines. The profile is easy to generate and the motion is uniform throughout the cycle of operation. However, the disadvantage of this configuration lies in the fact that the designer has no control over the process-cycle of the engine. In the case of polynomial profile based engines, a longer or shorter stroke of the piston is easily possible by proper design of the cam profile. This feature is completely absent in the case of a sinusoidal profile guided engine.

In the CFD model, the sinusoidal profile-guided piston motion is achieved using CEL expression for imparting the motion to the piston boundaries. The energy of combustion is input to the cylinder boundary using a source term. The effect of combustion is simulated in the CFD model without applying the complicated combustion model. The pressure distribution, temperature distribution, turbulence effects, heat transfer, and mass flow rates through the ports were all obtained with this method of modelling. The only difference from the actual combustion model was that this model did not use a reacting mixture and so did not predict products of combustion inside the combustion chamber.

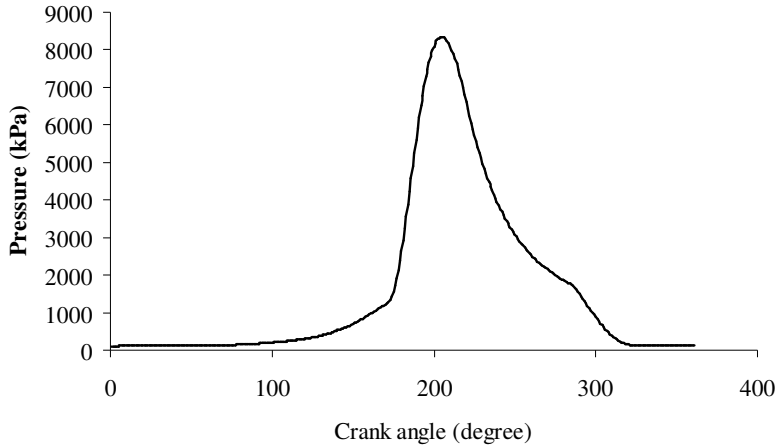

Figure 5.4: Pressure-Crank angle plot of Uniport, Sinusoidal cam-plate engine

Figure 5.4, shows a maximum pressure reading of 8.3 MPa at around 204^{o}CA position. This process-cycle follows the exact operation as in the spreadsheet model that makes it easy to compare between the CFD and spreadsheet models. The slower drop in pressure during expansion stroke as compared to the compression stroke is due to the lower rate of heat removal from the cylinder after the energy release stroke in the cylinder that resembles combustion.

In Figure 5.5, a high temperature of 4737 K at 222^{o}CA observed inside cylinder. The high temperature was found to persist inside the cylinder volume for 120 crank angle degrees, which might have influenced the slow drop of pressure inside cylinder volume. However, this high temperature predicted by the CFD model is significantly higher than that predicted by the spreadsheet model, and the reason for this discussed later in chapter 7 in this thesis.

Figure 5.6 shows the mass flow rates through the inlet and outlet ports of the CFD model. The volumetric efficiency of this engine configuration was observed to be 91.2% from an analysis of the CFD results. This predicts detaining of around 8% of the burnt gas in the combustion chamber even after the exhaust stroke. The negative spike in the inlet mass flow is a result of the back flows observed at the respective ports against the normal flow direction envisaged for those boundaries.

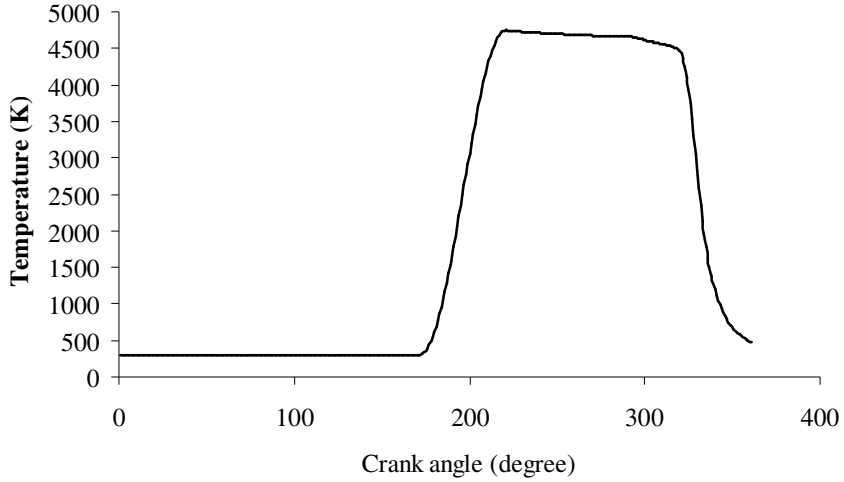

Figure 5.5: The Temperature-Crank angle diagram of uniport, sinusoidal motion cam-plate engine

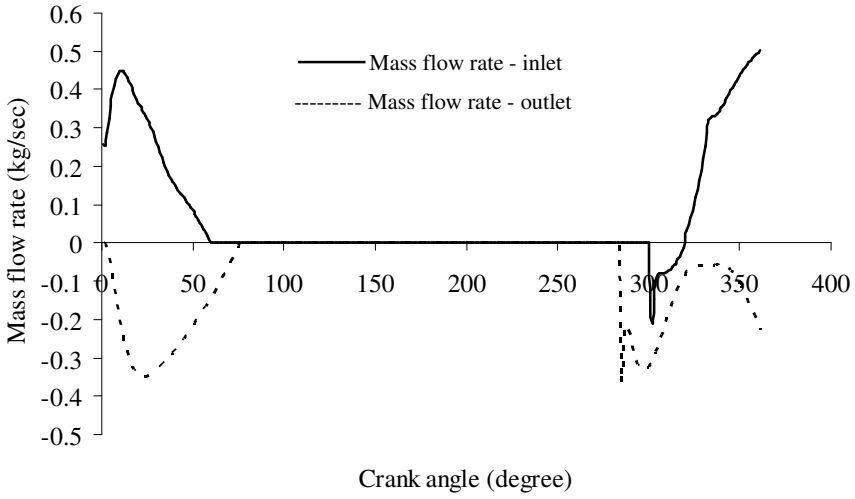

Figure 5.6: The Inlet and Outlet mass flow rates plotted against crank-angle diagram of uniport, sinusoidal motion cam-plate engine

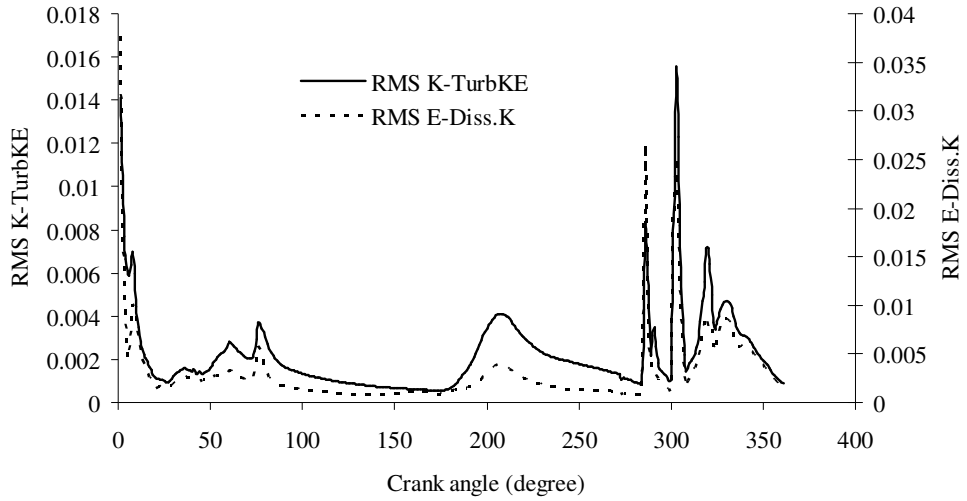

Figure 5.7: The RMS kinetic energy and eddy dissipation plotted against crank angle diagram for the uniport, sinusoidal profile cam-plate engine

5.5.2 Polynomial profile piston motion

The polynomial profile-guided piston motion is achieved in CFX using the piston motion values obtained in the spreadsheet model from polynomial expressions generated for the cam-plate profile. CFX allows the user to take data input from spreadsheet files as functions. The advantage of using polynomial cam profile is that the engine designer has full control over the configuration of the engine. For instance, a longer stroke during exhaust for better exhaust gas removal, or a longer stroke at TDC to extract maximum power and to ensure complete fuel burning etc. This theory is widely covered in the previous study by the author that mainly discussed the spreadsheet modelling (Thomas, 2008).

The series of plots in Figure 5.8 shows the contours of pressure at a middle plane inside the engine cylinder. Figure 5.8 (a), shows high pressure at the top of the cylinder, and this is due to the gas inflow when the pistons are at BDC. As pistons come close to TDC the pressure is seen to be distributed uniformly inside the cylinder, and higher values of pressure are observed close to the cylinder wall. At 180^{o}CA, the low pressure spot visible at the center of the cylinder is due to the vortex flow inside the cylinder. As the pistons move back to BDC the high pressure spot is observed to shift downwards.

Figure 5.9, reports a peak pressure of around 6.9 MPa at 198°CA. This pressure is low compared to that observed in the sinusoidal profile cam-plate engine, but happens at an earlier crank position. This property is a desirable advantage for this model when the thermodynamic properties are considered, as the earlier the peak pressure is reached inside the combustion chamber, the greater the energy extracted for useful work.

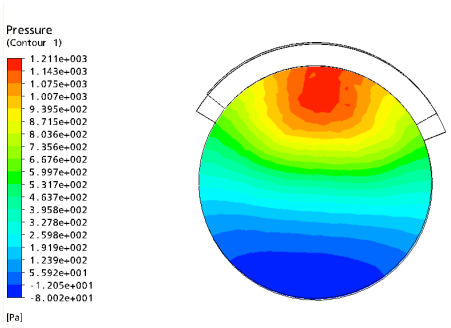

a. Pressure contours at cylinder mid-plane, 1°CA

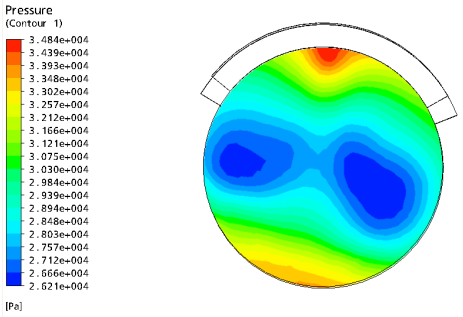

b. Pressure contours at cylinder mid-plane, 45°CA

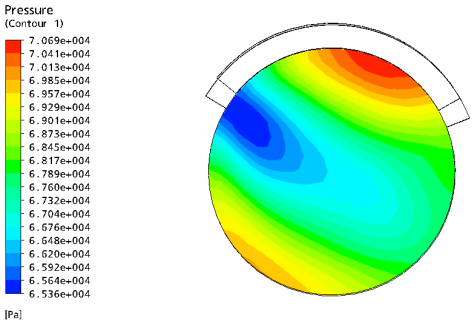

c. Pressure contours at cylinder mid-plane, 90°CA

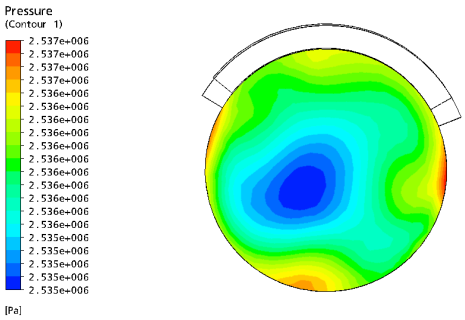

d. Pressure contours at cylinder mid-plane, 180°C

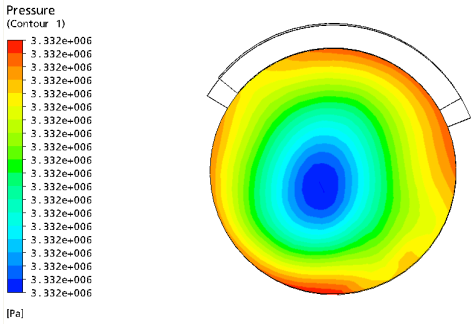

e.Pressure contours at cylinder mid-plane, 245°CA

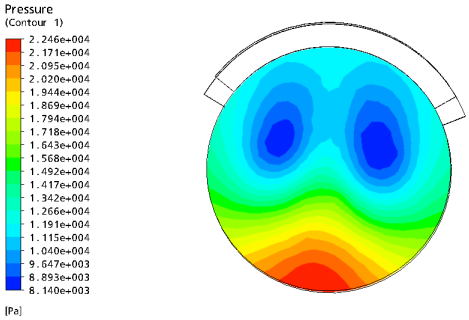

f.Pressure contours at cylinder mid-plane, 330°CA

Figure 5.8: The pressure contour plots (local) of the uniport, sinusoidal profile cam-plate engine at different crank angle positions

Figure 5.10 shows a prediction of back-flow at the inlet port at the start of exhaust stroke. The reason for this back-flow is due to the high pressure prevailing inside the combustion chamber at the end of the combustion process. The volumetric efficiency of this engine configuration observed to be around 94%.

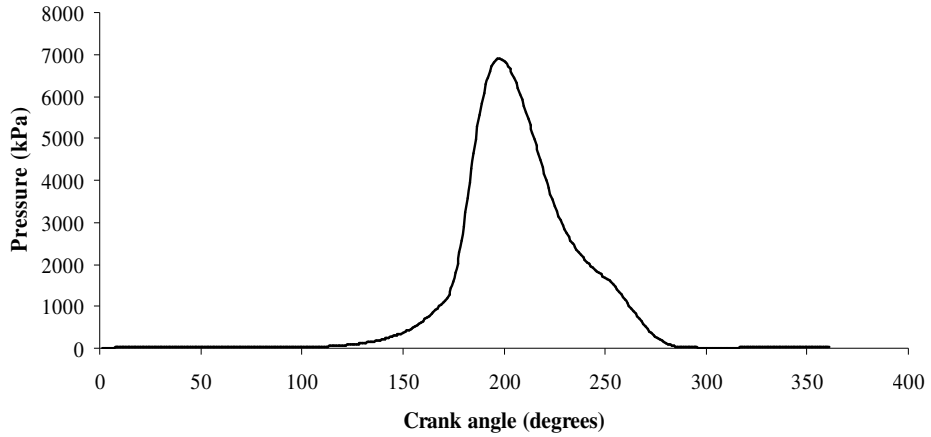

Figure 5.9: Pressure-crank angle diagram of uniport, polynomial cam-plate engine

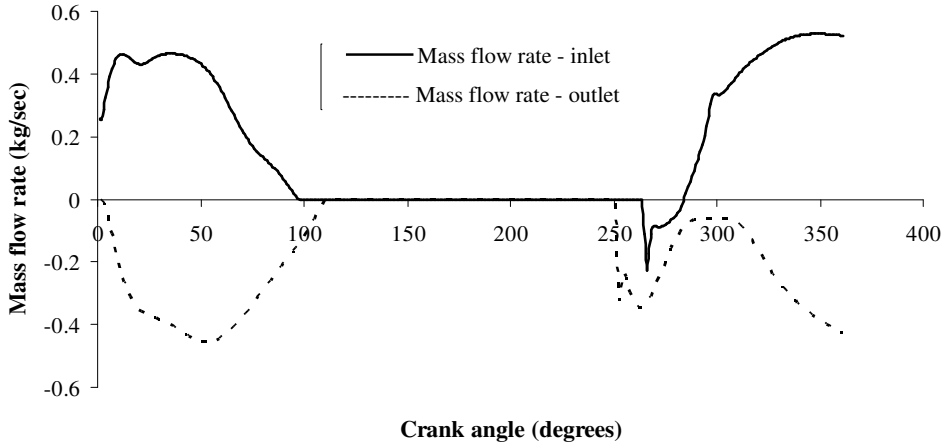

Figure 5.10: Mass flow rate vs CA plot for uniport, polynomial cam-plate engine

From Figure 5.11, the in-cylinder turbulence observed to be very high during the beginning of suction. As the ports closes, the turbulence drops to a lower value and maintain the same level until the beginning of exhaust stroke. In Figure 5.13 a detailed review of the temperature contour plots are included for this model. The temperature profile plotted is for the middle plane in the cylinder. As the piston

approaches the TDC, the temperature seems to be increasing, and the maximum value was observed at 180°CA due to the compression and combustion effects.

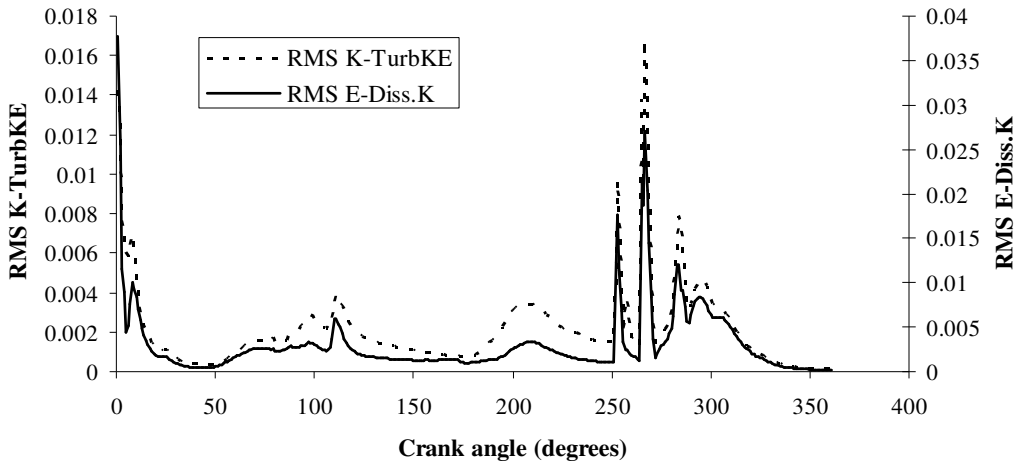

Figure 5.11: The RMS Turbulence kinetic energy and Eddy dissipation of the uniport, polynomial profile cam-plate engine

5. 6 Multiport Domain Source Model

In the multiport design, instead of a single port running almost more than half the way around the cylinder periphery as in the uniport design, the idea is to use multiple ports ensuring volumetric efficiency, uniform charge distribution inside the engine, and better cooling of the cylinder using input charge stream. In addition, this eliminates the possibility of breaking of piston rings when it pops out through ports due to heating, and any chances for piston locking.

In Figure 5.12, the arrows at the inlet and outlet boundaries show the 'Opening-type' boundary condition applied to these ports. Interfaces applied permit relative motion between the cylinder and port domains. The smaller ports are the inlet ports and the bigger ones are the outlet ports. The reason for this design is the same as that discussed in the uniport engine model. Using a series of ports with more refined mesh considerably increased the computational load of the computer system and software. Simulations were performed in cluster with the educational purpose serial-run license. It took a complete day to finish the run on the cluster system for the multiport engine model.

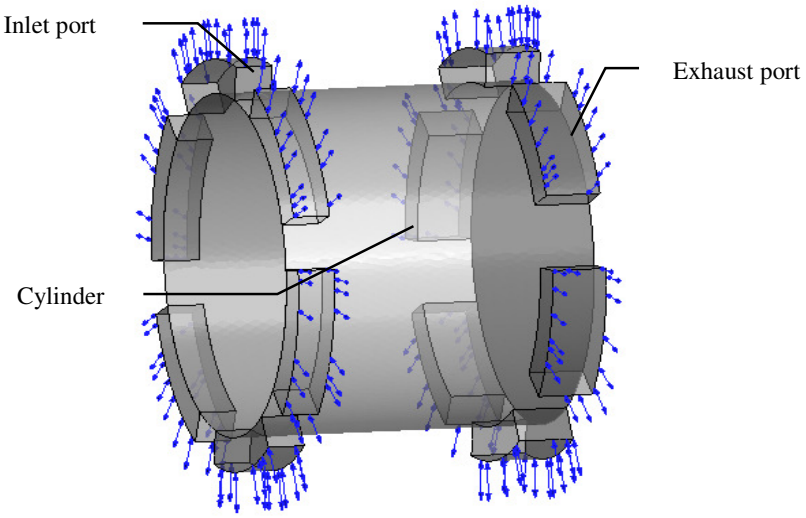

Figure 5.12: The multiport engine model designed in Ansys DM V11.0

With the available system and software capabilities, the tendency for the calculation to crash was significantly high for this model simulation. The software license and cluster system capacity did not permit mesh refinement beyond a certain limit. The present model has 25742 nodes and 96894 tetrahedral elements in the meshed geometry. The volume of the entire model is 732.52 cc. The k-ε turbulence model is used for this design. The results obtained from the analysis are discussed further in this session.

Figure 5.13 shows the temperature distribution inside the cylinder at the middle plane for different crank angles. As the piston moves from BDC to TDC (a to e) the high temperature seems to be uniform shifting from top of the cylinder to fill the entire volume. Later, during the motion of piston from TDC back to BDC, the temperature profile seems to be of a uniform distribution inside the combustion space.

5.6.1 Sinusoidal profile piston motion

Figure 5.14 shows a peak pressure of 7.6 MPa at 206^{o}CA position. The pressure drop during the expansion stroke is slower, as observed for the uniport engines. A possible reason for this is the high heat content prevailing inside the cylinder soon after combustion, and a slower heat transfer rate. The steep rise in pressure during the

compression stroke is visible in the diagram. All the other features of the model are kept the same as in the uniport design. Therefore, the results are comparable between the models and conclusions are easily drawn.

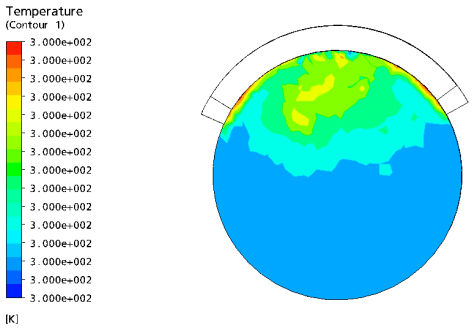

a. Temperature contours at mid-plane, 1°CA

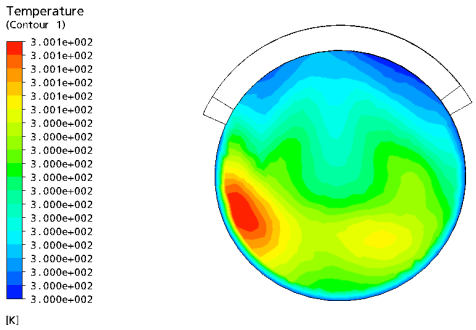

b. Temperature contours at mid-plane, 45°CA

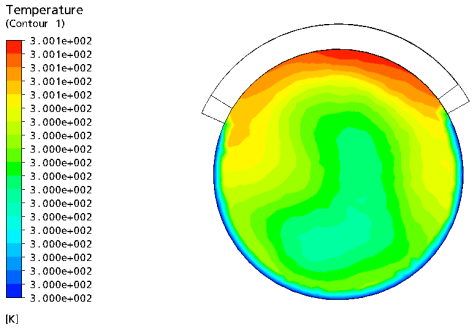

c. Temperature contours at mid-plane, 90°CA

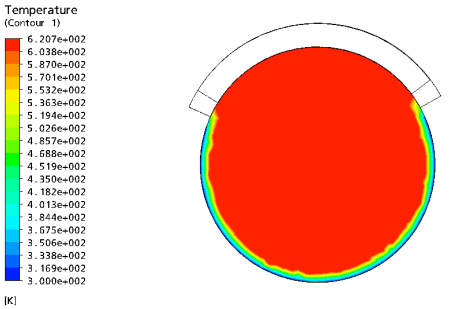

d. Temperature contours at mid-plane, 180°CA

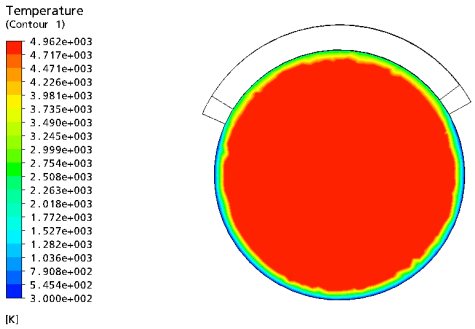

e. Temperature contours at mid-plane, 245°CA

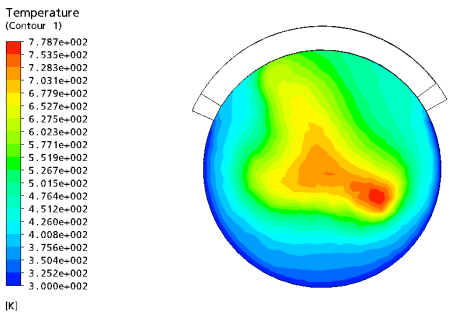

f. Temperature contours at mid-plane, 330°CA

Figure 5.13: The temperature contour plots of the uniport, polynomial profile cam-plate engine, plotted for different crank angles

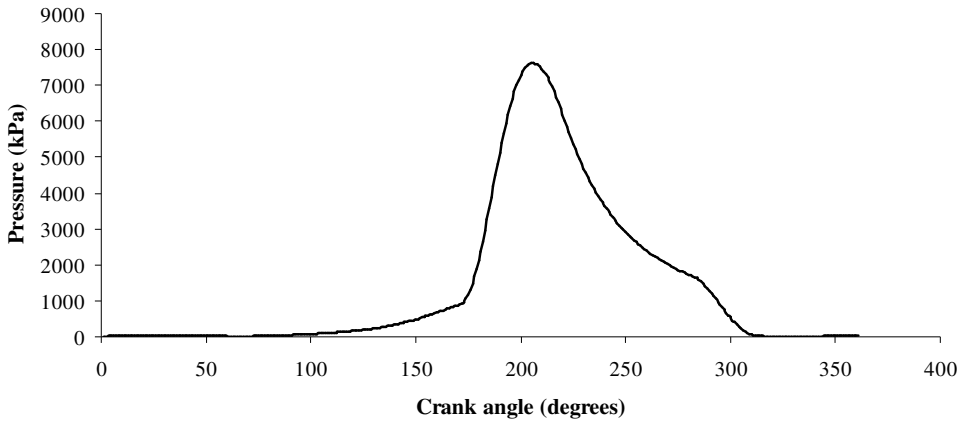

Figure 5.14: Pressure vs CA plot for multiport, sinusoidal cam-plate engine

Figure 5.15 shows the variation in mass flow rate for the particular engine configuration. The multiport model predicted considerably higher mass flow rate as compared to the single port model for the same boundary flow conditions. The volumetric efficiency was observed to be around 95.3%, which is quite appreciable as compared to the previous models. Slight discrepancies that are visible in the starting region of the cycle might be because the engine model ran for one cycle only, and so the initial assumptions made for the model caused the discrepancies in the beginning of the cycle. A few more runs of the same model with reference to the previous run results may hopefully solve this issue. However, this was not performed here, as the server does not seem to support the idea of using previous run results as initial values for another run.

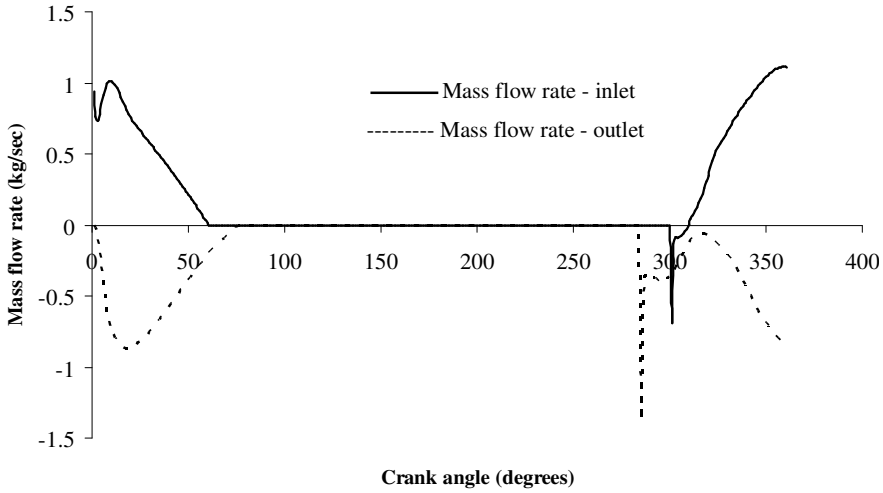

Figure 5.15: Mass flow rate vs CA plot for multiport, sinusoidal cam-plate engine

The discrepancy in the initial part of the cycle (Figure 5.16) is due to the high level of turbulence in the system due to entry of working fluid from all the ports into the cylinder, which sets up a complicated flow pattern. The turbulence effects during the cycle running time are not significantly high as shown in the diagram. The other discrepancy observed at around 270^{o}CA is because of the opening of ports after the expansion stroke.

In Figure 5.17, the pressure profile is plotted at the middle plane inside the cylinder for different crank angle positions. A high-pressure spot is observed to exist at the centre of the combustion chamber throughout the cycle of operation. As the pistons come closer, the high-pressure spot expands, and finally it spreads out in the entire cylinder. The working fluid is seen to undergo constant rotary motion inside the combustion chamber. To a certain extent, this phenomenon is desirable as it will ensure proper mixing of air-fuel mixture and promote flame propagation. However, if this goes out of control it can lead to early flame extinction and resulting flameout that is not desirable for proper functioning of the engine.

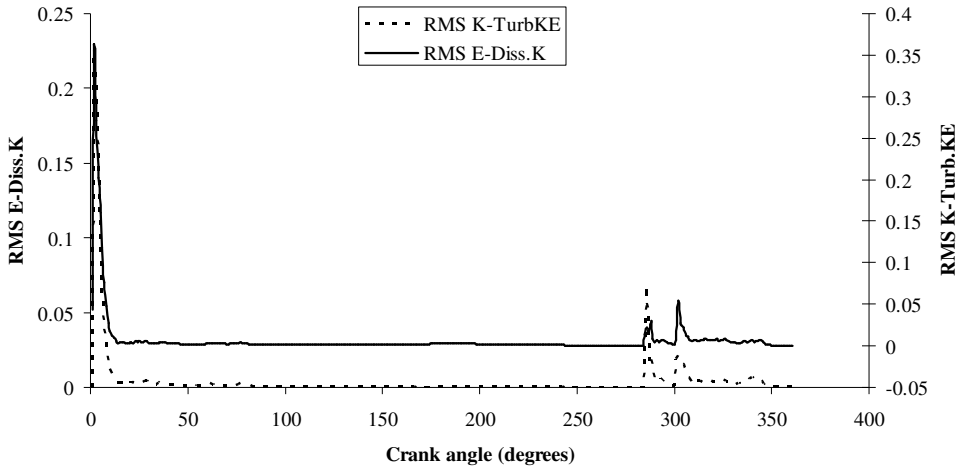

Figure 5.16: The RMS values of turbulence and eddy dissipation, plotted for multiport, sinusoidal profile cam-plate engine

5.6.2 Polynomial profile piston motion

The multiport engine model with polynomial profile guided piston motion is discussed now. The procedure of analysis is similar to that used in the uniport

polynomial profile cam-plate engine model. The geometry and all the features of the previous model are the same as used in this model.

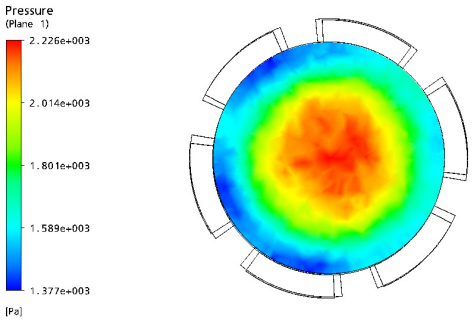

a. Pressure contours at cylinder mid-plane, 1°CA

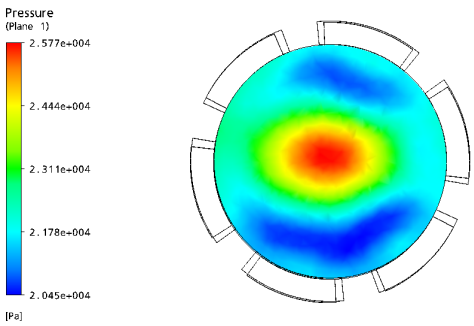

b. Pressure contours at cylinder mid-plane, 45°CA

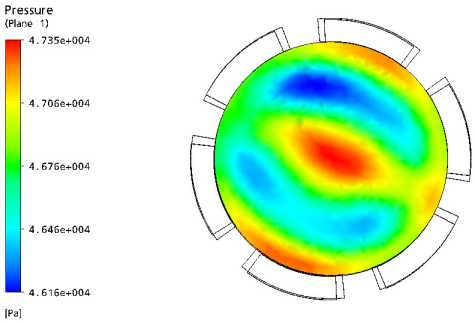

c. Pressure contours at cylinder mid-plane, 90°CA

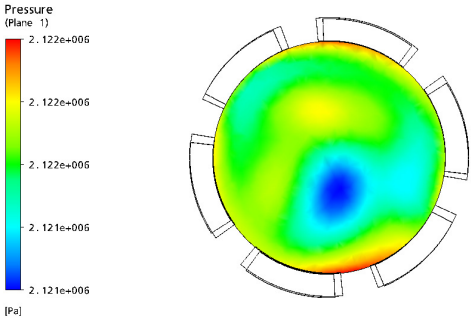

d. Pressure contours at cylinder mid-plane, 180°CA

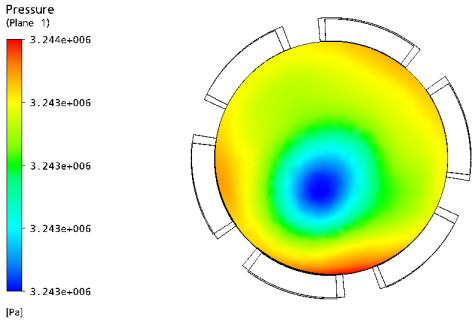

e.Pressure contours at cylinder mid-plane, 245°CA

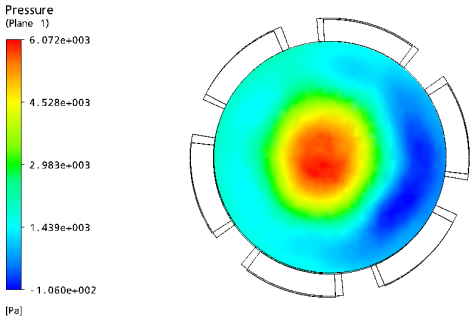

f.Pressure contours at cylinder mid-plane, 330°CA

Figure 5.17: The in-cylinder pressure distribution, plotted for multiport, sinusoidal cam-plate engine at different crank angles

In Figure 5.18, similar to that observed in the uniport engine analysis, the polynomial cam-plate model also predicted a low pressure compared to the sinusoidal motion model. The reason for this is the slower rise of piston in the polynomial model compared to sinusoidal motion model. The predicted peak pressure is around 6.36 MPa, which is 1 MPa lower than that of the sinusoidal motion model.

Figure 5.19 shows the result for a single run. A further run using the current results can remove the initial assumption errors for the model. Similar to the previous model analysis, the negative flow observed at the inlet port soon after the ports opened is due to the high pressure prevailing inside the cylinder volume. A high initial flow is observed at the exhaust port as soon as it is opened during the exhaust stroke, which then settles to flow driven by pressure gradients.

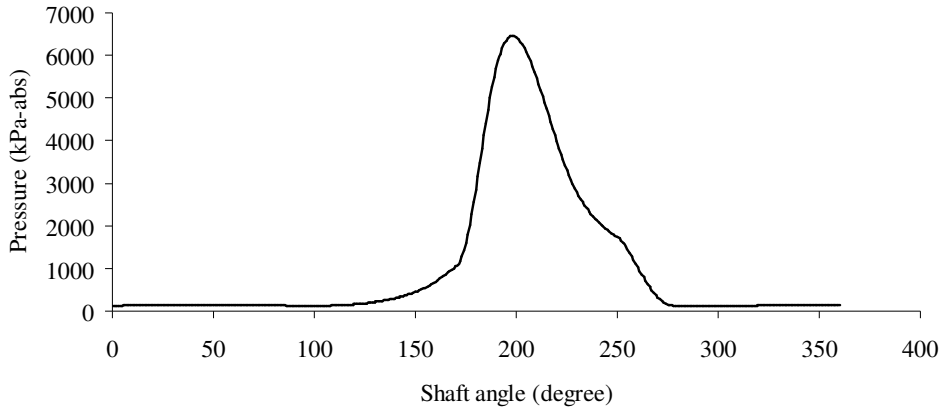

Figure 5.18: Pressure vs CA plot for multiport, polynomial cam-plate engine

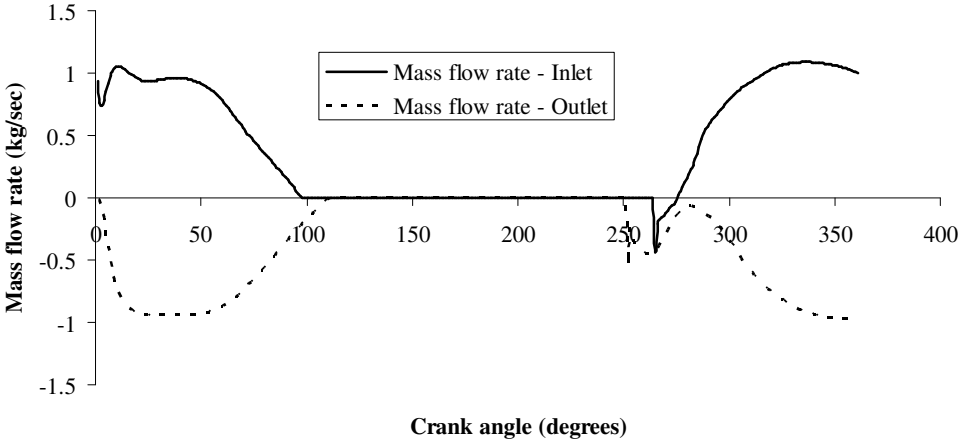

Figure 5.19: Mass flow rate vs CA plot for multiport, polynomial cam-plate engine

Figure 5.20 shows the turbulence effects predicted by the CFD model. The high level of in-cylinder turbulence predicted in the beginning of the cycle is probably due to the inlet flow disturbances in the model. A slight discrepancy is again visible in the cylinder during opening of ports after the expansion stroke similar to that observed in the previous model analysis. No significant turbulence effects are visible during the compression and power strokes.

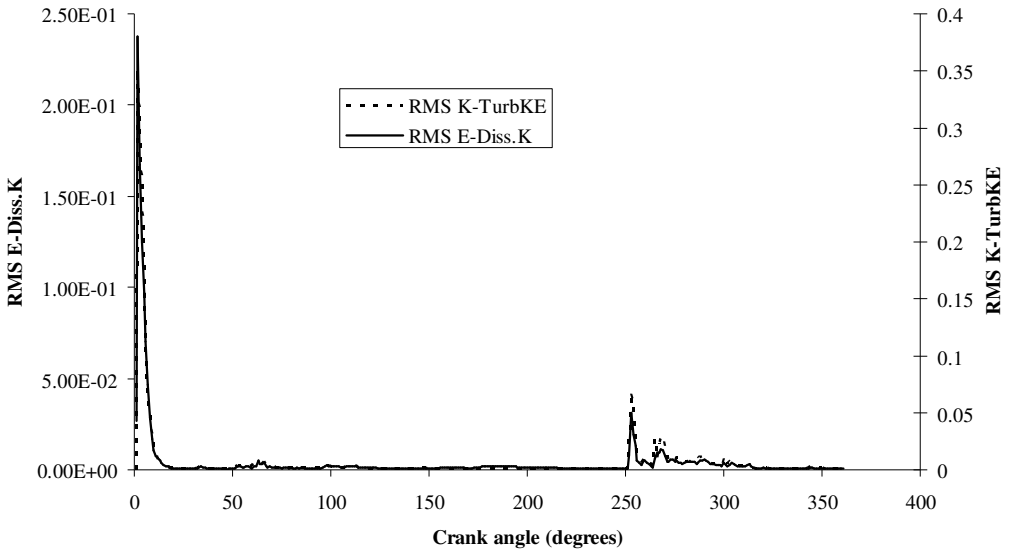

Figure 5.20: The RMS E-Diss.K and, plotted for multiport, polynomial profile cam-plate engine at different crank angles

From Figure 5.21, the pressure plots obtained here compared against the results from sinusoidal profile guided piston motion to draw conclusions. The pressure distribution predicted inside the cylinder is different for both the models as clearly visible from the pressure plane plots. A high-pressure spot is visible in the beginning of suction stroke at the cylinder centre. This high-pressure spot later spreads out evenly inside the cylinder. The effect of piston motion on pressure development is therefore confirmed from the plots below.

The velocity plots at the middle plane of the combustion chamber at various crank angles are shown in Figure 5.23. The in-cylinder velocity is very small initially, and later increases considerably to some value of around 106.8 m/sec, and then drops to a tenth of that value as the pistons reach TDC position. During the expansion stroke,

the velocity is small initially, and as pistons advance towards BDC the velocity is observed to be increasing to a maximum value of 237.9 m/sec at around 330^{o}CA.

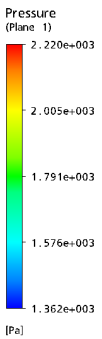

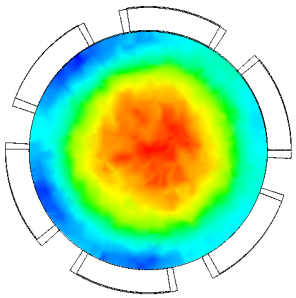

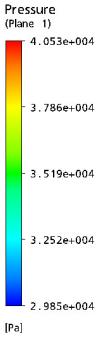

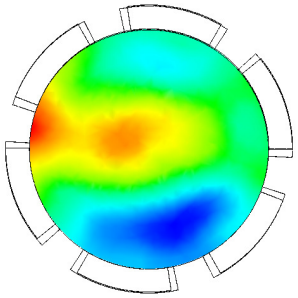

a. Pressure contours at cylinder mid-plane, 1^{o}CA b. Pressure contours at cylinder mid-plane, 45^{o}CA

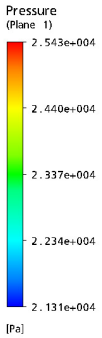

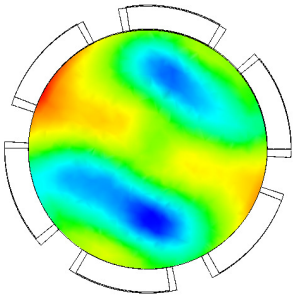

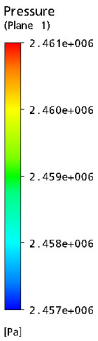

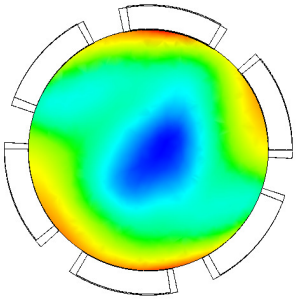

c.Pressure contours at cylinder mid-plane, 90^{o}CA d.Pressure contours at cylinder mid-plane, 180^{o}CA

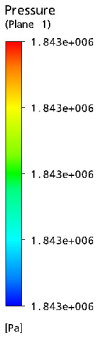

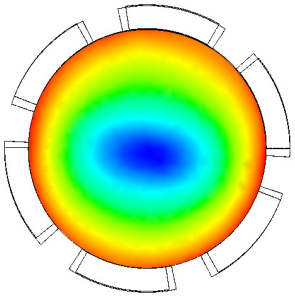

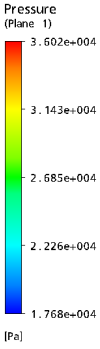

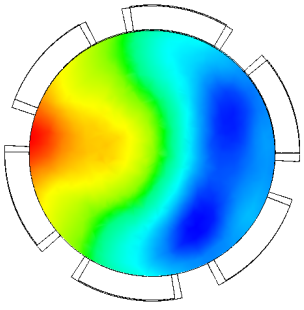

e.Pressure contours at cylinder mid-plane, 245^{o}CA f.Pressure contours at cylinder mid-plane, 330^{o}CA

Figure 5.21: The pressure plots in the middle plane, plotted for multiport, polynomial cam-plate engine at different crank angles

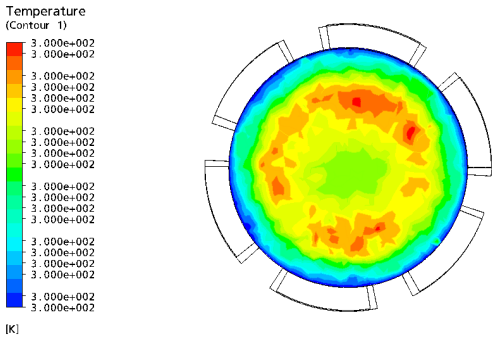

a. Temperature contours at mid-plane, 1°CA

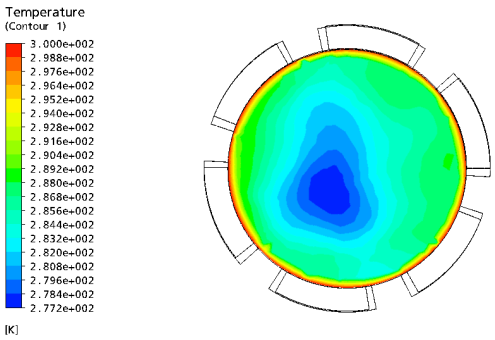

b. Temperature contours at mid-plane, 45°CA

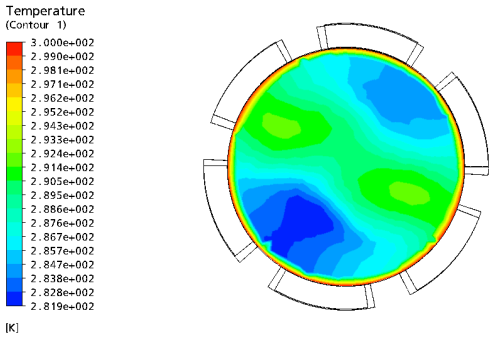

c. Temperature contours at mid-plane, 90°CA

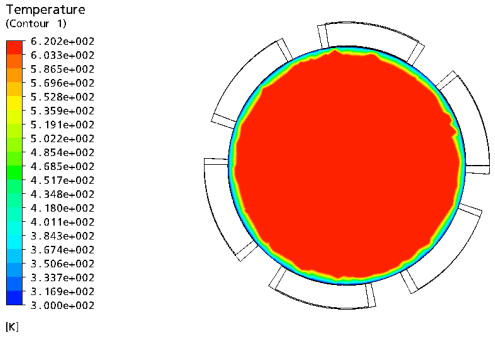

d. Temperature contours at mid-plane, 180°CA

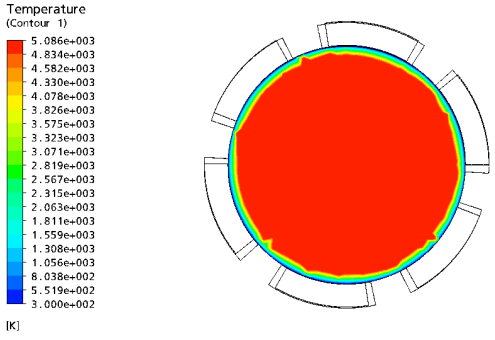

e. Temperature contours at mid-plane, 245°CA

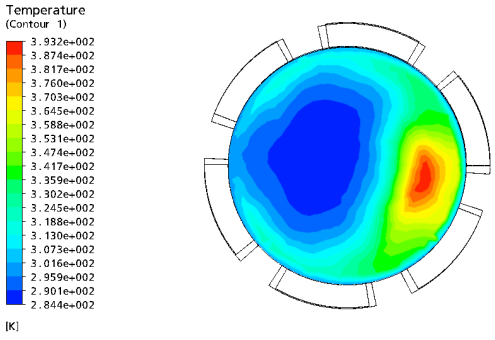

f. Temperature contours at mid-plane, 330°CA

Figure 5.22: The local temperature plots in the middle plane, plotted for multiport, polynomial cam-plate engine at different crank angles

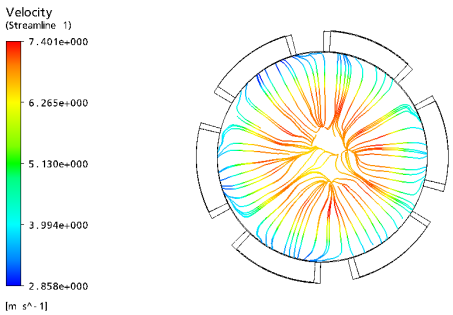

a. Streamline plot at cylinder mid-plane, 1°CA

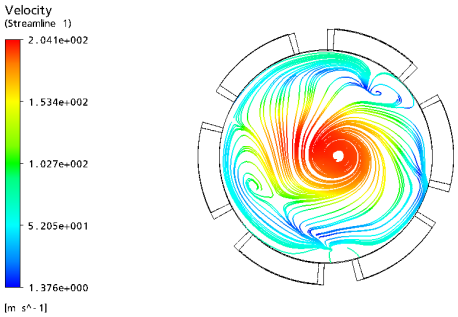

b. Streamline plot at cylinder mid-plane, 45°CA

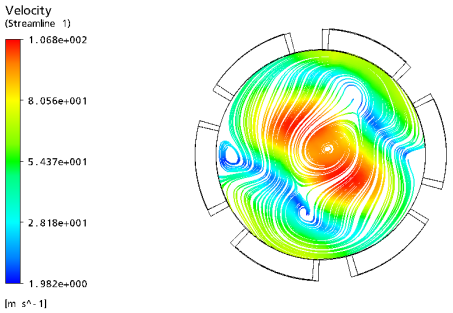

c.Streamline plot at cylinder mid-plane, 90°CA

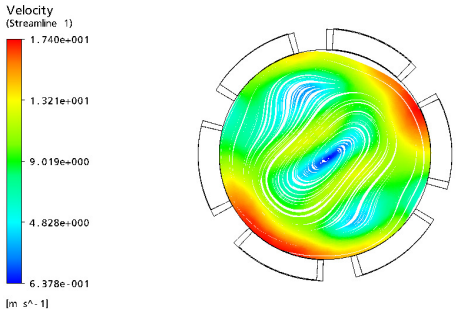

d. Streamline plot at cylinder mid-plane, 180°CA

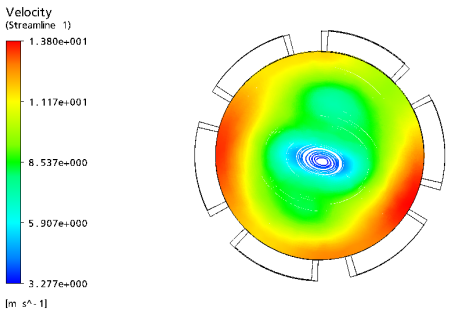

e. Streamline plot at cylinder mid-plane, 245°CA

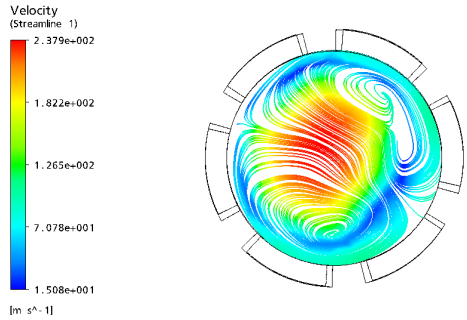

f. Streamline plot at cylinder mid-plane, 330°CA

Figure 5.23: The velocity streamlines as plotted in the middle plane of the cylinder for multiport, polynomial cam-plate engine at different crank angles

The swirling motion generated is clearly visible in the Figure 5.23 (b). A single vortex is formed initially, which intensifies as the piston approaches TDC. During the expansion stroke, at 330°CA two vortices are visible. Vortex motion plays a major role in the proper mixing, combustion and functioning of the engines (Horrocks, 2001).

5. 7 Summary

The geometry modelling of the engine is explained. Meshing of the model done using tetrahedral mesh is discussed. Important boundary conditions and parameters used in the model are explained. Domain Source Modelling as a potential method for initial stage process modelling of the engine instead of the expensive combustion modelling in CFD is detailed. An analysis of uniport models and multiport models is carried out using CFD. The significant advantage of polynomial cam-plate guided motion over sinusoidal profile guided piston motion is established. Results from the analysis are presented. The important results obtained are further compared between different models in detail in chapter 7.

Chapter 6

COMBUSTION MODELLING USING SIM AND EDM/FRC MODELS

The Domain Source Model (DSM) is introduced in this thesis as an initial step for modelling combustion in IC engines. However, the DSM method is not capable of producing a complete combustion simulation. As discussed earlier the DSM replaces the actual combustion process in engine with energy addition. The DSM model uses air as an ideal gas as the working fluid, and so does not predict the combustion products or after burn effects.

For a detailed analysis of the premixed-combustion in the CFD model, Eddy Dissipation Model/Finite Rate Chemistry (EDM/FRC) or Spark Ignition Model (SIM) should be used. The SIM is a latest addition to CFX and to most of the CFD tools. The EDM/FRC model has been in use for quite some time. Preliminary works are already done to use these models to simulate combustion in the present CFD model. Due to strict time and resource limitations, it was not possible to implement these models in this thesis as complete combustion simulations.

6. 1 Spark Ignition Model (SIM)

CFD simulation using SIM is expected to deliver results that are comparable with the experimental results. Unlike the other methods of combustion modeling, the SIM has an integrated spark ignition feature that can be used to locate the position of the spark plug. In CFX the SIM model is incorporated with the Burning Velocity Model (BVM) that can handle both the premixed and partially premixed combustion reactions.

The geometry of the CFD model used here is the same as that discussed for the DSM simulation of a multiport engine. The piston motion of the CFD model is based on profile of polynomial cam-plate. The $k-\varepsilon$ model is used for turbulence modelling

in the system. The BVM model works only with flamelet library(FLL) mixtures. The CFX-RIF tool is necessary to create FLL fuel mixtures, otherwise one can use only the two sample fuel mixtures available in the CFX, the Hydrogen–Air mixture and Methane-Air mixture.

Several attempts were made to use the Methane-Air mixture in the BVM model. After several simulation attempts it was observed that a proper combustion is not achievable with the available fuel mixture. However, the spark ignition was successfully simulated using BVM model. Some of the results obtained from the initial stage of this model are presented here. The spark ignition kernel is specified at the centre of the cylinder volume by specifying the coordinates. As seen in Figure 6.1, the temperature distribution inside the cylinder domain at different crank angles.

As seen in Figure 6.1, spark ignition is achieved at the specified kernel location, at the set time, using BVM model. However, proper combustion of air-fuel mixture could not be incorporated to produce pressure rise as predicted by the DSM and analytical models. With the availability of enough time and resources the SIM simulation can be achieved, and an initial guess is that the method is quite promising in engine performance predictions.

Figure 6.1 shows the temperature plots at the cylinder middle plane for this model. The spark ignition is visible in Figure 6.1 (e), and the flame propagation is shown in Figure 6.1 (f, g & h). The intensity of the flame front is quite low as seen in the diagram, and this is possibly due to the improper air-fuel mixture used in this model for combustion reaction. A proper air-fuel mixture is needed for the successful modelling of combustion in the BVM model.

6. 2 Eddy Dissipation/Finite Rate Chemistry (EDM/FRC)

Simulation using combined EDM/FRC is also in the early stage of development. The theory behind this model is discussed in chapter 4 and so is not repeated here.

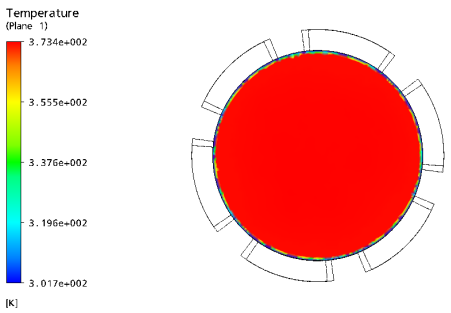

(a) Temperature contours at mid-plane, 1°CA

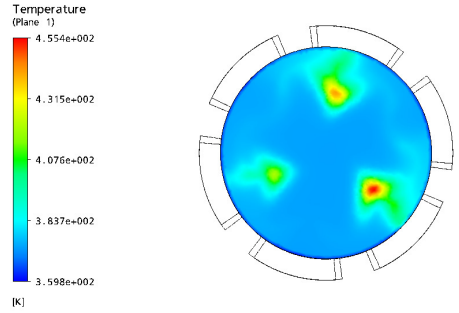

(b) Temperature contours at mid-plane, 45°CA

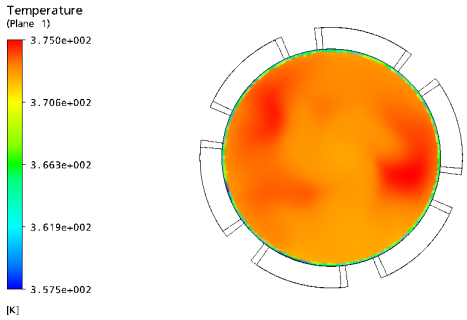

(c) Temperature contours at mid-plane, 90°CA

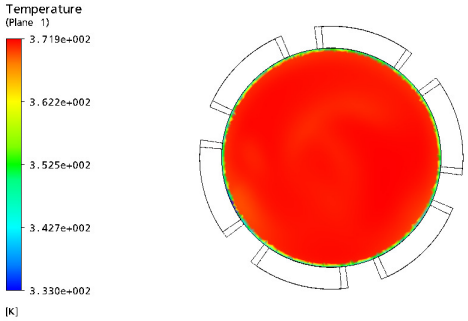

(d) Temperature contours at mid-plane, 165°CA

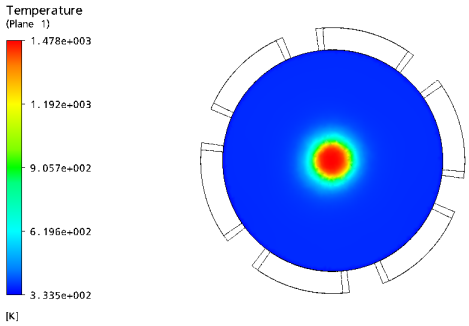

(e) Temperature contours at mid-plane, 171°CA

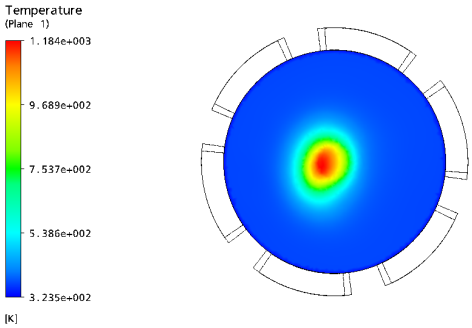

(f) Temperature contours at mid-plane, 180°CA

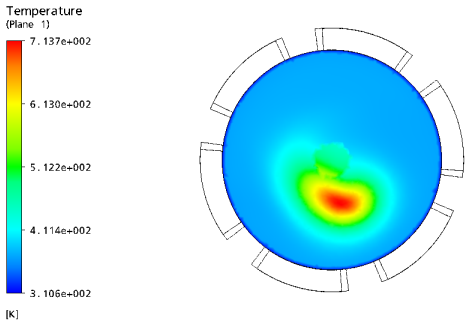

(g) Temperature contours at mid-plane, 210°CA

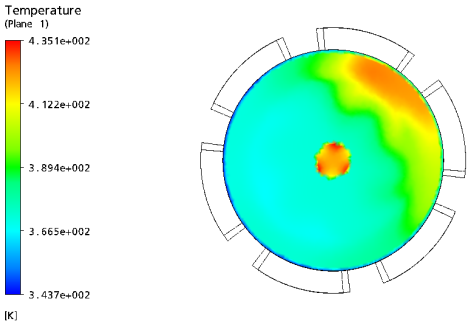

(h) Temperature contours at mid-plane, 290°CA

Figure 6.1: The temperature contours plotted for the Spark Ignition Model (SIM)

Methane-Air mixture is used as the working fluid in this model, and this is a predefined fuel available in CFX. A heat source is specified for initiating reaction as the EDM/FRC model needs initiation of reaction using some energy source. A smeared volume is assumed so that the reaction progress smoothly in the combustion volume. As discussed in the CFX manual a hyperbolic tangent function is used for modelling reaction and flame propogation (ANSYS, 2006).

A subdomain is created to apply the energy source to activate the reaction at a preset time. A maximum flame temperature of 5000K is assumed in order to avoid the model becoming unstable under high reaction conditions. The combustion model assumed a simple reaction between CH_4 and O_2 to produce CO_2 and H_2O, and NO is set as constraint. The model did not successfully predict the combustion yet with the available air-fuel mixture. This led to the conclusion that both the BVM and EDM/FRC models need to use a properly defined air-fuel mixture, which can be developed using CFX-RIF.

6. 3 Summary

The SIM and EDM/FRC methods of combustion modelling seemed to be quite promising for the current application. In these models, a reacting air-fuel mixture can be used that resembles the actual combustion working fluid. With the currently available time and resources, it was not possible to achieve these objectives. Furthermore, any chances to incorporate experimental analysis to validate the CFD and analytical results can confirm the acceptability of the discussed DSM, EDM/FRC, BVM, and analytical models in IC engine analysis.

Chapter 7

COMPARISON OF CAM-PLATE ENGINE MODELS

This chapter discusses the results obtained from the Domain Source Model (DSM). A comparison of results based on port configuration and piston motion configuration is performed. Conclusions are drawn about based on which model gives the most reasonable performance and results.

7. 1 Comparison based on port configuration

Based on the port configuration we have uniport engine models and multiport engine models for comparison. In the earlier discussion of port configuration, the disadvantages of uniport design were discussed and so are not repeated here. The comparison of results is presented in the form of in-cylinder pressure and mass flow rate through ports.

The uniport and multiport configurations are compared for sinusoidal piston motion configuration. Figure 7.1 shows that both models have almost the same pressure variation with crank angle even if they predicted slightly different values of peak pressure. Both models predicted similar pressure values at critical areas like combustion and expansion. However, the multiport model has an advantage over the uniport model due to the practical shortcomings in applying uniport model for operation.

From Figure 7.2, it can be observed that the multiport model predicts more mass flow rate than the uniport model for the same port open area. This is more evident from the analysis of numerical model results obtained. The uniport model predicted only one third of the mass of gas inside the cylinder domain as compared to the multiport model. This can significantly affect the engine model performance.

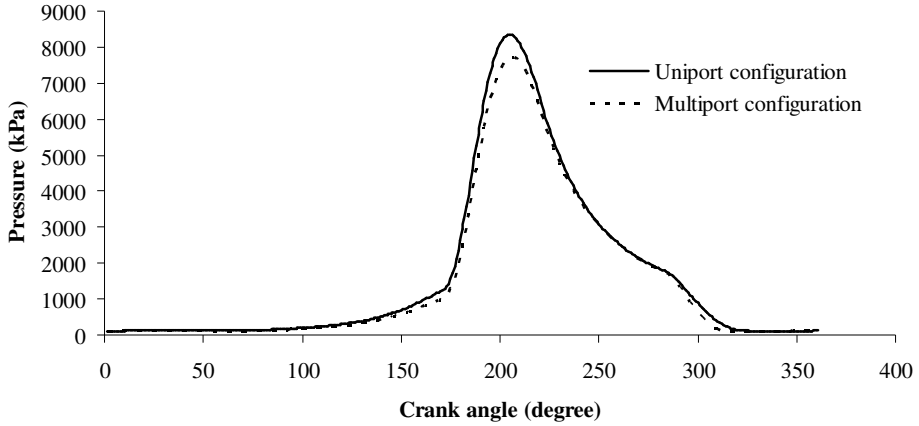

Figure 7.1: Pressure vs CA plot for the uniport and multiport engine models using sinusoidal cam-plate

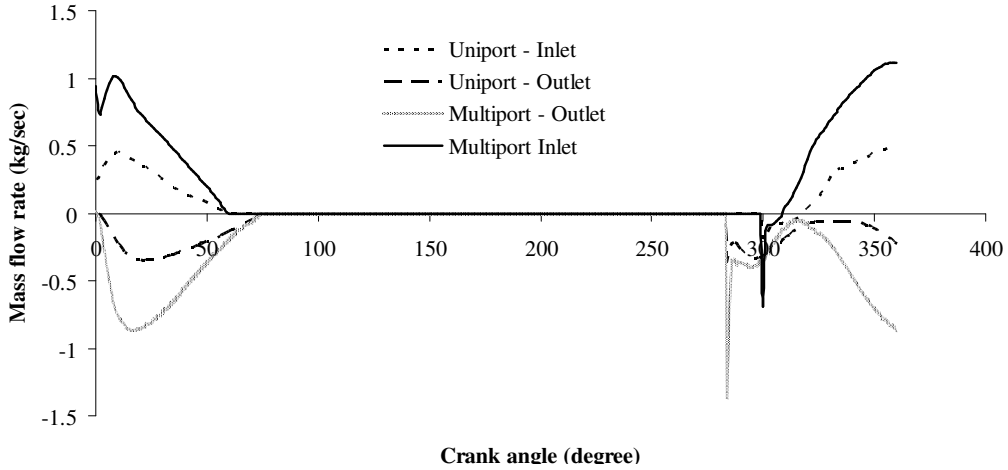

Figure 7.2: Mass flow rate vs CA plots for uniport and multiport engine models using sinusoidal cam-plate

It can be seen in Figure 7.3 that the pressure - crank angle diagram predictions are very similar to those for sinusoidal piston motion engine models. The uniport model predicted slightly higher pressure compared to the multiport model for the same configuration. The pressure profile looks very similar for both the models. Even though both the profiles have different rise and fall rate, this does not seem to have significant influence over the pressure diagram.

Figure 7.4 shows that the mass flow rate diagram is very similar to that observed for the sinusoidal motion models. The multiport model predicted a higher mass flow rate than the uniport model. The slight discrepancies visible for all the models are due to

the initial assumptions made for these models, which could have been avoided if the model was run for another cycle.

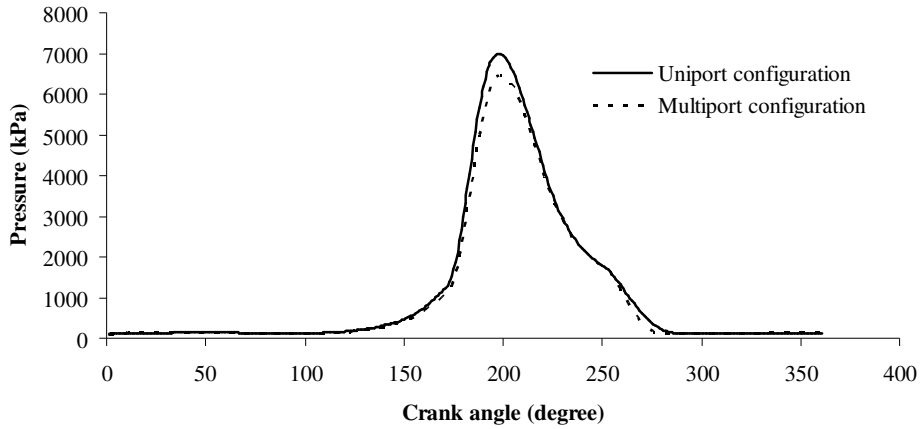

Figure 7.3: Pressure vs CA plots for the uniport and multiport engine using polynomial cam-plate profile

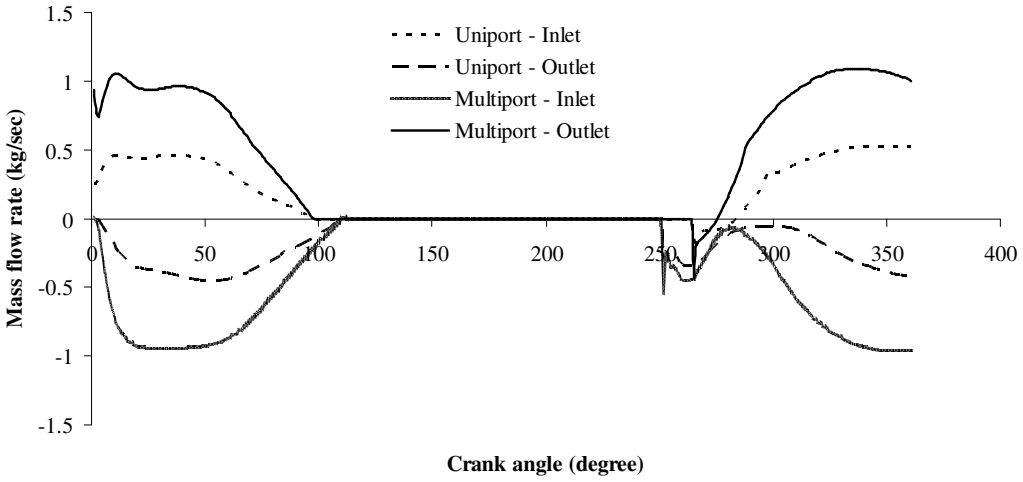

Figure 7.4: The inlet and outlet mass flow rates through ports for uniport and multiport engine using polynomial cam-plate profile

7. 2 Comparison based on piston motion configuration

Here, the in-cylinder pressure and mass flow rate through ports are compared based on piston motion configuration. Separate analysis is performed for the uniport and multiport models with sinusoidal and polynomial cam-plate guided piston motions.

From Figure 7.5, it is clear that both models predict the expansion stroke of the cycle differently. The sinusoidal profile-guided piston motion predicts a higher peak pressure compared to the polynomial profile guided piston motion configuration even if they have same stroke length. The reason could be that in the case of sinusoidal profile guided motion, the piston motion curve is steeper, the amount of mass inflow is less, and consequently the temperature predicted inside the cylinder is higher. These can lead to a higher pressure inside the cylinder. However, the profile of both the pressure curves is almost similar.

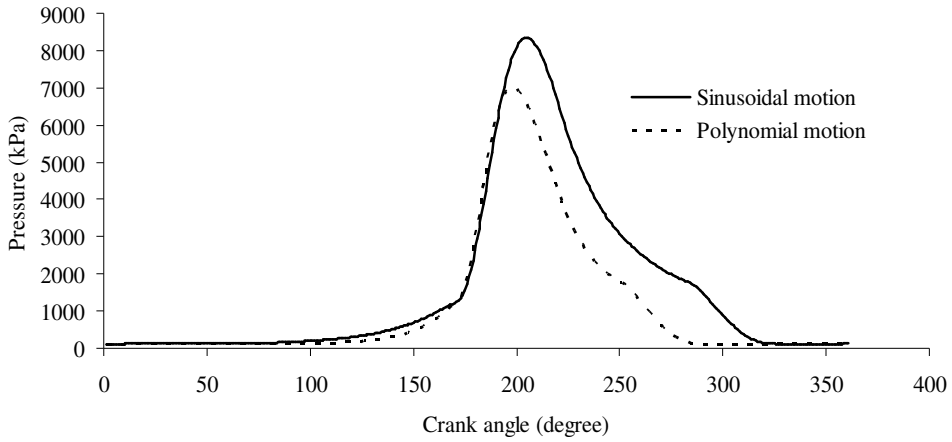

Figure 7.5: Pressure vs CA plots for uniport engine with sinusoidal and polynomial cam-plate profiles compared

The mass flow rate at the inlet and outlet ports of the uniport model for sinusoidal and polynomial profile-guided piston motion configurations are shown in Figure 7.6. The polynomial cam-plate engine ports close after the sinusoidal cam-plate engine ports close, and again they open prior to the sinusoidal cam-plate engine ports. This helps to draw in more air and increase the volumetric efficiency that helps to achieve lean mixture possible in polynomial profile guided piston motion engines. The negative flow visible for the inlet ports of both the engine configurations after expansion stroke is due to the high pressure inside the cylinder soon after combustion stroke.

The pressure – crank angle diagram shown in Figure 7.7 is similar to that obtained for the uniport engine in Figure 7.5. The reasons for the lower pressure values predicted by the polynomial cam-plate engine compared to sinusoidal cam-plate

engine are the same as discussed in the earlier section. The peak pressure is reached earlier in the case of the polynomial profile guided engine compared to the other one. This means that the piston velocity of polynomial cam-plate engine is higher as compared to the sinusoidal cam-plate engine.

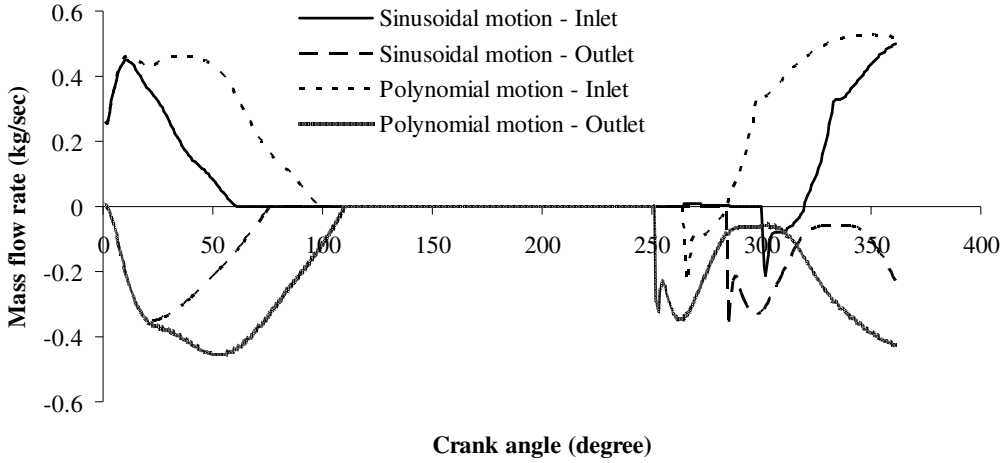

Figure 7.6: Mass flow rate through ports of the uniport engine configuration with sinusoidal and polynomial cam-plate engine

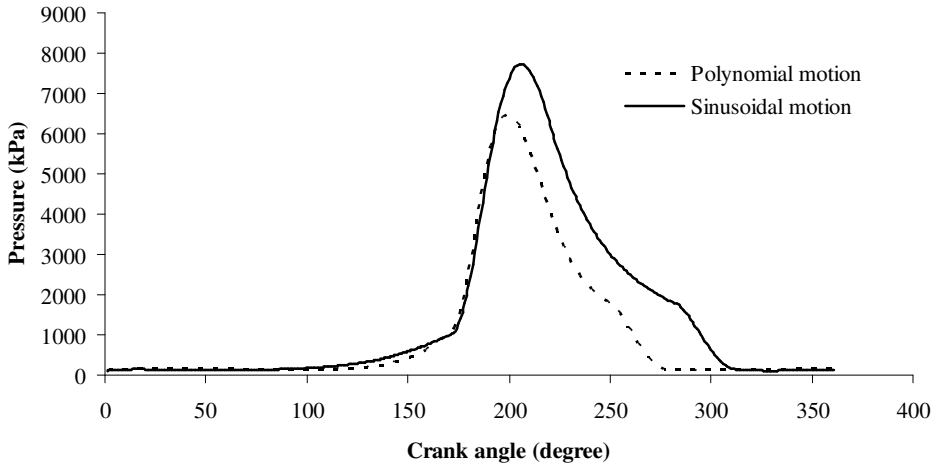

Figure 7.7: Pressure vs CA plots for multiport engine configuration with sinusoidal and polynomial cam-plate engine

Figure 7.8 shows that the polynomial profile cam-plate engine ports close slowly and open faster compared to the other one. In both methods, soon after the power stroke, it is predicted that the inlet ports have some reverse flow due to high pressure inside

the cylinder domain. The mass flow rate of working fluid entering the polynomial cam-plate engine is higher as compared to the sinusoidal cam-plate engine. The mass flow rates at the outlet ports in Figure 7.8 are zero initially, which is due to the initial assumptions made.

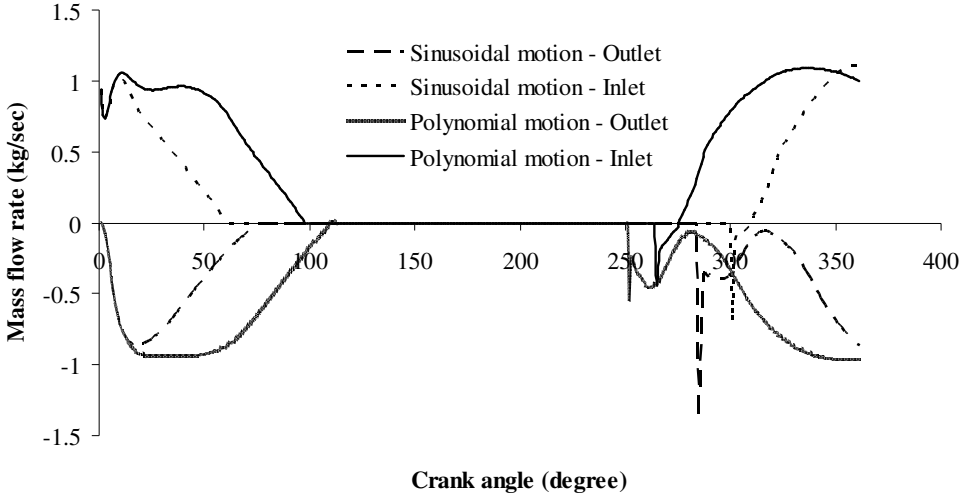

Figure 7.8: Mass flow rate through ports of the multiport engine configuration with sinusoidal and polynomial cam-plate engine

7. 3 Comparison of analytical and CFD models

The results obtained from the CFD analysis and analytical model analysis are compared. After the analysis of CFD results, the multiport engine model with polynomial cam-plate is the best choice for further discussion. Slight discrepacies are expected in the CFD model results as the simulation was run for one cycle only, while in the case of analytical model, four cycles were run to optimise the final results.

Both the analytical and CFD models predict almost same pressure values, and the variations over crank angles for both the models look similar. The analytical model predicts an early rise in pressure as compared to the CFD model. The spreadsheet model do not consider turbulence effects and other dynamic loads on the system. It is observed that that CFD model predicted higher mass flow rates to the system compared to the analytical model. These factors might have influenced the behavior of both the models.

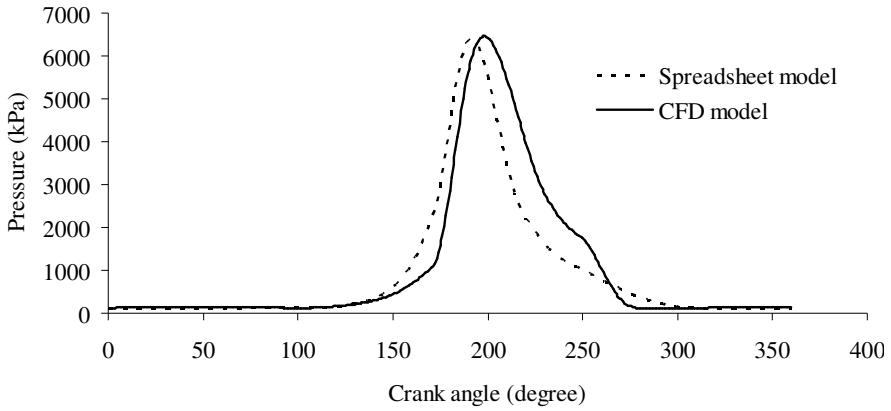

Figure 7.9: Pressure vs CA plots from CFD and analytical models compared

The temperature distribution predicted by the analytical model was observed to be well below that predicted by the CFD model as shown in Figure 7.10. The slight drop in temperature visible for the spreadsheet model at around 210^{o}CA might be due to the increased heat transfer immediately after combustion. The higher temperature prediction for the CFD model is linked to the less mass of air inside the CFD model. With less mass, the same fuel energy supplied to CFD model is distributed over a smaller air mass, and so the temperature predictions are higher for CFD model based on the air ideal gas equation.

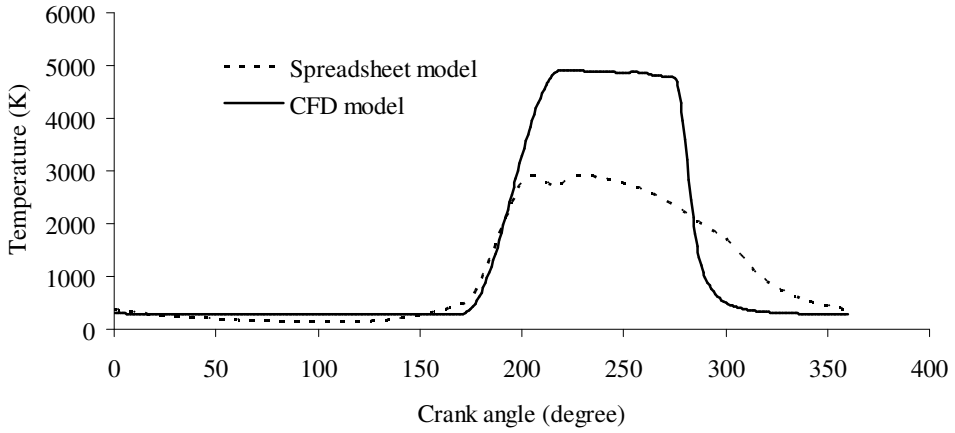

Figure 7.10: Temperature vs CA plots from CFD and analytical models compared

Figure 7.11 shows that the mass flow rate predicted by the CFD model is higher than that predicted by the analytical model. This means that the quantity of working fluid is smaller in the analytical model as compared to the CFD model. The temperature

and pressure characteristics inside the engine model are influenced by the amount of working fluid inside the combustion chamber and hence the mass flow rate.

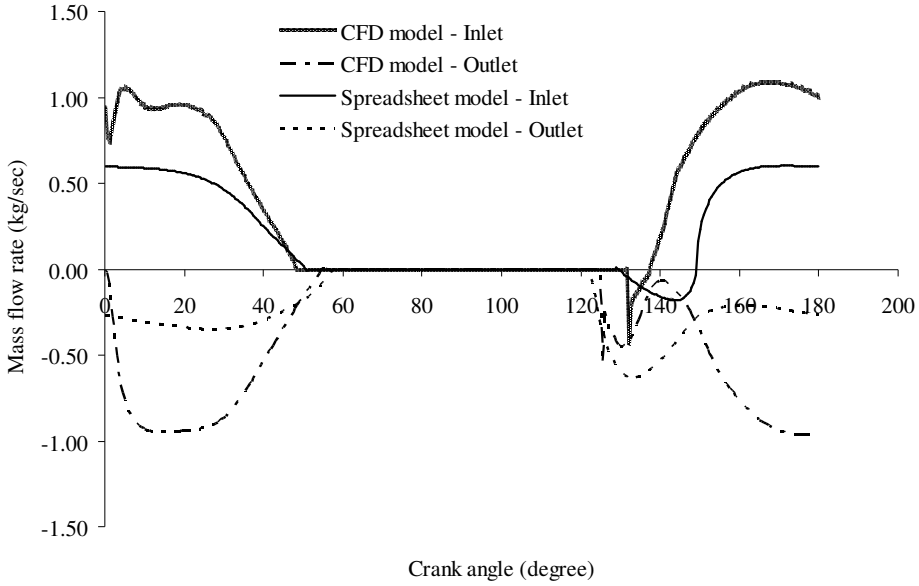

Figure 7.11: Mass flow rate through inlet and outlet ports, plotted from CFD and analytical model compared

Both the analytical model and CFD model predict negative flow at the inlet port boundary as the port is opened at the end of expansion stroke. The reason, as we have already noted several times in this thesis, is due to the high pressure inside the cylinder domain after the combustion stroke. The discrepancy due to single run performed on the CFD model is visible in the diagram.

7. 4 Summary

In this chapter, comparisons of engine operating characteristics were made based on the piston motion configuration and ports configuration, and conclusions are drawn. In an IC engine process cycle it is desirable that the maximum pressure is achieved rapidly so that the maximum power can be extracted from the system before the exhaust port opens. This can be easily achieved using a polynomial cam-plate engine as evident from the results discussed in Figures 7.5 and 7.7. In addition, it was observed that the multiport engine model has a higher volumetric efficiency and allows use of a very lean combustion mixture compared to the sinusoidal cam-plate

engine. Comparison of Figures 7.6 and 7.8 proved that the polynomial cam-plate engine design helps to draw in comparatively higher amount of charge as compared to the sinusoidal cam-plate piston motion configuration.

The analytical model was compared with the multiport polynomial cam-plate engine CFD model, and it was observed that both models match in their operation characteristics. Some slight differences observed are due to the assumptions made in the models, complexities of the models, different equations used to define parameters etc. The CFD model is observed to be quite good in predicting the operation characteristics accurately. Compared to the polynomial cam-plate guided piston motion configuration, it is observed that the conventional crankshaft guided engine do not have the advantage of control over the engine operation cycles. Moreover, the crankshaft based engine has more moving parts than a simple cam-plate guided engine which introduces more losses and increased chances to get damaged, and requires a bigger crankcase to occupy the entire crankshaft assembly.

Chapter 8

CONCLUSIONS AND RECOMMENDATIONS

This chapter discusses the main outcomes of the current research, the conclusions drawn and the possible future works on Opposed Piston engine.

8. 1 Outcomes of the current research

This study presents research conducted by the author on an opposed-piston IC engine using analytical and CFD modelling. Mainly three different methods of combustion modelling were studied: the Domain Source Model (DSM), combined Eddy Dissipation Model/Finite Rate Chemistry (EDM/FRC), and Spark Ignition Model (SIM)/Burning Velocity Model (BVM). The BVM and EDM/FRC methods of combustion modelling are still in the development stage and were not fully applied. As a result these models are not discussed much in this thesis. The DSM results were discussed in Chapters 5 and 7.

The DSM method of modelling is introduced with the intention of modelling the IC engine process cycle in the simplest way so as to check the mesh, geometry and boundary conditions before applying the more complicated combustion models. The model is successfully validated against analytical model results, and found that the idea can be applied in similar methods of combustion analyis. Also, the analytical model has been proved versatile in that it gives quite lot of information needed for modelling and comparing the CFD model, and provides an easy way of engine process analysis for a user who is not an expert in CFD analysis and do not have access to experimental results. The analytical model can virtually handle any configuration of the engine and predict engine operation characteristcs.

The BVM was attempted to apply on the engine model, but the task could not be finished in the limited time and with the limited resources available. It was observed that a flamelet library needs to be created for the reaction and reacting material to

model the combustion. This is possible only with the use of CFX-RIF, which is a standalone software that needs to be purchased. Since the project was not funded at the time of the course, purchasing additional resources was not feasible and the time limits were very stringent. However, some promising results were obtained, and they are presented in this thesis. SIM was achieved successfully even though complete combustion modelling was not achieved.

Application of EDM/FRC was also tried to apply on the present engine model. This model needs reaction activation using some energy source. A heat source is applied in the present model with the idea of smeared volume so that the combustion grows smoothly. However, this model did not work as expected. The combustion mixture did not combust at all. Since no time was available to further investigate the model the idea of using EDM/FRC was dropped for the time, but in a later stage can be hopefully achieved with some modifications in combustion activation and flame propagation section. If possible both the BVM and EDM/FRC models will be included in future publications by the author which will be based on the current thesis.

Achievements of the current thesis are:

- The advantages of a polynomial profile guided piston motion over sinusoidal profile guided piston motion is discussed and verified.
- The performance of multiport and uniport engine models are compared, discussed and verified.
- The multiport model was seen to be the best choice as it offers better volumetric efficiency, better cooling of engine parts using inlet air stream and allows lean mixture combustion.
- The multiple port model was found the best choice from the viewpoint of practical application of the engine model as otherwise will result in piston locking as discussed earlier.
- The CFD simulation of the cam plate engine is achieved and combustion is modelled using DSM model.

- Preliminary work for implementing complete combustion simulation using BVM and EDM/FRC models has been carried out.

8. 2 Future work

A lot of further analysis can be performed in the present model as a part of future work. The first priority should be to make the Spark Ignition Model (SIM) working so that the results from analytical model can be compared and validated. This is a tremendous task as the model needs the development of a combustible air-fuel mixture using software. Once the BVM model is achieved, the next target should be to make the EDM/FRC model working so that the BVM, DSM and analytical mode results can be checked against the EDM/FRC results. Also, as a part of future work experimental analysis of the engine is suggested so that the experimentally obtained results from the real engine can be then compared with the CFD and analytical model results to validate these models. Experimental validation of all CFD and analytical results is an important step to confirm that the mathematical predictions are correct.

REFERENCES

ABBOTT, M. B. (1989) *Computational fluid dynamics,* New York, Longman Scientific & Technical.

AFFES, H., TRIGUL, N., SMITH, D. & GRIAZNOV, V. (1998) Shape Optimization of IC engine ports and chamber. *SAE Special Publications*.

AGLAVE, R., REIDEL, U. & WARNATZ, J. (2008) Turbulence - chemistry interactions in CFD modelling of diesel engine. *Combustion Theory and Modelling,* 12**,** 303 - 323.

ANDERSON, J. D. (1995) *Computational fluid dynamics: the basics with applications,* New York, McGraw-Hill.

ANNAND, W. J. D. (1963) Heat Transfer in the cylinders of reciprocating Internal Combustion Engines *Proc. Inst. mech. Engrs.,* 177**,** 973 - 990.

ANNAND, W. J. D. & MA, T. H. (1970) Instantaneous heat transfer rates to the cylinder head surface of a small compression-ignition engine. *Pro.IMechE,* 185**,** 976-987.

ANNAND, W. J. D. & PINFOLD, D. (1980) Heat transfer in the cylinder of a motored reciprocating engine. *SAE paper*.

ANNAND, W. J. D. & ROE, G. E. (1974) *Gas flow in the Internal Combustion Engine,* Somerset, G T Foulis.

ANSYS (2006) ANSYS Documentation Notes. Mississippi.

ARMSSTRONG, L. V. & HARTMAN, J. B. (1959) *The Diesel Engine: Its Theory, Basic Design, and Economics,* New York, The Macmillan Company.

ARREGLE, J., LOPEZ, J. J., GARCIA, J. M. & FENOLLOSA, C. (2003) Development of a zero-dimensional Diesel combustion model Part 2: Analysis of the transient initial and final diffusion combustion phases. *Applied Thermal Engineering,* 23**,** 1319-1331.

BACKREEDY, R. I., FLETCHER, L. M., MA, L., POURKASHANIAN, M. & WILLIAMS, A. (2006) Modelling pulverised coal combustion using a detailed coal combustion model. *Combust.Sci. and Tech.,* 178**,** 763-787.

BARALDI, D., HEITSCH, M. & WILKENING, H. (2007) CFD simulations of hydrogen combustion in a simplified EPR containment with CFX and REACFLOW. *Nuclear Engineering Design,* 237**,** 1668-1678.

BARDINA, J. E., HUANG, P. G. & COAKLEY, T. J. (1997) Turbulence modeling, validation, testing and development. *NACA technical memorandum 110446.*

BARLOW, R. S. & FRANK, J. H. (1998) Effects of turbulence on species mass fractions in methane/air jet flames. *Proc. Combust. Inst. ,* 27**,** 1087 - 1095.

BATTIN-LECLERC, F., GLAUDE, P. A., WARTH, V., FOURNET, R., SCACCHI, G. & COME, G. M. (1999) Computer tools for modelling the chemical phenomena related to combustion. *Chemical Engineering Science,* 55.

BATTIN-LECLERC, F., GLAUDE, P. A., WARTH, V., FOURNET, R., SCACCHI, G. & COME, G. M. (2000) Computer tools for modelling the chemical phenomena related to combustion. *Chemical Engineering Sciences,* 55.

BAYRAKTAR, H. (2005) Experimental and theoretical investigation of using gasloine-ethanol blends in spark-ignition engines. *Renewable Energy,* 30**,** 1733-1747.

BENSON, R. S. (1960) Experiments on a Piston Controlled Port. *The Engineer*.

BENSON, R. S. & WHITEHOUSE, N. D. (1979) *Internal Combustion Engines,* New York, Pergamon Press.

BERNARD, C. & BARANESCU, R. (1999) *Diesel engine reference book,* England, Butterworth-Heinemann.

BLARIGAN, P. V. & KELLER, J. O. (1998) A hydrogen fuelled internal combustion engine designed for single speed/power operation. *Int. J. Hydrogen Energy,* 23**,** 603-609.

BORMAN, G. & NISHIWAKI, K. (1987) Internal - Combustion Engine Heat Transfer. *Prog. Energy Combust. Sci.,* 13.

BORMAN, G. L. & RAGLAND, K. W. (1998) *Combustion Engineering,* Madison, McGraw-Hill.

BOSE, T. K. (1988) *Computational fluid dynamics,* New York, Wiley.

BOYER, G. C. (1943) *Diesel and gas power plants,* New York, McGraw Hill.

BRAY, K. N. C. (1996) The challenge of turbulent combustion. *26th Symposium (International) on Combustion.* Pittsburgh, The Combustion Institute.

BREWSTER, K. (2003) Mustang-II Engine Choices.

BROATCH, A., MARGOT, X., GIL, A. & DONAYRE, C. (2007) Computational study of the sensitivity to ignition characteristics of the resonance in DI diesel engine combustion chambers. *International journal for Computer-Aided Engineering and Software,* 24.

BROEZE, J. J. (1963) *Combustion in Piston Engines: Spark-Ignition and Compression-Ignition,* Keulen, De Technische Uitgeverij H. Stam N.V.

BUSEMANN, A. (1933) *Die expansionsberichtichtigong der Kontactioziffer von Blenden*, Forsch. Ing. Wes.

CALLAGHAN, E. E. & BOWDEN, D. T. (1949) Investigation of flow coefficients of circular, square and elliptical orifices at high pressure ratios. *NACA technical note.*

CHEN, J. H., CARD, J. M., DAY, M. & MAHALINGAM, S. Direct Numerical Simulation of Tuubulent Non-premixed Methane-Air Flames. California, Department of Energy.

CHEN, Y. & SHIH, M.-H. (1997) CFD applications to internal combustion engine port-flow designs. *1997 ASME Fluids Engineering Division Summer Meeting.* ASME.

CHENG, X.-B., HUANG, R.-H., ZHI, W. & ZHU, M.-L. (2002) Experimental investigation and numerical modelling of spray combustion and emission in a diesel engine. *ICE Spring Technical Conference.* ASME.

CHIAVOLA, O. (2002) Multi-dimensonal CFD-transmission matrix modelling of IC engine intake and exhaust systems. *Joournal of Sound and Vibration,* 256**,** 835-848.

CHOW, P. H. P., WATSON, H. C. & WALLIS, T. (2006) Combustion in a high-speed rotary valve spark-ignition engine. *Proc. IMechE,* 221.

D'ERRICO, G. (2007) Prediction of the combustion process and emission formation of a bi-fuel SI engine. *Energy Conservation and Management,* 49**,** 3116-3128.

DAS, S. & CHMIEL, D. M. Computational and Experimental Study of In-cylinder Flow in a Direct Injection Gasoline (DIG) Engine. New York, Delphi Automotive Systems.

DELTIC, N. (1960) The DPS Gallery. The Deltic Preservation Society Limited.

DENT, J. C. & SULAIMAN, S. J. (1977) Convective and Radiative Heat Transfer in a High Swirl Direct Injection Diesel Engine. *SAE Trans,* 86.

DFD, D. T.-. (1947) Oldengine. Toledo's TBBS.

DIXON, T. F., MANN, A. P., PLAZA, F. & GILFILLAN, W. N. (2003) Development of advanced technology for biomass combustion - CFD as an essential tool. *Fuel,* 84**,** 1303-1311.

DRAKE, M. C., FANSLER, T. D. & LIPPERT, A. M. (2005) Stratified-charge combustion: modelling and imaging of a spray-guided direct-injection spark-ignition engine. *Proceedings of the Combustion Institute,* 30**,** 2683-2691.

DRAKE, M. C. & HAWORTH, D. C. (2007) Advanced gasoline engine development using optical diagnostics and numerical modelling. *Proceedings of the Combustion Institute,* 31**,** 99-124.

DURBIN, P. A. (2007) *Fluid dynamics with a computational perspective,* New York, Cambridge University Press.

ECKERT, E. R. G. (1950) *Introduction to the transfer of heat and mass,* New York, McGraw Hill.

FERZIGER, J. H. (1996) *Computational methods for fluid dynamics,* New York, Springer-Verlag.

FINOL, C. A. & ROBINSON, K. (2005) Thermal modelling of modern engines: a review of empirical correlations to estimate the in-cylinder heat transfer coefficient. *Proceedings of the Institute of Mechanical Engineers* 220.

FLETCHER, C. A. J. (1991) *Computational techniques for fluid dynamics,* New York, Springer-Verlag.

FLOYD, J. E., MCGRATTAN, K. B., HOSTIKKA, S. & BAUM, H. R. (2003) CFD Fire Simulation Using Mixture Fraction Combustion and Finite Volume Radiative Heat Transfer. *Journal of Fire Protection Engineering,* 13.

FLYNN, P., MIZUSAWA, M., UYEHARA, O. & MYERS, P. (1972) An experimental determination of the instantaneous potential radiant heat transfer within an operating diesel engine *SAE Trans*.

FOSTER, A. (1998) Transient flow in IC engines. *CFX Update.*

FRANK, J. H., KAISER, S. A. & LONG, M. B. (2002) Reaction-rate, mixture-fraction, and temperature imaging in turbulent methane/air jet flames. *Proceedings of the Combustion Institute,* 29**,** 2687 - 2694.

GALINDO, J., LUJAN, J. M., SERRANO, J. R. & HERANDEZ, L. (2005) Combustion simulation of turbocharger HSDI diesel engines during transient operation using neural networks. *Applied Thermal Engineering,* 25**,** 877-898.

GEORGE, W. K., WANG, H., WOLLBLAD, C. & TOHANSSON, T. G. (2001) *14th AFMC.* Adelaide, Australia.

GOLOVITCHEV, V. I., BERMAN, M. & MONTORSI, L. (2007) CFD modelling of diesel oil and DME performance in a two-stroke free piston engine. *Combust.Sci. and tech.,* 179**,** 417-436.

GOSMAN, A. D., LAUNDER, B. E. & REECE, G. J. (1985) *Computer-aided engineering: heat transfer and fluid flow,* England, Halsted Press.

HEEL, B., MALY, R., WELLER, H. G. & GOSMAN, A. D. (1998) Validation of SI combustion model over range of speed, load, equivalence ratio, and spark timing. *The fourth International Symposium COMODIA 98.*

HEYWOOD, J. B. (1988) *Internal Combustion Engine Fundamentals,* New York, McGraw-Hill.

HEYWOOD, J. B. & SHER, E. (1999a) *The Two-Stroke Cycle Engine,* New York, SAE International.

HEYWOOD, J. B. & SHER, E. (1999b) *The Two-Stroke Cycle Engine: Its Development, Operation, and Design,* New York, Taylor and Francis.

HILL, P. G. & ZHANG, D. (1994) The effects of swirl and tumble on combustion in spark-ignition engines. *Progress in Energy and Combustion Science,* 20**,** 373-429.

HOFBAUER, P. (1999) Stroke of genius OPOC takes two. Engine Technology International

HOFFMAN, K. A. (1993) *Computational fluid dynamics for engineers,* Wichita, Engineering Education System.

HOHENBERG, G. F. (1979) Advanced Approaches for Heat Transfer Calculations *SAE Transactions,* 88.

HOLT, M. (1984) *Numerical methods in fluid dynamics,* New York, Springer-Verlag.

HORROCKS, G. (2001) A Numerical Study of a Rotary Valve Internal Combustion Engine. *Engineering.* Sydney, University of Technology, Sydney.

HUA, J., WU, M. & KUMAR, K. (2005) Numerical simulation of the combustion of hydrogen-air mixture in micro-scaled chambers.Part 1 Fundamental study. *Chemical Engineering Sciences,* 60**,** 3497-3506.

HUANG, H. C. (1994) *Finite element analysis for heat transfer: theory and software,* New York, Springer-Verlag.

HUANG, J. & BUSHIE, W. K. (2007) Simulation of transient turbulent methane jet ignition and combustion under engine-relevant conditions using conditional source-term estimation with detailed chemistry. *Combustion Theory and Modelling,* 11**,** 977-1008.

ILBAS, M. (2005) The effect of thermal radiation and radiation models on hydrogen-hydrocarbon combustion modelling. *International Journal of Hydrogen Energy,* 30**,** 1113-1126.

INCORPERA, F. P. & DEWITT, D. P. (1990) *Introduction to heat transfer* New York, John Wiley and Sons Inc.

INCROPERA, F. P. (2006) *Fundamentals of heat and mass transfer,* New Jersey, Wiley.

JAZBEC, M., FLETCHER, D. F. & HAYNES, B. S. (2000) Simulation of the ignition of lean methane mixtures using CFD modelling and a reduced chemistry mechanism. *Applied Mathematical Modelling,* 24**,** 689-696.

JOBSON, D. A. (1955) On the flow of a compressible fluid through orifices. *Proc. I Mech. E.,* 160**,** 767.

JUDGE, A. W. (1955) *Modern Petrol Engines,* Norwich, Chapman and Hall Ltd.

KIDO, H., NAKAHARA, M. & HASHIMOTO, J. (1998) A turbulent burning velocity model taking account of the preferential diffusion effect. *The fourth International Symposium COMODIA*.

KNIGHT, B. E. (1964) The problem of predicting heat transfer in diesel engines. *proceedings of the Institution of Mechanical Engineers,* 179**,** 93-106.

KNOP, V., BENKENIDA, A., JAY, S. & COLIN, O. (2008) Modelling of combustion and nitrogen oxide formatrion in hydrogen-fuelled internal combustion engines within a 3D CFD code. *International Journal of Hydrogen Energy,* 33**,** 5083-5097.

KONG, S.-C. & REITZ, R. D. (2003) Numerical study of premixed HCCI engine combustion and its sensitivity to computational mesh and model uncertainties. *Combustion Theory and Modelling,* 7**,** 417-433.

KOPF, G. (1981) *The engine,* London, Heinemann Educational.

KURNIAWAN, W. H. & ABDULLAH, S. (2007a) Numerical analysis of the combustion process in a four-stroke compressed natural gas engine witrh direct injection system. *The 9th Asian International Conference on Fluid Mechinery.* Korea.

KURNIAWAN, W. H. & ABDULLAH, S. (2007b) Numerical analysis of the combustion process in a four stroke compressed natural gas engine with direct injection system. *Asian National Conference on Fluid Machinery.*

KURNIAWAN, W. H., ABDULLAH, S., NOPIAH, Z. M. & SOPIAN, K. (2007a) The Development of Artificial Neural Network for Prediction of Performance and Emissions in a Compressed Natural Gas Engine with Direct Injection System. *SAE International*.

KURNIAWAN, W. H., ABDULLAH, S., NOPIAH, Z. M. & SOPIAN, K. (2007b) Multi-objective optimization of combustion process in a compressed natural gas direct injection engine using coupled code of CFD and generic algorithm. *Society of Automotive Engineers of japan*.

KURNIAWAN, W. H., ABDULLAH, S. & SHAMSUDEEN, A. (2007c) Turbulence and heat transfer analysis of intake and compression stroke in automotive 4-stroke direct injection engine. *Algerian Journal of Applied Fluid Mechanics,* 1**,** 37 -50.

KUZNETSOV, V. R. & SABEL'NIKOV, V. A. (1990) *Turbulence and Combustion,* Washington, Hemisphere Publishing Corporation.

LEFEUVRE, T., MYERS, P. S. & UYEHARA, O. A. (1969) Experimental Instantaneous heat Fluxes in a Diesel Engine and their Correlations. *SAE Trans,* 78.

LEICHER, S., FRITZ, W., GRASHOF, J. & LONGO, J. Mesh generation strategies for CFD on complex configurations West Germany.

LUMLEY, J. L. (1999a) *Engines: An Introduction,* Melbourne, Press Syndicate of The University of Cambridge.

LUMLEY, J. L. (1999b) *Engines: an introduction: using the Stanford Engine Simulation Program,* Cambridge, Cambridge University Press.

MAMERI, A., KAABI, A. & GOKALP, I. (2008) TFC modelling of hydrogenated methane premixed combustion. *CISM 2008.* Oum El Bouaghi, Institut de Combustion, France.

MATHUR, M. L. & SHARMA, R. P. (2003) *Internal Combustion Engines,* New Delhi, Dhanpat Rai Publications.

MCNEILL, D. H. (2005) Minimum ignition energy for laser spark ignition *Proceedings of the Combustion Institute,* 30.

MENTER, F. R. (1994) Two equation eddy viscosity turbulence models for engineering application. *AIAA Journal,* 32**,** 1598-1605.

MIDDLEMAN, S. (1998) *An introduction to fluid dynamic: principles of analysis and design,* New York, Wiley.

MIKALSEN, R. & ROSKILLY, A. P. (2007) Performance simulation of a spark ignited free-piston engine generator. *Applied Thermal Engineering,* 28**,** 1726–1733.

MILLS, A. F. (1995) *Heat and mass transfer,* Burr Ridge, Irwin.

MILTNER, M., MILTNER, A., HARASEK, M. & FRIEDL, A. (2005) Process simulation and CFD calculations for the development of an innovative baled biomass-fired combustion chamber. *Applied Thermal Engineering,* 27**,** 1138-1143.

MIYAGAWA, H., NOMURA, Y., KOIKE, M. & TOMODA, T. (2003) CFD simulation of Stratified Combustion Process in a Direct Injection Spark Ingition Engine. *JSME Internation Journal,* 46**,** 332-339.

MOAVENI, S. (2008) *Finite element analysis: theory and application with Ansys,* New Jersey, Prentice Hall.

MOHAMMADI, A., YAGHOUBI, M. & RASHIDI, M. (2007) Analysis of local convective heat transfer in a spark ignition engine. *Internal Communications in Heat and Mass Transfer,* 35**,** 215 - 224.

NAG, P. K. (1995) *Engineering Thermodynamics,* New Delhi, Tata McGraw-Hill Publications.

NEVIS, N. E.-. (2009) DynaCam engine.

NEWTON & STEEDS (1927) THE MICHELL AXIAL SWASHPLATE ENGINE. Iliffe.

PALIPANA, A. S., MALALASEKERA, W. & JAMES, E. H. (1999) A CFD parametric study of natural gas engine combustion. *1999 Spring Technical Conference* ASME

PAOLA, G. D., MASTORAKOS, E., WRIGHT, Y. M. & BOULOUCHOS, K. (2008) Diesel engine simulations with multi-dimensional conditional moment closure. *Combust.Sci. and Tech.,* 180**,** 883-899.

PAYRI, F., BENAJES, J., MARGOT, X. & GIL, A. (2003) CFD modelling of the in-cylinder flow in direct-injection Diesel engines. *Computers and Fluids,* 33.

PETERS, N. (1986) Laminar Flamelet Concepts in Turbulent Combustion. *Twenty first symposium (International) on Combustion* Germany, The Combustion Institute.

PETERS, N. (2000) *Turbulent Combustion,* Germany, Cambridge University Press.

POPE, S. B. (2000) *Turbulent Flows,* Cambridge, Cambridge University Press.

POWELL, P. E. C.-. (2006) THE NUSTROKE ENGINE.

PYE, D. R. (1953a) *The Internal Combustion Engine,* London, Oxford University Press.

PYE, D. R. (1953b) *The Internal Combustion Engine Vol II: The Aero-Engine,* London, Oxford University Press.

RABBATH, C. A., DESIRA, H. & BUTTS, K. (2001) Effective modelling and simulation of Internal combustion engine control systems. *Proceedings of the American Control Conference.* Arlington, VA, AACC.

RAMOS, J. I. (1989) *Internal Combustion Engine Modelling,* New York, Hemisphere Publishing Corporation.

REDDY, J. N. (1994) *The finite element method in heat transfer and fluid dynamics,* Boca Raton, CRC Press.

REITZ, R. D. & RUTLAND, C. J. (1995) Development and testing of diesel engine CFD models. *Progress in Energy and Combustion Science,* 21**,** 173-196.

RICHARD, S., COLIN, O., VERMOREL, O., BENKENIDA, A., ANGELBERGER, C. & VEYNANTE, D. (2007) Towards large eddy simulation of combustion in spark ignition engines. *Proceedings of the Combustion Institute,* 31**,** 3059-3066.

SAIJYO, K., NISHIWAKI, K. & YOSHIHARA, Y. (2003) Numerical analysis of the Interaction between Thermo-Fluid Dynamics and Auto-Ignition reaction in SI engines. *JSME International Journal,* 46**,** 44-51.

SARLI, V. D., MARRA, F. S. & BENDETTO, A. D. (2007) Spontaneous oscillations in lean premixed combustors: CFD simulation. *Combust.Sci. and Tech.,* 179**,** 2335-2359.

SCHMIDT, F. A. F. (1965) *Internal combustion engine,* London, Chapman and Hall.

SEQUEIRA, A. (1995) Navier-Stokes equations and related nonlinear problems. *Proceedings of the third international conference on Navier-Stokes Equations and related nonlinear problems.* Madeira Islands.

SETRIGHT, L. J. K. (1979) *Some Unusual Engines,* London, Mechanical Engineering Publications Limited.

SHAW, C. T. (1992) *Using computational fluid dynamics,* New York, Prentice Hall.

SHAYLER, P. J., CHICK, J. P. & MA, T. (1997) Correlation of engine heat transfer for heat rejection and warm-up modelling. *SAE Trans,* 106.

SHINJO, J., MIZOBUCHI, Y. & SATORU, O. (2004) Combustion Dynamics in a lean premixed gas turbine combustor. *Computational fluid dynamics,* 13**,** 348-354.

SIHLING, K. & WOSCHNI, G. (1979) Experimental investigation of the instantaneous heat transfer in the cylinder of a high speed diesel engine. *Society of Automotive Engineers***,** 95-103.

SINGH, K. (2004) *Automobile Engineering,* New Delhi, Standard Publishers Distributors.

SOUTHWELL, R. V. & VAISEY, G. (1948) Relaxation methods applied to Engineering Problems: XII Fluid Motions Characterized by Free Streamlines. *Phil. Trans. Roy. Soc.,* 246**,** 117.

SPALDING, D. B. & AFGAN, N. H. (Eds.) (1989) *Heat and Mass Transfer in Gasoline and Diesel Engines,* New York, Hemishpere Publishing Corporation.

STONE, R. (1999a) *Introduction to internal combustion engines,* London, Macmillan Press.

STONE, R. (1999b) Particulate matter from Diesel engines *CFX Update*.

STOPFORD, P. J. (2002) Recent applications of CFD modelling in the power generation and combustion industries. *Applied Mathematical Modelling,* 26**,** 351-374.

TAKAGI, Y. (1998) A new era in spark-ignition engines featuring high-pressure direct injection`. *Twenty-Seventh Symposium (International) on Combustion.* The Combustion Institute.

TALLIO, K. V. & VOLELLA, P. C. (1997) A multi-fluid CFD turbulent entrainment combustion model: Formulation and one-dimensional results. *Society of Automotice Engineers*.

TAN, Z. & REITZ, R. D. (2006) An ignition and combustion model based on the level-set method for spark ignition engine multidimensional modelling. *Combustion and Flame,* 145**,** 1-15.

TARDEC, U. S. A. T. A. R. D. A. E. C.-. (2009) Opposing piston opposing cylinder engine (OPOC).

TAYLOR, C. E. (1985a) *The Internal Combustion Engine in theory and practice,* Cambridge, MIT Press.

TAYLOR, C. E. & TOONG, T. Y. (1985) Heat transfer in internal combustion engines. *ASME*.

TAYLOR, C. F. (1960) *The Internal Combustion Engine in Theory and Practice,* Massachussets, The Technology Press of The Massachussets Institute of Technology and John Wiley & Sons, Inc.

TAYLOR, C. F. (1984) *The Internal combustion engine,* Pennsylvania, International Co.

TAYLOR, C. F. (1985b) *The internal-combustion engine in theory and practice* Massachusetts, MIT Press, Cambridge.

TAYLOR, C. F. & TAYLOR, E. S. (1950) *The Internal Combustion Engine,* Pennsylvania, International Textbook Company.

THOMAS, G. (2008) Numerical and CFD modelling of Internal Combustion Engines, analysis and optimization of Conventional and Opposed piston configurations. Master of Engineering Thesis. *Engineering.* Wollongong, University of Wollongong.

TOMODA, T., KUBOTA, M., SHIMIZU, R. & NOMURA, Y. (2003) Numerical analysis of misture formation of direct injection gasoline engine. *JSME International Journal,* 46**,** 2-9.

TU, J., YEOH, G. H. & LIU, C. (2008) *Computational Fluid Dynamics: A Practical Approach,* New York, Butterworth-Heinemann.

VERSTEEG, H. K. & MALALASEKERA, W. (2007) *An Introduction to Computational Fluid Dynamics,* Harlow, Pearson Education Limited.

VEYNANTE, D. & VERVISCH, L. (2001) Turbulent Combustion Modeling. *Progress in Energy and Combustion Science,* 28**,** 193 - 266.

VITA, A. D. & ANGELO, L. D. (2003) CFD analysis of engine: An advanced approach based on codes dynamically coupled. *2003 Spring Technical Conference of the ASME Internal Combustion Engine Division.* Austria, ASME.

WALKER, S. (1996) Mitchell, Anthony George Maldon (1870 - 1959). Australian Dictionary of Biography.

WATSON, N. & JANOTA, M. S. (1982) *Turbocharging the Internal combustion engine,* London, Macmillan Education.

WEAVING, J. H. (Ed.) (1990) *Internal Combustion Engineering: Science and Technology,* London, Elsevier Applied Science.

WIJESINGHE, J. & HONG, G. (2008) Study of the autoignition combustion operation region of a small two-stroke engine *Pro.IMechE,* 223**,** 651 - 659.

WINTERBONE, D. E. & PEARSON, R. J. (1999) *Design Techniques for Engine Manifolds: Wave Action Methods for IC Engines,* London, Professional Engineering Publishing Limited.

WITHWORTH, A. (1977) Opposed piston steam engine. Armstrong Withworth and Company Limited.

WOSCHNI, G. (1967) A Universally Applicable Equation for the Instantaneous Heat Transfer Coefficient in the Internal Combustion Engine. *SAE Transactions*.

YAHYA, S. M. (2004) *Fundamental of compressible flow,* New Delhi, New Age International Publishers.

YASAR, O. (2001) A new ignition model for spark-ignited engine simulations. *Elsevier,* 27**,** 179 - 200.

YEDIDIAH, S. (2008) A study in the use of CFD in the design of centrifugal pumps. *Engineering application of computational fluid mechanics,* 2**,** 331-343.

ZHANG, Y. Z., KUNG, E. H. & HAWORTH, D. C. (2005) A PDF method for multidimensional modelling of HCCI engine combustion: effects of turbulence/chemistry interactions on ignition timing and emissions *Proceedings of the Combustion Institute,* 30**,** 2763-2771.